

Use Authorization

In presenting this dissertation in partial fulfillment of the requirements for an advanced degree at Idaho State University, I agree that the Library shall make it freely available for inspection. I further state that permission to download and/or print my dissertation for scholarly purposes may be granted by the Dean of the Graduate School, Dean of my academic division, or by the University Librarian. It is understood that any copying or publication of this dissertation for financial gain shall not be allowed without my written permission.

Signature _____

Date _____

High-Precision PMT Gain Measurement With Subsequent Quartz Cerenkov Detector
Characterization

by

Brady Lowe

A thesis
submitted in partial fulfillment
of the requirements for the degree of
Master of Science in the Department of Physics
Idaho State University
Summer 2019

Copyright (2019) Brady Lowe
All rights reserved.

To the Graduate Faculty:

The members of the committee appointed to examine the dissertation of Brady Lowe find it satisfactory and recommend that it be accepted.

Dr. Dustin McNulty,

Major Advisor

Dr. Steve Shropshire,

Committee Member

Dr. Robert Fisher,

Graduate Faculty Representative

Acknowledgments

First of all, I would like to acknowledge my wife, Lwin, who has supported me through school no matter how hard our lives get. I love our home life, I love the cooking, the decorations, the cuddles. Thank you for understanding when I am overwhelmed by stress. Thank you for letting me work on my research at any odd hour of the day or night to match my motivation level. I hope I can offer you the same support as you finish your degrees.

I would like to acknowledge all the worries, investments, and love of my parents, Mike and Lori Lowe. You have both supported me to the best of your ability despite my age and poor decisions. You continue to help me to this day with babysitting, family gatherings, and anything else that I happen to need. Thank you for the years of hard work and advice to care for myself. Thank you for the years of constant encouragement and unconditional love that I know I will have even if I accomplish nothing (else).

I want to acknowledge my advisor, Dr. McNulty for his patience and understanding over the years. We have had some push and shove in the lab that has motivated me to do a thorough job and be sure of what I am saying. You have given me guidance in many areas of life and helped me to see a bigger, better world in many ways. Thank you for the many opportunities to expand my horizons.

I want to acknowledge Dr. Steve Shropshire who advised me many times throughout each semester on career path choices, classes, thesis topics, and camping matters. You have helped my family through college, and you have given us many activities to get out of our comfort zones, into public, and talking about science.

I also want to acknowledge my classmates and labmates. Daniel Sluder, I owe an incredible amount to you. Watching you perform your research, take classes, write your thesis, and snowboard at pebble every day put me in awe and inspired me. I followed in your footsteps to get where I am now. Carlos Bula, I have known you now for many years, you have come to multiple parties of ours and a few other outings. You are so caring and solid in your views

of the world, you have encouraged me and given me a different perspective, and I thank you. Joey McCullough, I have gotten to know you during our graduate studies, and it has been a great time. You have shown me how to live as a bachelor, what it means to be a dude. You have had many heart to heart talks with me, you have felt my pain, and I have felt yours. Thank you for the companionship and help with the homework. Devi Adhikari, I have also gotten to know you over the past 2 years. You are a great man with a great family, you have taught me what life can be like in a different world, you have helped me develop deep thoughts about physics as well as ethics and spirituality. Last, but not least, I'll thank Rob Lewis. Out of everyone involved, you have certainly taken the most time and effort to dive deep into this project that only I really know about. You have strained your brain, looking at countless numbers, scripts, and plots to help me sort it all out.

I am very grateful to have been blessed with such an amazing group of friends and family.

Contents

List of Figures	ix
List of Tables	xiii
Abstract	xiv
1 Introduction	1
1.1 Motivation	1
1.2 Experimental Setup	3
1.2.1 The PMTs	4
1.2.2 Light source	6
1.2.3 Electronics	7
1.2.4 Data Acquisition	7
1.3 Summary of Other Chapters	10
2 PMT Models	12
2.1 PMT Basics	12
2.1.1 The photo-cathode	13
2.1.2 Amplification	13
2.1.3 Gain Vs. High Voltage	14
2.2 Monte Carlo simulation	15
2.2.1 Simulating the PMT	15
2.2.2 Using the Simulation For Calibration	17
2.3 Assuming a Distribution Shape	18
2.3.1 Gaussian Models	19
2.3.2 Beyond the Gaussian Model	20
2.4 Implementing the Model Using Root	22
2.5 Example Fit Results	24

3 Precise Low-Light Gain Measurement at High Voltages	31
3.1 Turning on the PMT	31
3.2 Data Acquisition	34
3.2.1 Taking Good Data With PMT 1	34
3.2.2 Taking Good Data with PMTs 4 and 5	36
3.3 Taking Bad Data	37
3.3.1 Gain is Too Low	37
3.3.2 Light Level is Too High	38
3.3.3 Statistics are Too Low	40
3.4 Producing a Great Fit	42
3.4.1 High-Energy Bump	42
3.4.2 Non-Gaussian ADC Distribution	43
3.4.3 Fit Inputs: Constraints	43
3.4.4 Fit Outputs: Gain and Light Level	45
3.4.5 Measurement Error	46
3.5 MySQL For Managing Many Fit Results	47
3.5.1 Filling the Database	48
3.5.2 Analyzing a Full Database	49
4 Light Level Calibration	66
4.1 Calibrating Light Levels With the Gain Data	66
4.2 Calibrating Filter Transparency	69
5 High-Light Gain Measurement at Low Voltages	72
5.1 Gain measurement at low voltage	72
5.1.1 Examples of individual results	73
5.1.2 Trends in the results	74
5.1.3 Comparison to Poisson Results	76

6 Characterizing Cerenkov Detectors with PMTs	82
6.1 Intro to Cerenkov Detectors	82
6.1.1 Angle Dependence	83
6.1.2 Quartz Requirements	84
6.2 Thin Quartz	85
6.2.1 Tandem Design	85
6.2.2 Tandem Data	86
6.3 ShowerMax Detector	87
6.3.1 ShowerMax Data	88
6.3.2 Benchmarking Apparatus	89
6.3.3 Benchmarking Data Using Gain Measurements	90
6.4 Comparison With Simulation	91
6.5 Future Studies	92
A Gain Measurement Software	106
B Gain Measurement Results	113

List of Figures

1.1	Dark box with PMT	4
1.2	PMT holders	5
1.3	CAEN SP5601 LED Driver	6
1.4	Optical elements	7
1.5	Pulse generator	8
1.6	NIM and VME	9
2.1	PMT schematic	12
2.2	QE vs. Wavelength	16
2.3	Example of Pedestal Data	20
2.4	Low-light high-voltage fits	27
2.5	Medium-light high-voltage fits	28
2.6	High-light Poisson fits	29
2.7	High-light Gaussian fits	30
3.1	Gate pulse	32
3.2	1-PE scope signal	33
3.3	Multiple PE scope signal	34
3.4	PMT 1 @ 2,000 V	52
3.5	PMT 1 @ 1,900 V	53
3.6	PMT 4 @ 2,000 V	54
3.7	PMT 5 @ 1,350 V	55
3.8	High voltage scan @ light level 40	56
3.9	Full light level scan @ high-gain	57
3.10	Spread in statistics	58
3.11	High-energy bump at high statistics	59

3.12	Triple-Gaussian CAEN ADC distribution	60
3.13	MySQL scripts command line output	61
3.14	Gain Vs Voltage for all PMTs	62
3.15	Gain Vs Voltage with and without exponential decay	63
3.16	Gain Vs Light Level for PMT 1	64
3.17	Gain Vs Gain Constraint	65
4.1	Low light calibration for all PMTs	68
4.2	Filter/Light calibration with PMT 6	69
4.3	Filter/Light calibration with PMT 6 (high gain)	71
5.1	High-light model results PMT 1 @ 2,000 volts (1-PE)	73
5.2	High-light model results PMT 1 @ 2,000 volts (many PE)	78
5.3	High-light model gain curves for PMTs 1, 2, 5, and 6	79
5.4	High-light model filtered results	80
5.5	High-light model compared to low-light models	81
6.1	Tandem Detector Optical Simulation	83
6.2	Thin Quartz Angle Dependence	84
6.3	Tandem Detector	86
6.4	Tandem Detector PMT Response	95
6.5	ShowerMax Detector	96
6.6	ShowerMax 1A and 1B Simulation	97
6.7	ShowerMax 1A and 1B Data	98
6.8	ShowerMax Benchmarking Detector	99
6.9	Benchmark 1A Data (No Tungsten Vs Tungsten)	100
6.10	Benchmark 1B Data (2 and 3 stacks)	101
6.11	Benchmark Full Stack Energy Comparison	102
6.12	Benchmark 1A Simulation (0 and 1 stacks)	103

6.13 Benchmark 1A Simulation (2, 3, and 4 stacks)	104
A.1 Low-Light Fit Setup	108
A.2 Drawing the Fit Results	109
A.3 Fitting to Background	110
A.4 Fitting to Signal	111
A.5 Post-Processing Fit Results	112
B.1 Gain Curve PMT 1: Error	113
B.2 Gain Curve PMT 1: Light Level	113
B.3 Gain Curve PMT 1: Model	114
B.4 Gain Curve Fit PMT 1	114
B.5 Light Level Curve PMT 1	115
B.6 Gain Curve PMT 2: Error	115
B.7 Gain Curve PMT 2: Light Level	115
B.8 Gain Curve PMT 2: Model	116
B.9 Gain Curve Fit PMT 2	116
B.10 Light Level Curve PMT 2	116
B.11 Gain Curve PMT 3: Error	117
B.12 Gain Curve PMT 3: Light Level	117
B.13 Gain Curve PMT 3: Model	117
B.14 Gain Curve Fit PMT 3	118
B.15 Light Level Curve PMT 3	118
B.16 Gain Curve PMT 4: Error	118
B.17 Gain Curve PMT 4: Light Level	119
B.18 Gain Curve PMT 4: Model	119
B.19 Gain Curve Fit PMT 4	120
B.20 Light Level Curve PMT 4	120

B.21 Gain Curve PMT 5: Error	120
B.22 Gain Curve PMT 5: Light Level	121
B.23 Gain Curve PMT 5: Model	121
B.24 Gain Curve Fit PMT 5	122
B.25 Light Level Curve PMT 5	122
B.26 Gain Curve PMT 6: Error	122
B.27 Gain Curve PMT 6: Light Level	123
B.28 Gain Curve PMT 6: Model	123
B.29 Gain Curve Fit PMT 6	124
B.30 Light Level Curve PMT 6	124

List of Tables

2.1	Tuning a single parameter	23
2.2	Tuning two parameters	24
3.1	PMT 1 gain measurement at 2,000V and 1,900V	35
3.2	PMT 4 gain measurement @ 2,000V	36
3.3	PMT 5 gain measurement @ 1,350V	37
3.4	High voltage scan @ light level 40	37
3.5	High-gain fit applied to low gain	39
3.6	Full light level scan @ high-gain	40
3.7	Spread in statistics	41
3.8	Fit inputs description	45
3.9	Fit outputs	46
3.10	Scripts for filling MySQL tables	49
3.11	Scripts for filling MySQL tables	50
4.1	Low-light calibration for PMT 1	67
4.2	Low-light calibration for PMT 1 (best fits)	67
4.3	Low-light calibration for all PMTs	68
4.4	Low-light filter 8 calibration	70
A.1	Root C++ Objects	106
A.2	Root Fitting Functions	107

High-Precision PMT Gain Measurement With Subsequent Quartz Cerenkov Detector
Characterization

Thesis Abstract—Idaho State University (2019)

High-purity, quartz Cerenkov detectors can be used to count extreme flux rates of relativistic electrons with very high precision. This allows for many indirect measurements of the universe including the cross-sections of weakly-interacting electrons with lead, calcium or liquid hydrogen targets. With this goal, several Cerenkov detectors were designed and constructed. Data was collected at Stanford Linear Accelerator Center (SLAC) to test these detectors. The data collected at SLAC shows the light yield and resolution of several configurations of the detectors. A calibration of six photo-multiplier tubes (PMTs) was completed to analyze the electron testbeam data. The PMT calibration included a precise measurement of the gain using a low-light method only applicable at high voltage, a light source calibration, and a measurement of the gains at low voltages using the calibrated light source. A description of the gain measurement apparatus is presented along with the measurement technique and results.

Keywords:

Particle Physics, PMT calibration, Photo-multiplier characterization, gain measurement, Poisson statistics, Quartz Cerenkov detectors

Chapter 1

Introduction

This thesis contains a detailed analysis of the measurement of the gain of six photomultiplier tubes (PMTs) over a range of voltages and light levels. A high-precision measurement is made at high voltages and used to measure gain at lower voltages. These gain calibrations are required for the quartz Cerenkov detector characterizations discussed in Chapter 6. The six PMTs were calibrated at high voltage (gain) using a Poisson fitting model at very low light (single photon) conditions, where possible. For the low-gain measurements, use of a calibrated light source at high light levels is required. Calibrated PMTs are required for the benchmarking of simulations that aid in detector development, and are indispensable measurement tools to have for almost any particle physics experiment.

This chapter discusses the motivation for the gain measurements, the experimental setup, and gives an overview of the chapters to follow.

Motivation

Our lab at Idaho State University designs and builds quartz Cerenkov detectors for use in Parity-Violating Electron Scattering (PVES) experiments such as PREx [1], CREx [2], and MOLLER [3]. Parity-violating experiments study the weak interaction by exploiting its characteristic parity violation. Electrons, protons, and neutrons all interact via the electromagnetic force and the weak force. Protons and electrons interact very often via the Lorentz force because they are both charged, whereas the neutron is uncharged. When it comes to the weak force, however, it is the interactions between neutrons and electrons that dominate. This means that if an electron scatters electromagnetically off of a target, it most-likely scattered off a proton, and if the electron scatters weakly in the target, it most likely interacted with a neutron. Observing the weakly interacting electrons allows measurement of the neutron distribution of the target rather than the more commonly

observed proton distribution.

The characteristic parity violation of the weak force manifests itself when both the target and beam are polarized. When polarized, primarily left-handed electrons will interact weakly with the nuclear target. Of course, most of the electrons will interact electromagnetically with the target¹. This means that with one beam helicity, the observed scattering distribution will include electrons that interacted with both protons and neutrons, whereas the other beam helicity distribution will be predominantly from electromagnetic proton scattering. The neutron distribution is found in the difference of the cross sections for the two beam helicities. This difference divided by the sum of the two distributions is called the parity-violating asymmetry, A_{PV} [1, pp. 5-6]. Forming an asymmetry measurement allows for much of the electromagnetic contribution to be canceled out. A_{PV} is very small (around 1 part per million) due to the weak coupling of the weak force, as well as the small scattering angles (small Q^2) observed in these experiments. This means that the measurement of the distributions must be very precise in order to resolve anything reliably. Meeting the precision requirements here amounts to being able to count electrons traversing the detector at better than the 1 ppm level.²

Quartz Cerenkov detectors are able to count charged particles with decent precision. The main motivation in using a quartz Cerenkov detector is the extreme resistance to damage quartz exhibits in continuous exposure to radiation. These detectors will be able to record the large number of interactions necessary for good resolution. A quartz Cerenkov detector is basically a piece of high-purity fused silica (quartz) and a photo-sensitive device (PMT). Cerenkov refers to radiation from a charged particle moving through a medium faster than light can travel in that medium. This phenomenon is analogous to a sonic blast, where a particle moves through the air faster than sound can travel through it. The disturbances (waves) in the medium pile up behind the source of the disturbances and travel outward in a powerful front at an angle defined by the velocity of the particle and the speed of

¹Not really all of them will, but a million times more will.

²Achieving this precision requires careful attending to all statistical errors and sufficient statistics.

wave propagation. The medium here is the high-purity quartz crystal with polished surfaces allowing only 0.1% of light loss from inside the quartz.³ This Cerenkov radiation is very regular and reliable; even for minimum-ionizing particles such as muons, the number and color of Cerenkov photons created in the traversal of a piece of quartz is unavoidable and highly regular.⁴ With a calibrated PMT, the flash of light produced by a single electron traversing the quartz can be well characterized.

Monte Carlo simulations facilitate development of the detectors by predicting how the PMT distribution will depend on various elements such as light guides, polish, etc. To achieve the precision required for A_{PV} measurement, the resolution must be optimized. Calibrating the PMTs is necessary for comparing simulations to real PMT data. The goal of this thesis is to give a measurement of the gain of six PMTs over their operating voltages and light levels, and use this measurement for the analysis of real data taken at Stanford Linear Accelerator Center (SLAC) with ISU's quartz Cerenkov detectors and PMTs. The light level mentioned above is very important and thoroughly discussed in this thesis. Light level here refers to the number of photo-electrons ejected from the photo-cathode PER event (i.e. per flash of LED light or per Cerenkov pulse). The number of photo-electrons ejected from the PMT cathode depends on light source intensity, distance to PMT, light guide design, PMT model, filters used, etc., but is independent of the gain of the PMT. This light level is predicted by the Monte Carlo simulations used and compared to the results seen in the Poissonian PMT response model. This model and the process of photo-electron ejection will be described in detail in Sections 2.3 and 2.1 respectively.

Experimental Setup

This high-precision gain measurement takes place at a very low light level where Poissonian statistics describe the PMT distribution. A black plastic box of approximate dimensions

³These detectors rely on total internal reflection inside the quartz to guide the light to the PMT.

⁴Cerenkov is only produced for charged particles with sufficient speed (greater than light speed).

0.25 m x 0.25 m x 1 m, with a deep groove in the lid, was used to shut out the ambient light. Inside the box rests an aluminum plate used as an optical beam line base platform. To this base platform mounts the PMT, fiber optic from the light source, filters, a shutter, and a diffuser. This setup is shown in figure 1.1.



Figure 1.1: The PMT is mounted to the filter wheel apparatus which is mounted to the base plate in the dark box. The fiber optic cable along with control and HV lines are routed out of the box. A black cloth wraps around everything in the box before the lid is secured.

The PMTs

All six PMTs measured are designed to receive UV and visible light of around 200-500 nm from the Cerenkov pulse. This includes bi-alkali photo-cathodes and quartz windows to allow UV detection and transmission. The quartz windows also ensure that minimal window degradation will occur from incident radiation during the experiment. The transmission of the PMT window should remain constant throughout the experiment. Four of the PMTs are made by Hamamatsu, model R7723Q, with 2" windows and bases modified for better signal linearity. The operating range of voltages for these tubes is -700V to -2000V with a gain of around 10^3 to 10^6 respectively. They multiply the signal over 8 dynode stages with voltage ratios of 4:1:2:1:1:1:2:1. These four tubes are referred to as PMTs 1 - 4.

The other two PMTs are from ET Enterprises, model 9305KBQ, and referred to as

PMTs 5 and 6. PMT 6 has a base modified for better pulsed-linearity; PMT 5 does not. These tubes have 10 dynodes and 3" quartz windows. PMT 5 has voltage divider ratios of 3:1:1:1:1:1:1:1:1:1 and operating voltages of -500V to -1350V. The high pulsed-linearity model has ratios of 3:1:1:1:1:1:2:3:4:3 and operating voltages of -400V to -1000V⁵. These tubes give gains of 10^3 to around 10^7 .

The PMTs mount to the filter wheel apparatus via 3D printed custom holders. Figure 1.2 shows splices for the 2" and 3" PMTs. The 2" PMTs use an end-cap system. One end-cap attaches to the PMT base via set screws. A PVC tube is slipped around the PMT and mates to the printed end-caps. The end-cap that mounts to the filter wheel has threads printed into it for this mate. Figure 1.1 shows the PMT inside the PVC tube with end-caps on. The 3" PMT holders have a similar cap for mating to the filter wheel apparatus, but rather than a PVC tube and another end-cap, a custom sleeve is printed to hold the PMT.



Figure 1.2: The left image shows a 2" PMT with end cap attached to its base. The middle image shows the 3D printed 3" PMT sleeve empty. The right image shows a quartz detectors with 3" PMT and sleeve mounted. The quartz is inside the black box.

⁵For the rest of this document, the negative sign will be neglected when referring to voltages. All voltages are assumed negative.

Light source

The SP5601 LED Driver made by CAEN is used as a source of 2-4 nanosecond light pulses (see figure 1.3).



Figure 1.3: Front and back of the light source. The front has the light level dial and the fiber optic attachment. The back has a switch for internal/external trigger source, trigger input, and trigger output, as well as a switch for internal trigger frequency (fast or very fast).

This source uses an LED deep into the violet end of the spectrum that is able to be triggered at up to 100 MHz. The source can produce anywhere from 0 to around 10,000 photons per pulse and delivers a very steady amount of light wherever it is set. The light box sits outside the dark box and delivers the pulses to the PMT via 5' of fiber optic cable. This light source is suitable for a low-light measurement by itself; no filtering is necessary to observe Poissonian statistics if the CAEN LED driver dial is set right⁶. Upon exiting the fiber optic, the light pulse then passes through the shutter (if open), travels through a filter (if one has been placed), and then travels through a diffuser to deliver light to the photo-cathode as homogeneously as possible. Filters are used for allowing calibration of high light levels using the low light fitting model described in Section 2.3.

Edmond Optics offers a variety of filter wheels for mechanical filter strength selection. A wheel with 8 filters that range from 0.1% transmission to around 70% transmission was used for part of this analysis. These filters are neutral density meaning that light is attenuated uniformly for wavelengths of 400-700 nm. Figure 1.4 shows the filter wheel setup.

⁶Filtered data was acquired for comparison with unfiltered data.

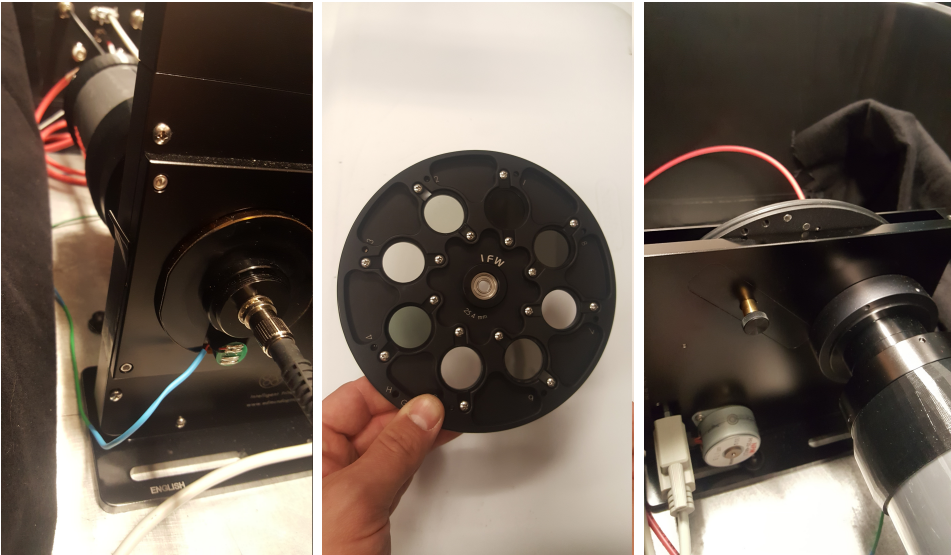


Figure 1.4: The left image shows a close-up of the electronic shutter connecting the fiber optic cable to the filter wheel apparatus. The blue wire is for remote control of the shutter. The middle picture shows the filter wheel with its 8 filters. It connects to the computer via an RS-232 connection. The right picture shows the top of the filter wheel exposed.

Electronics

The rest of the setup includes the oscilloscope, function generator (Figure 1.5), high voltage power supply (CAEN N470), and NIM/VME modules including the ADC (CAEN V965), a dual timer (CAEN N93B), an and/or logic module, and a NIM/TTL translator. See Figure 1.6 for electronics images.

Data Acquisition

The function generator is the source of the data collection cycle. The function generator is set to 3,000 Hz and is used to trigger the light source. Immediately, the light source sends a pulse of light into the fiber optic as well as an output trigger pulse. The output pulse is shaped in a gate generator in preparation for triggering the data acquisition system (DAQ).

In parallel with this stream of events, a 400 Hz signal is generated from the other channel of the function generator. This pulse is sent directly to the gate generator for pulse timing shaping. These pulses will trigger data acquisition but not the light source. This will



Figure 1.5: The pulse generator shown has two output channels with two copies of each channel. Each channel can have its own frequency, amplitude, phase, and duty cycle. Synchronization of the channels is used for pedestal injection.

guarantee at least 400 Hz of "pedestal" events. Pedestal events are recorded in the absence of light to quantify the noise floor and the zero of the ADC.

The 3,000 Hz pulse train triggering the light source is merged with the 400 Hz pulse train via an "or" operation in the logic unit. Channel synchronization and proper offset are necessary to avoid overlapping the 3,000 Hz pulses with the 400 Hz pulses. The output 3,400 Hz pulse train goes into the ADC to trigger data acquisition.

A charge-integrating ADC made by CAEN, model V965, was used to digitize the PMT output pulses. This 12-bit ADC has a high-sensitivity conversion factor of 25 femtoCoulombs (fC) per ADC channel as well as a high range, 200 fC scale. When the ADC receives a trigger pulse, it integrates the charge received on each of its 16 input channels and stores these values in a buffer as a number between 0 and 4095 ($2^{12} - 1$). After recording the charge from an event, the ADC puts an interrupt request on the backplane of the VME crate, signaling the readout controller (ROC) to collect the data.

The ROC is the brains of the VME crate, running a light-weight Linux operating system. Drivers exist on this computer for operating modules such as the V965 ADC. The pedestal mean and other characteristics of the digitized distribution can be tuned by modifying these drivers. The ROC is responsible for operating the ADC by initializing it for use and then

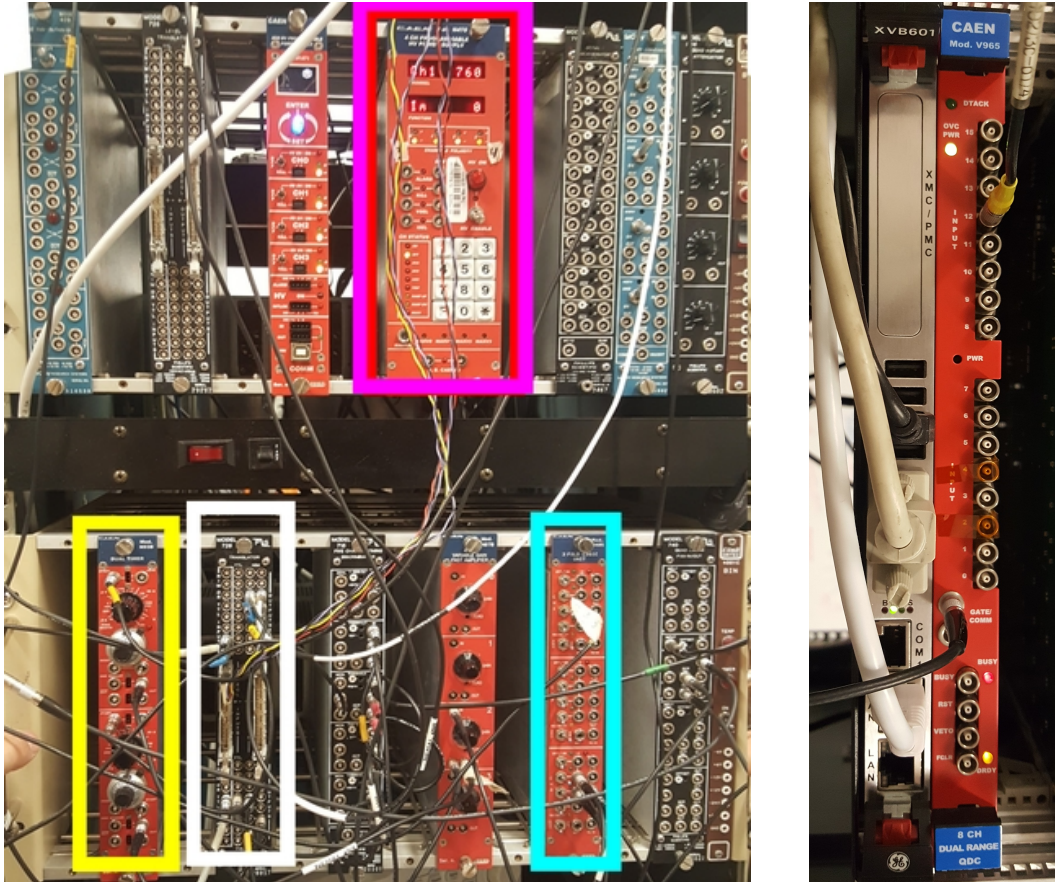


Figure 1.6: The left image is the NIM bin with the translator (white), power supply (magenta), logic unit (cyan), and dual timer (yellow). The right image is the VME crate with the readout controller (ROC) and CAEN ADC.

reading and writing to and from its buffers during data acquisition. This computer is not powerful enough to process the incoming data, however. The ROC very quickly passes the data on to a powerful modern desktop computer via ethernet.

Jefferson Lab has developed a software called CODA (CEBAF Online Data Acquisition system) to orchestrate the gathering and storing of data into binary data files. CODA runs on CentOS 7 on a powerful desktop computer.

To summarize, the CAEN ADC is plugged into the VME crate with the ROC and communicates with it via the backplane. The ROC grabs the data from the ADC buffers and sends it to CODA via ethernet to be put into the current data file.

Summary of Other Chapters

This thesis details multiple measurements with the ultimate goal of counting charged particles with high precision. Discussion of errors takes place throughout all chapters.

Chapter 2 is all about modeling the PMT. Some pro's and con's are given for common models. The Monte Carlo method is extremely powerful but computationally intensive and difficult to tune. Fitting distributions with mathematical functions is quick and easy, but at the expense of the model's accuracy. The model used for the high-precision gain measurement in this thesis is a convolution of a Poissonian distribution with a sum of Gaussians, each convoluted with a decaying exponential distribution. This fit is fairly detailed, but still uses a relatively low computation time.

Chapter 3 gives details of the high-precision gain measurement in low-light such as experimental run parameters, model constraints and inputs, and how all of these parameters were chosen. The model is only useful with appropriate data; the Poissonian distribution is characteristic of very low light. Even with good data, due to the model's complexity, good fit results can only be achieved with appropriate starting values and bounds for certain model parameters. Examples of bad fits and bad data are shown in this chapter as well as the use of MySQL to handle large data sets.

Chapter 4 uses the gain and data from Chapter 3 as well as some additional data to perform a calibration of the light levels for each PMT. Measuring the filter transparencies is necessary for obtaining low light fits to large light pulses. The light calibration process must be performed for each tube due to the differences in quantum efficiency. The quantum efficiency is a property of the photo-cathode; it gives the number of electrons ejected from the cathode per incident photon. Absolute calibration of the number of photons in each light pulse requires knowledge of the quantum efficiency whereas calibration of the number of liberated photo-electrons for each pulse does not.

Chapter 5 details the measurement of the gain of a PMT given a known light level. This

procedure is used to measure the PMT gains at low voltage where the size of the single photo-electron signal is imperceptibly small. Measuring PMT gain with a known light level is as easy as comparing the means of two well-separated Gaussian distributions⁷.

Chapter 6 is a full chapter that briefly describes the characterization of the quartz Cerenkov detectors used in this project. Multiple theses could be written on the contents of this chapter and almost certainly will be. The theory behind Cerenkov detectors is discussed in this chapter as well as analysis of electron beam data collected at Stanford Linear Accelerator Center (SLAC) and comparison to simulation.

Appendix A includes examples of the code used to perform the calculations in this thesis along with explanation.

Appendix B gives comprehensive gain measurement results for all 6 PMTs.

⁷The signal is not exactly Gaussian, but certainly simple and easy to fit.

Chapter 2

PMT Models

This chapter begins by reviewing the operation of a PMT followed by a discussion of the immense complexity and power of the Monte Carlo simulation. After that, the simple Gaussian model for a PMT response is described, and finally, the full low-light Poissonian model is defined in detail.

PMT Basics

The PMT is a very simple device that converts light waves into electronic signal, much like a microphone does for sound¹. The conversion mechanism is the photo-electric effect described by Einstein in his Nobel Prize winning paper. Just a single photon can elicit a signal from a PMT. Of course, the PMT could be struck by 5 or 10 photons and get a bigger signal. Figure 2.1 shows a PMT schematic for the discussions in this section.

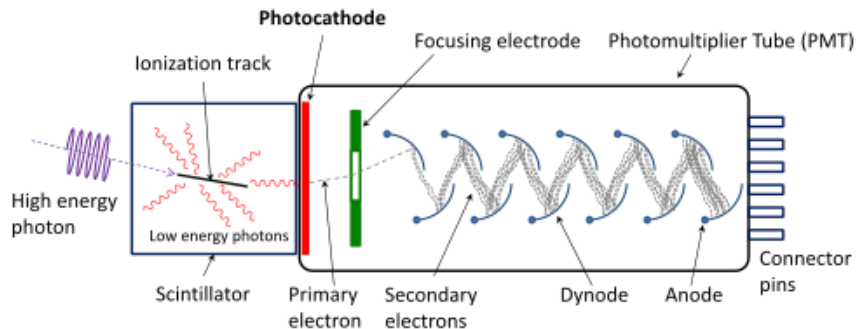


Figure 2.1: This is a schematic taken from [4]. This diagram helps to show the light creation, conversion, and amplification in the different stages of the PMT. Creation happens in a scintillator such as quartz, the light is converted at the photo-cathode, and amplified through the dynodes. The anode receives the final output signal.

¹Like a microphone, modern PMTs are quite complex for advanced signal shaping.

The photo-cathode

The photons strike a filament-like piece of metal called the photo-cathode, and electrons are ejected via the photoelectric effect. Due to the probabilistic nature of particle interactions and the large number of atoms in the cathode, each photon that strikes may or may not eject an electron. Quantum efficiency is the probability of photo-electron ejection for a given photon and a given wavelength.² This acts as a bit of a filter which helps give rise to the Poisson distribution. Many applications employ filters before the light reaches the photo-cathode to ensure a low light level; however, the photo-cathode can also handle thousands of photons at a time. The quantum efficiency of a typical PMT peaks at around 25% for the blue/visible part of the spectrum, as seen in Figure 2.2 later in this chapter.

Amplification

The tens or hundreds of PEs, or photo-electrons (electrons ejected from the photo-cathode), are too small for even the great electronics in most particle physics labs to detect; amplification is required to detect a single PE (photo-electron) in event-mode. Event-mode, where each event is quantized, is required for the method chosen in this thesis. To process every single event, the data collection rate must be low (in the thousands of Hertz) for the computer to keep up. The alternative to event-mode data collection is integration mode where events come in the millions per second. Very little, if any, amplification is needed for integration-mode data collection.

Between the cathode and anode are a series of dynode stages responsible for electron amplification. These stages are metal plates, each at a lower potential than the last. Electrons accelerate from one stage to the next, knocking out extra electrons with their recently gained kinetic energy upon impact. By the end of the cascade, one single ejected PE can result in around a million electrons reaching the anode. These million electrons will make a

²Actually, this is only true if a single electron is ejected for any given incoming photon. Double electron ejection is possible for certain cathodes and wavelengths.

measurable blip on sufficiently fancy electronics (≈ 5 ADC channels on the V965), and **this** factor of a million is the gain of the PMT.

Unfortunately, this "factor of a million" is actually different for each individual cascade. When the photo-electrons reach the first dynode stage, they will have some hundred eV of kinetic energy, but how many electrons will they knock loose from the metal? Can this be calculated exactly? Of course not, it is another probabilistic interaction like the photo-electric effect, but this is the electro-electric effect. This means that the gain of a PMT is not necessarily a well-defined quantity.

Gain Vs. High Voltage

The number of secondary electrons each incoming electron will eject from the next stage depends on its kinetic energy. The kinetic energy of the incoming electron is equal to the voltage drop over that stage. Because the number of secondaries is approximately proportional to incoming kinetic energy, the Gain Vs HV curve has the following trend:

$$G_n(V) = g \left(\frac{V}{n}\right)^n, \quad (2.1)$$

where G is the PMT gain, V is the voltage drop from cathode to anode, n is the number of dynode stages in the PMT, and g is some proportionality constant that has to do with the number of electrons knocked loose at each stage. This model assumes, however, that the voltage drop is equal at each stage. This is not true, especially for modified bases (voltage divider circuitry) for improved PMT response linearity. Something like

$$G_n(V) = g * \frac{4V}{14} * \frac{V}{14} * \frac{2V}{14} * \frac{V}{14} * \frac{V}{14} * \frac{V}{14} * \frac{V}{14} * \frac{2V}{14} * \frac{V}{14} \quad (2.2)$$

is more realistic for the Hamamatsu tubes (PMTs 1 - 4),

$$G = g * \frac{3V}{13} * \frac{V}{13} \quad (2.3)$$

for the ET Enterprises tube using divider A (PMT 5), and

$$G = g * \frac{3V}{21} * \frac{V}{21} * \frac{V}{21} * \frac{V}{21} * \frac{V}{21} * \frac{V}{21} * \frac{2V}{21} * \frac{3V}{21} * \frac{4V}{21} * \frac{3V}{21} \quad (2.4)$$

for the ET Enterprises tube with voltage divider B (PMT 6). Of course, each PMT may have its own value for g . This value can only be measured for a given tube after the gain of that tube had been measured at each high voltage value. These models won't help to measure the gain, but they should help to compare gain measurements obtained from other models.

The following sections describe the distribution of signal sizes seen at the PMT anode for a given high voltage and light level, as well as models that can be applied to these distributions to extract the gain. For discussion on methods to measure the gain without making assumptions of the shape of the PMT distribution, look at [**Model-Independent-Gain**].

Monte Carlo simulation

To really do a great job modeling the PMT, a simulation engine with kinematics, relativity, and quantum mechanics is required. This is very achievable via the very common Monte Carlo simulation technique. Many groups have used this method to model PMTs. For instance, [5] gives a walk-through on Monte Carlo code for PMT simulation. To perform a thorough Monte Carlo simulation, a performant GPU or two may be required. For instance, [**GPU-Boosted-Gain**] discusses how to utilize GPU's to fit using more realistic PMT models.

Simulating the PMT

Even when doing a Monte Carlo simulation, there are choices to make on what to model. The first step is to model the QE (quantum efficiency) of the photo-cathode by turning 8 incoming photons into, say 3 PEs. Normally, a constant quantum efficiency is assumed across

the entire cathode for a given wavelength. This would be represented in code as an array of floats describing some arbitrary function, perhaps 10 terms of a polynomial that represent the QE (quantum efficiency) vs. wavelength curve. If a measurement of the number of electrons coming off the cathode is made, and if the number of incident photons is known (over the range of wavelengths of interest), it is possible to calibrate this floating point array for any given cathode. Refer to Figure 2.2 to see the QE curves for the Hamamatsu and ET tubes used here.

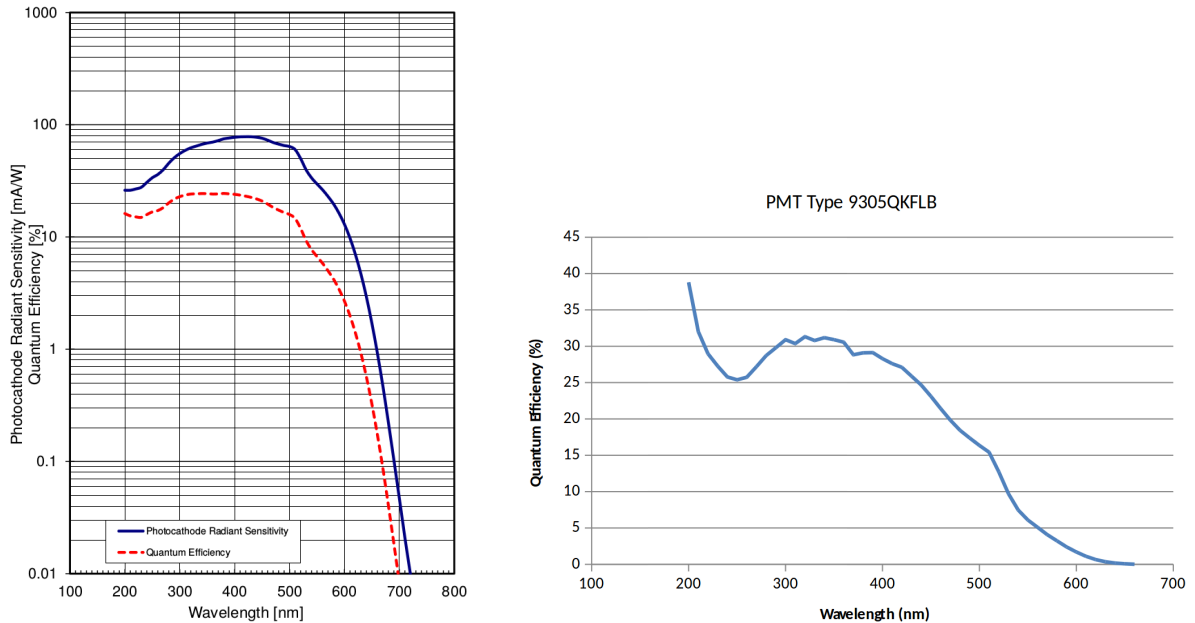


Figure 2.2: The left plot shows the quantum efficiency curve for the Hamamatsu tubes (red dashed line). The right image is for the ET tubes. Both of these plots were obtained from the companies by special request. These plots may differ from similar plots of the same model tubes that don't employ a quartz PMT window since regular glass attenuates UV light.

For some researchers, this model of the cathode is too simple for their purposes. In reality, photons that strike near the edge of the photo-cathode are less likely to eject an electron. These photons follow a "non-ideal" trajectory. This introduces a few more parameters to our model of QE for describing the distribution as a function of position. A few additional lines of code are needed to support position-dependent QE. Also, photons can and do pass through the photo-cathode. When they do, they are likely to hit the first dynode stage

and have some probability of producing a PE. Modeling this equates to modeling *another* quantum efficiency, now for the first dynode stage. Bi-alkali cathodes such as the ones used here are prone to having 2 PEs ejected from a single photon of certain wavelengths; simply add a single floating point probability to the code to model this effect. By now, the parameter tuning process is getting tricky since correlating the incoming photon position or trajectory to output signal size is incredibly difficult.

In the cathode, there are photons colliding with electrons; in the dynodes, electrons are hitting electrons. It is a very similar process, and it can be modeled in a very similar manner. Some sort of efficiency parameter for each stage just like the QE of the cathode is needed. Position dependence as well as incoming electron energy dependence probably impact the number of ejected electrons at each stage. Besides all that, the electric field through the dynode chain must be in the Monte Carlo model. This includes fluctuations in the electric field that may be specific to each model and device due to imperfections in design or wear-and-tear. These imperfections are important because electrons can and do miss the dynode stages sometimes. The biggest contributor to this effect is when a PE from the cathode misses the first dynode stage. This electron will produce a signal N times smaller than normal, where N is the number of electrons that would have been ejected from the first dynode stage. If an electron misses the *last* dynode stage, the total number of electrons at the anode goes from M to $M - N$ (where $M \gg N$); this is negligible compared to missing the first stage. The modified base circuits try to reduce the number of PEs missing the first dynode by increasing the voltage drop between the cathode and the first stage.

Using the Simulation For Calibration

Once the simulation code is written, and a parameter list for all the functions and probabilities of events is defined, simulation farming begins. Simulations must be run where 1 photon hits the cathode, 2 photons hit, 3 photons hit, etc., in different proportions to create a single distribution for a given light level and gain. One full distribution contains anywhere

from 10,000 to around 10^6 depending on the statistical error limit for the application. The first few distributions produced with a new Monte Carlo will likely be bad due to incorrect parameters. Some sort of multivariate analysis must be applied to change the parameters incrementally until the output distribution matches the real data. This process is called "benchmarking" the simulation. The more physical the model is (more aspects included), the harder this tuning process will be and the more likely convergence is on a false set of parameters, not representative of reality.

Once the simulation is benchmarked, the total number of electrons at the anode of the PMT after N incoming PEs will be "computable", at least the mean and standard deviation are computable. The number of anode electrons per cathode electron is the gain of the PMT. The model should produce correct results at all high voltage settings, unless there is some physical process that is not being accounted for.

Assuming a Distribution Shape

As discussed briefly in Chapter 1, knowledge of distribution shapes can be used to perform high-precision indirect measurements via fitting models to distributions. In the Monte Carlo method, no distribution shape is assumed. The simulation can produce distributions of different shapes, but the shape is determined by the mechanics that produce the events, not the other way around. To make an assumption of shape makes a model much less general, but also much more useful and practical if the assumption is a true one. One very common distribution shape in nature is the Gaussian. If a distribution truly is Gaussian in shape, the entire (normalized) distribution can be described by two parameters: mean, and variance. Recall the equation of a normalized Gaussian:

$$\frac{1}{\sqrt{2\pi}} e^{-(x-\mu)^2/2\sigma^2}$$

The Gaussian distribution will play a big role in the chosen PMT model.

Gaussian Models

In order to use a charge-integrating ADC to measure just about anything, the distribution observed by the ADC when the signal is present must be compared to that observed in the absence of signal (light, in this case). Like Einstein said, everything is relative. ADCs give a non-zero distribution even when the voltage across the dynode chain is zero. The distribution observed in the absence of light (with PMT voltage on) is called the "pedestal". The pedestal comes from the dark current that is always flowing from the PMT when the high voltage is on as well as the dark current of the ADC itself. For most ADCs and PMTs, the pedestal is Gaussian in shape. The mean and RMS of the pedestal must be measured for each data run in order to subtract it from the signal. These two parameters are therefore required in our model, and they will be referred to as Q_0 and σ_0 for the mean and RMS respectively. These parameters have units of ADC channels which equate to units of charge. The pedestal characteristic of the CAEN ADC used in this work is actually a triple Gaussian shape, so the χ^2 value seen in Figure 2.3 is quite high; this is discussed more in Section 3.4.

When the light is barely on and a single photo-electron is ejected, another Gaussian distribution is observed, but with a larger mean and RMS than the pedestal. The 1-PE distribution does not show up by itself as a lone spike, though. Instead, the distribution is some convolution of pedestal events, 1-PE events, and some 2-PE as well as others! This is because of the statistical processes that filtered the light down to this level; these events cannot be controlled individually. If the gain is high enough that the 1-PE mean is clear of the pedestal, a cut can be made to single out the 1-PE distribution. If the 1-PE peak is isolated, a simple Gaussian fit will produce the mean and RMS. These two parameters are also necessary for measuring the gain, and they will be referred to as Q_1 and σ_1 . The gain of a PMT is well-characterized by $Q_1 - Q_0/e$, where e is the electron charge. This value represents the number of electrons that reach the anode when one PE leaves the photo-cathode.

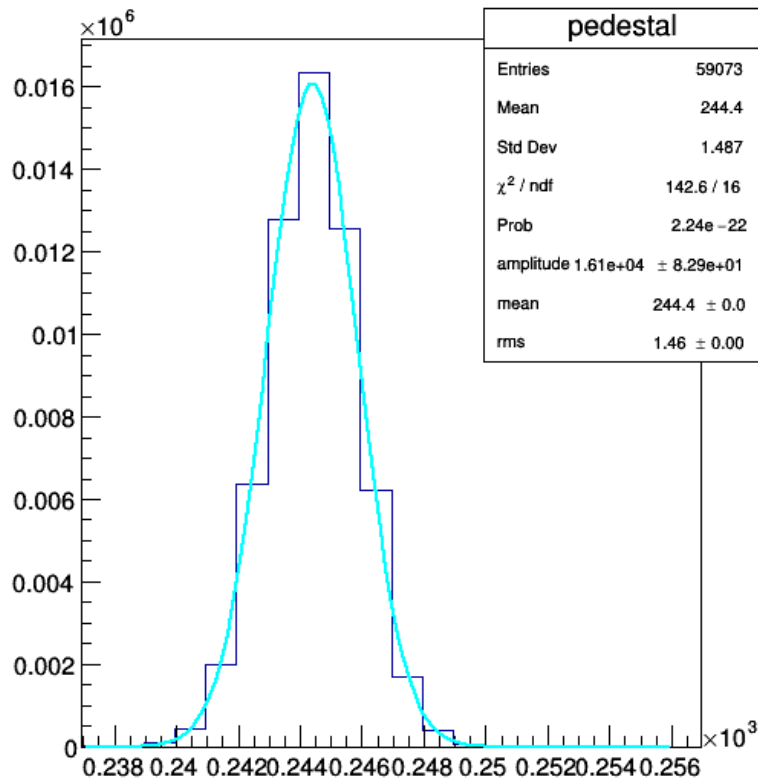


Figure 2.3: This histogram of over 100,000 events was all taken in complete darkness; this Gaussian represents the zero of the data at 2,000 volts for PMT 1, ADC channel 12.

Beyond the Gaussian Model

One problem with trying to single out a PE peak from the PMT is that the 0-PE and 2-PE distributions overlap with the 1-PE distribution. Simply trying to cut them apart is usually impractical as well as inefficient. Cutting apart the distributions would be followed by finding $2N$ parameters describing means and RMSs, where N is the number of peaks taken into consideration. This is not necessary because the means of each peak are correlated, as are the RMSs. Not only that, there is information about the light level found in the relative amplitudes of the Gaussian peaks. So far, the amplitudes have been completely ignored thanks to normalization; to consider them would add another N parameters. Again, all these parameters are correlated and can be characterized by a single parameter, μ . This

μ characterizes the Poisson distribution referenced repeatedly so far in the thesis. The frequency of 1-PE events is related to the frequency of 2-PE events, 3-PE events, and 0-PE events. For low light, many 0-PE events are observed and no 50-PE events, whereas at high light, many 50-PE and 51-PE events may be present, but very infrequently 1-PE or 2-PE events. μ represents the average number of photo-electrons ejected per pulse for a given light level. The Poissonian distribution observed in the PMT spectrum at low light is given in Equation 2.5.

$$P_n(\mu) = \frac{\mu^n e^{-\mu}}{n} \quad (2.5)$$

These 5 parameters ($Q_0, \sigma_0, Q_1, \sigma_1, \mu$) model the PMT spectrum pretty well, but there will almost certainly be unpredicted artifacts in the spectrum, e.g. small bumps or trends that are not present in the model. All the same phenomena that were present when building the Monte Carlo simulation (double PE ejection, PE ejection from first dynode, PE misses first dynode, etc.) are still unaccounted for in this model. From this list, the type of event impacting the PMT output the most is a photo-electron missing the first dynode stage due to poor trajectory.

There is an old NIM publication that describes a method of accounting for this process [6]. The paper suggests that signals resulting from under-amplified processes form an exponential distribution starting at the mean of each Gaussian and decaying to infinity from there. The decaying exponential distribution is convoluted with the Gaussian pedestal and each PE peak³. The decaying exponential is of course characterized by a decay constant, α , as well as the associated probability, W_α , that a given signal is the result of an under-amplified process. These parameters are used and studied in this analysis, though the correct values for α and W_α are unknown and not discussed [6].

The NIM publication details the 7-parameter fit described so far in this section. Look

³It is unclear if the pedestal should have the same exponential distribution as the signal peaks, but it is assumed so.

there to see the full functional form of the PMT model. To recap, there are the pedestal parameters Q_0 and σ_0 , the 1-PE parameters Q_1 and σ_1 , the Poissonian parameter μ , and the discrete background parameters W_α and α . The full PMT distribution is a sum of the pedestal distribution with the 1-PE, 2-PE, 3-PE, etc. Gaussian distributions, all of which are individually convoluted with the exponential signal and collectively convoluted with the Poisson distribution.

These 7 parameters almost entirely represent the fitting algorithm used to analyze the data in Chapter 3. There are two parameters not yet mentioned called W_{ped} and W_{real} , both of which should be between 0 and 1. W_{ped} represents the fraction of the data that is injected pedestal events; these events are inserted to ensure a good measurement of Q_0 and σ_0 . These events change the relative height of the pedestal peak which would disrupt the Poissonian model if not otherwise accounted for. The other parameter, W_{real} represents the proportion of data corresponding to the Poissonian process. This parameter is almost perfectly correlated with W_{ped} (the expression $W_{real} = 1 - W_{ped}$ is expected to be true). Most of the time, both of these parameters are constrained because their values are effectively known.

This concludes the description of the fitting algorithm used to acquire a high-precision fit result at low-light. For the rest of this chapter, some example fit results are shown in different voltage and light level regimes, and some strengths and weaknesses of the model are pointed out.

Implementing the Model Using Root

Having the mathematics down on paper is a great achievement, but the paper will not compute fit results for data runs. Computing them by hand is far from practical. Thinking about how to go about this process, however, is instructive.

To fit a data file to the model means to take a function defined by the seven parameters described earlier, overlay the curve on a distribution of data points, and adjust the seven

values one at a time until the shape of the function passes through the points. This is certainly a good exercise, and common; everyone has done this sort of thing while learning arithmetic, algebra and calculus. For a single parameter, the problem is as easy as starting with a value too low to be correct and watching the shape change as the single parameter value is increased. χ^2 is a number that can be calculated given a set of data points and a function or model (a set of continuous "true" points) that gives some measure of how well the given model describes the given data. χ^2 is calculated as the sum of squared deviations of data point locations from the model value at the corresponding location. The number of degrees of freedom for a set of data and a model is equal to the number of data points minus the number of parameters in the fit. χ^2 per n.d.f. will decrease until the optimal value for the parameter is reached. Scaling by the number of degrees of freedom allows comparison of χ^2 values between fits with different numbers of data points. A model that truly describes the given data should have χ^2 per n.d.f. nearly equal to 1. Table 2.1 gives an example of tuning a single parameter to find the best fit. The χ^2 value must be computed for every choice of value. An input of 7 is identified in the table as the best value, and now a more refined value search should be performed between 6 and 8. This will likely be followed by a more refined sub-search.

Param value	1	2	3	4	5	6	7	8	9
$\frac{\chi^2}{\text{n.d.f.}}$	978.2	478.5	234.3	89.2	23.7	8.23	3.89	18.4	39.6

Table 2.1: Example reduced χ^2 value for each parameter in a typical fit.

For two parameters, the difficulty of the problem is much more than doubled. Only one parameter can be changed at a time for correlations to be untangled, and this means that the other parameter values must be held constant. If the problem at hand is to fit a normalized Gaussian to a distribution, then the process may look like what is seen in Table 2.2. The χ^2 value in this example must be computed for each pair of values in a 2D scan. A single scan here requires 35 computations. A fine scan must be performed based off the results in this table.

Mean	RMS						
	1.0	2.0	3.0	4.0	5.0	6.0	7.0
972	inf	inf	inf	inf	inf	997.2	inf
973	inf	inf	inf	inf	923.7	808.3	838.9
974	inf	inf	934.3	839.2	732.7	511.3	551.9
975	898.4	658.6	446.4	429.2	378.4	358.23	359.9
976	683.3	474.2	234.8	92.7	32.7	18.3	27.4

Table 2.2: Example reduced χ^2 value for each parameter in a typical fit for two input parameters.

For seven or more parameters, the problem is intractable by humans with their slow mathematical pace. Root C++ Interpreter is a fantastic framework capable of compiling and running C++ meaning that the algorithm will be fast and powerful. Libraries are included in this framework for handling data histograms, reading and writing files, and statistical analysis. Root performs the deep, computationally intense task of iterative scanning of the 7-dimensional parameter-space as well as estimating the correlations and errors of the returned values.

Example Fit Results

Here are some examples of the Root fit of the model to some PMT data. Because of the huge parameter space, a plethora of different types of fit results are seen for the data. Knowledge of the experimental setup must be used to choose which fits most likely represent reality (χ^2 can be low for false fit results).

Figure 2.4 show very low, but increasing light levels. The distance between the pedestal and 1-PE mean is proportional to the gain, and it is the same distance observed between each pair of neighboring PE peaks; that is to say that the red and cyan peaks are all regularly spaced with distance Q_1 . When the light level increases, more 2-PE and 3-PE events are seen, but fewer 0-PE and 1-PE events.

Figure 2.5 shows a couple higher light levels, but still very dim. Notice how all the fits

choose different values for the parameters W_α , α , μ , and Q_1 and well as the Gaussian widths. all fits with parameters near reasonable values are considered "good" gain measurements. Good fits should also seem to converge around the same values and consistently produce low chi-squared and statistical error. Already at this light level, there is too much noise induced from the light, and the model begins to fail. Notice how the 0-PE peak is artificially large as the signal moves to the right; this is from injected pedestal events.

If the light level is low enough and the gain high enough, the PMT model might work on high light data as well, but as the light level becomes distant from the pedestal, Root can no longer reliably deconvolute the peaks and requires light level constraints to converge to believable values. Figure 2.6 shows some attempts at fitting a high light level using knowledge of the setup and fit constraints. The model doesn't work well when the light level leaves the single PE regime, but can be forced to produce results. These fits are forced to have light levels of around $\mu = 363$ PEs per flash.

Taking high-light data is necessary when the gain is too low to separate the individual PE peaks. In this regime, the analysis becomes incredibly simple. The entire PMT distribution approaches a Gaussian shape, and the mean and variance of the peak are dictated by that of the 1-PE distribution and light level distribution. Actually, perhaps due to the modified base circuitry present in this experiment, the distribution doesn't approach a perfect Gaussian, but rather has a decaying exponential tail. Taking this into account in the simple model is enough to extract the mean and RMS from the high light signal with low error. After subtracting the pedestal away, some large amount of charge, Q_{high} , remains. This charge is the 1-PE charge times the light level:

$$Q_{high} = \mu * Q_1 \quad (2.6)$$

and RMS [6]:

$$S_{high} = \sqrt{\mu * (\sigma_1^2 + \sigma_0^2)} \quad (2.7)$$

This is why the light level must be calibrated for low-gain measurements; μ is needed to calculate Q_1 . Figure 2.7 shows an example of this simple analysis.

The simple model used here at high light is a Gaussian peak convoluted with a decaying exponential from the Gaussian mean to infinity. The decay parameter is shown in the stats box as λ . This parameter is assumed to be related to, or perhaps equivalent to, the exponential decay parameter, α from the Poisson model. The shape of the distribution could come from the CAEN ADC used to collect the data, the modified base circuitry for improved gain linearity could shift the distribution in this way, or the PMT itself could have this characteristic decay from the under-amplified processes talked about earlier. Either way, this model appears to return the Gaussian mean and RMS that are needed for gain measurement.

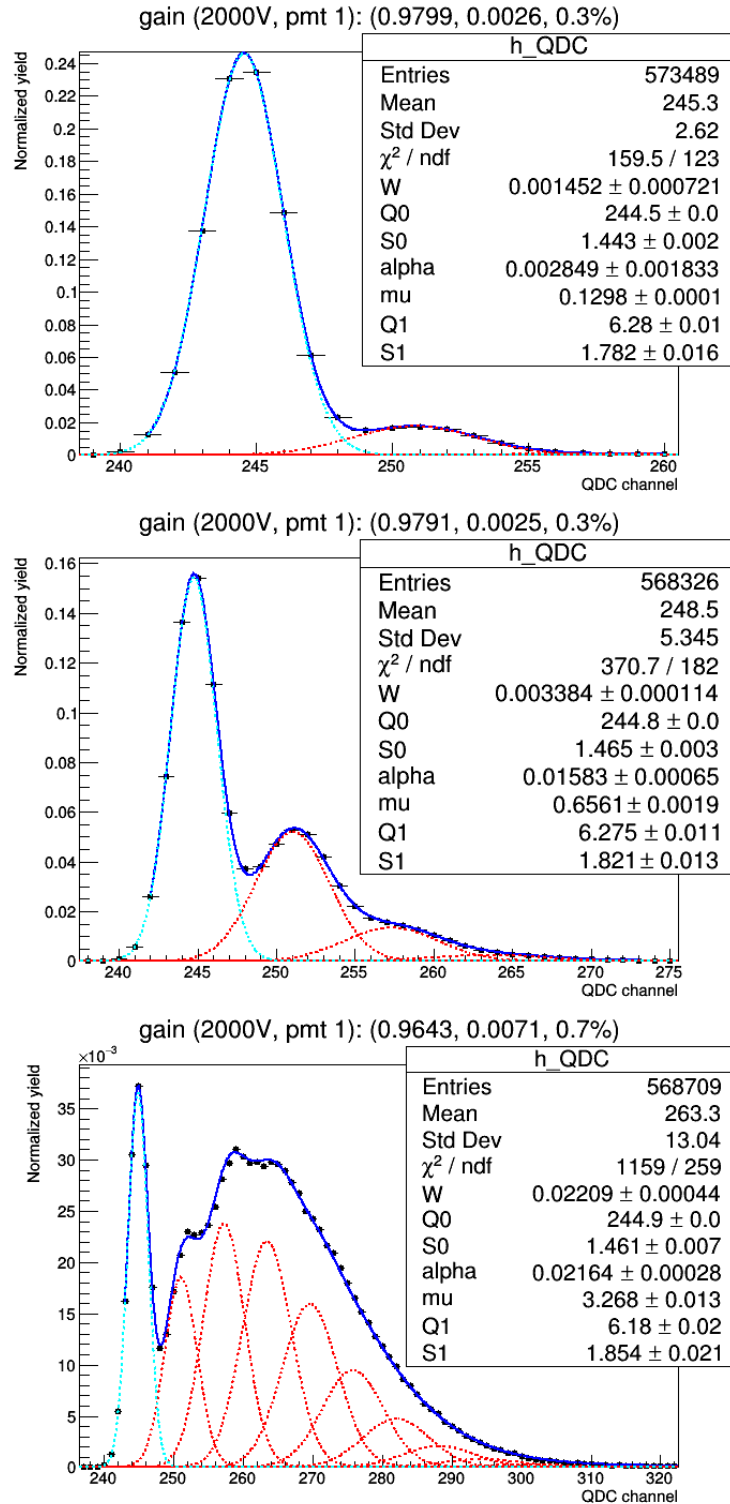


Figure 2.4: Very low light, high voltage data fits, the three runs increase in light level from top to bottom. The cyan line is pedestal, the red lines are PE peaks, and the blue line is overall best fit. As the light level changes, μ changes along with the overall distribution shape. The distance between the bumps (Q_1), however, should stay fixed.

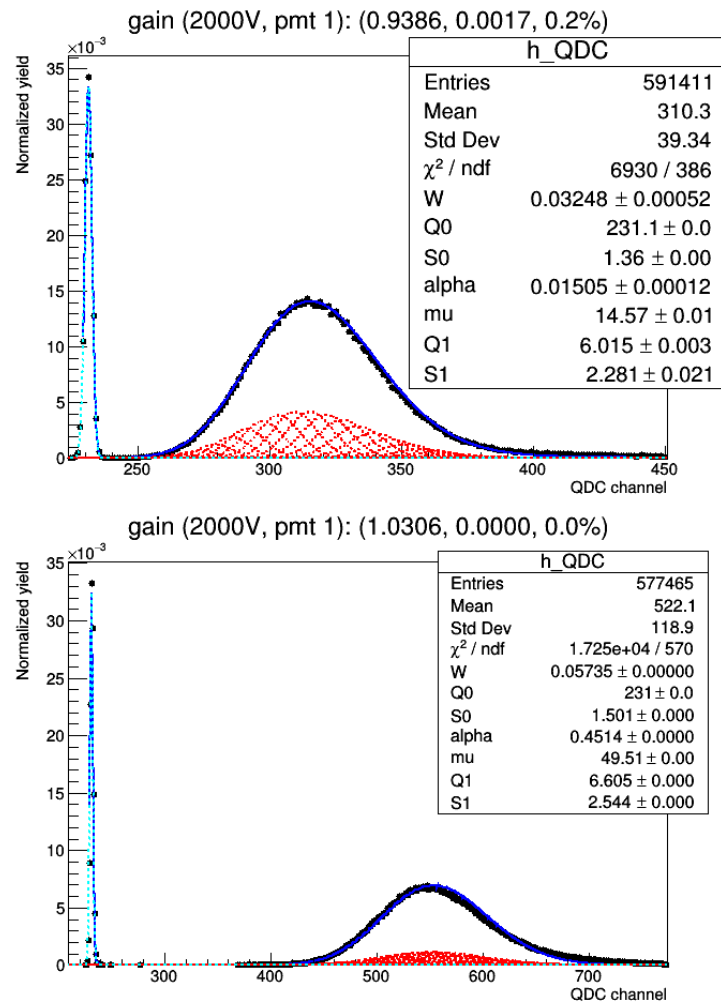


Figure 2.5: The first image shows light level $\mu = 15$. The second image shows light level $\mu = 50$.

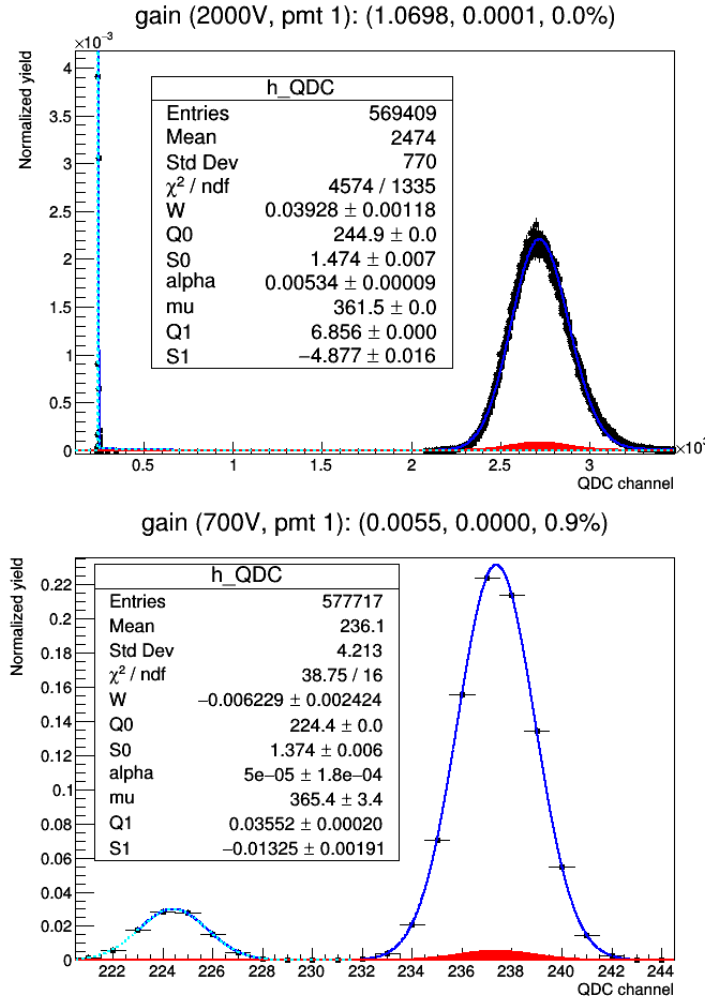


Figure 2.6: High light ($\mu = 360$) using full 7-parameter PMT model on data. Two images are shown. The first image shows the PMT distribution at 2,000 volts, the second shows the distribution at 700 volts.

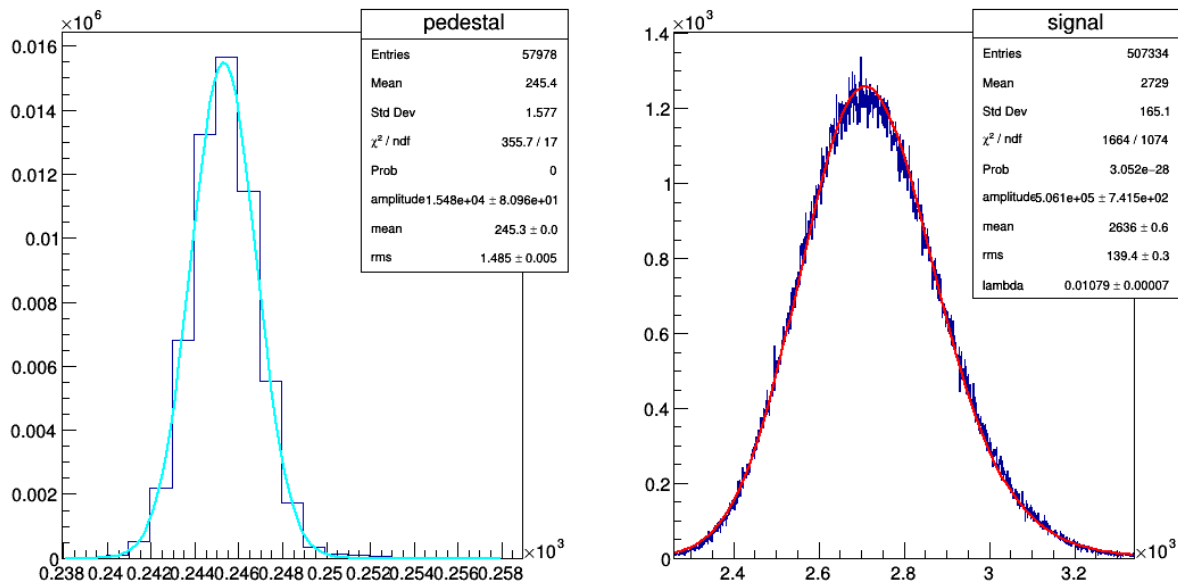


Figure 2.7: This image shows the same PMT distribution, taken at 2,000 volts, as in Figure 2.6. The whole distribution is shown in the left panel (the pedestal is a sharp peak to the left), the pedestal is fit with a simple Gaussian in the center panel, and the pedestal-corrected signal is fit with a Gaussian + Exponential in the right panel. The exponential decay parameter is listed as λ in the stats box.

Chapter 3

Precise Low-Light Gain Measurement at High Voltages

Now that the model is defined, it is time to gather and analyze data. This chapter gives details about how to collect great low-light data. Fit results will be shown to demonstrate data during the first few sections, though details of how to produce the fits aren't discussed until later in the chapter.

Much data was collected to explore the dependence of the gain measurement on experimental parameters, and many fits were produced in an effort to understand the dependence of the gain measurement and error on inputs to the fit. Results pertaining to dependence on number of events, light level, filter setting, etc. are included to justify the choice of model inputs and run parameters.

Turning on the PMT

After building the dark box, assembling the optical beam line, and routing all cables through the box, the PMT is inserted into its holder, and the entire assembly is wrapped in a black cloth just to ensure that there are no light leaks¹. Besides the DAQ, all the other components outside the dark box are plug-and-play. The filter wheel, shutter, and light source are all remotely controllable.

The function generator triggers the light source as well as the ADC for data acquisition. Too big a signal² could damage the digitizer, so it is important to verify the size of the PMT signal on the oscilloscope before taking data with the ADC. To verify that the ADC will not receive signals that are too big, a driver signal must come out of the function generator and go into the CAEN LED driver (which is set to external triggering). If after many pulses, there are no signals with too large of amplitude, then it is safe to take data.

¹Before wrapping up the PMT, verify that the filter wheel is operational and set to the most transparent filter, and that the shutter is open.

²Any signal with greater than a few positive millivolts could break the ADC channel it is plugged into; only negative signals are allowed.

In order to acquire the signals seen on the oscilloscope, a copy of the driver signal is taken out of the CAEN LED driver and sent to a gate generator for proper shaping and timing. The CAEN LED driver may not send a pulse that is suitable for the ADC to accept as a gate; the ADC expects a square pulse less than -1 volt deep and with a given duration. The duration of the gate pulse tells the ADC how long to integrate the incoming signal. At least 30ns is required and at most around 200 ns.³ This gate pulse, along with the output PMT signal can both go into the oscilloscope to tune their relative timing. The signal must arrive at the ADC at least 15 ns after the beginning of the gate pulse in order to be acquired. The gate pulse is shown in Figure 3.1.

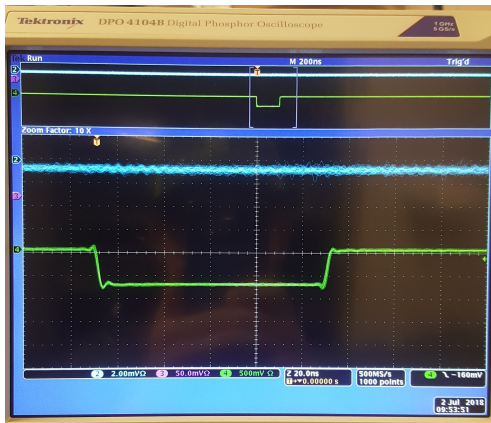


Figure 3.1: The gate signal shown on the green line here is 100 ns long and about -750 mV deep. This will trigger the CAEN ADC to capture the signal on the wire within the gate time window. The blue line shows no signal coming from the PMT which corresponds to a zero light level.

At this point, the PMT can be turned up to its maximum voltage, watching the signal on the oscilloscope for any surprising signals such as light leaks or light source malfunctions. Once the PMT is at the maximum voltage, the light source dial can be slowly turned up. The scale on the light source shown in Figure 1.3 ranges from 0,00 to 10,00 (referred to as light levels 0 to 100); the dial must be set above 2,00 (light level 20) with the current setup for a measurable amount of light to hit the PMT. At the lowest light levels, an empty gate is often observed on the scope, and once in a while a little bump from a single photon. A

³Too long a gate pulse will increase the likelihood of noise pulses being integrated with the signal.

low light level is shown in Figure 3.2.

Note the position of the PMT signal inside the gate. The CAEN ADC will not capture any signals falling within the first 15 ns of the beginning of the gate. Most of the data was taken with a 100 ns gate where the signal falls around 30 ns after the beginning of the gate; this ensures that any slow light pulses from reflections are included in the ADC integration.



Figure 3.2: The scope signal seen here on the blue line falls inside the gate (thanks to proper delay-cable lengths) and has a duration of around 4 ns. The size of these signals is ≈ 1 mV, incredibly hard to see. This was using the lowest gain tube (Gain < 700,000 @ 2,000 V for PMT 4). This light level is produced by about a 3.00 on the light dial (light level 30).

When the light is turned up, fewer and fewer pedestal events are seen, and more and more of these 1 mV events are seen. Some 2 mV events and 3 mV events start to show up as well as the light gets brighter. If the RMS of the gain was zero, the scope alone would offer a gain measurement based on pulse heights because each pulse would either be 1 mV or 2 mV or 3 mV, etc. In reality, all the 1-, 2-, and 3-PE events blur together on the screen as seen in Figure 3.3 because sometimes 1-PE will be 1 mV, sometimes 0.9 mV, sometimes 1.5 mV, etc.⁴ At least hints of the discrete event sizes can be seen at this small gain. This indicates that the ADC could contain measurable results.

⁴It is actually the area of each pulse that is proportional to signal size (amount of charge in the pulse is $Q=V*t$), but looking at the height of the pulse is easier on the oscilloscope.

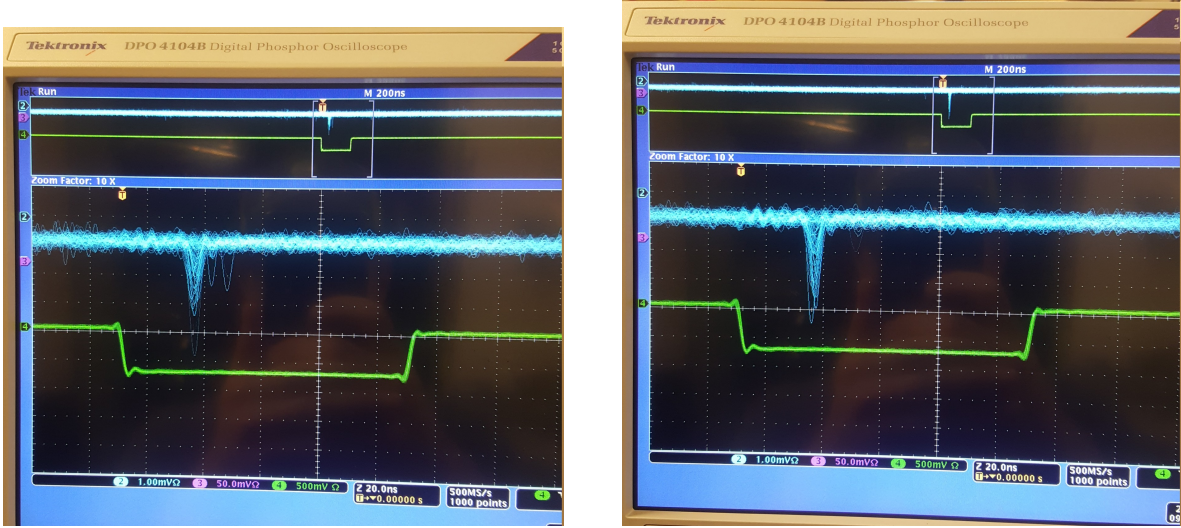


Figure 3.3: The signals seen in these images come from the same PMT. In the left plot, many pedestal events are visible, some single PE events, and a few 2-PE events (light level 40). The right image shows multiple 3-PE events (light level 50). In these plots, some stray signals can be seen 5-10 ns later than the rest; these are reflected photons with modified light level, introducing noise.

Data Acquisition

The light levels seen on the scope are examples of single-PE events. The distribution of these events for a given light level are needed to use the model from Chapter 2. This light level is sampled thousands of times, and the resulting distribution is described by a series of Gaussians scaled by a Poisson distribution. Some fit results are shown below to demonstrate the data in this regime. Exactly how to produce these fits will be discussed in Section 3.4.

Taking Good Data With PMT 1

All of the runs in this section were taken with 3,000 Hz data rate, 400 Hz pedestal injection rate, at least 500,000 flashes of the light (events), and no filter. Almost all of the data taken for this measurement was on ADC channel 12. This channel will always be used unless otherwise specified. Some results from PMT 1 (a Hamamatsu tube) are shown below. Table 3.1 gives the run parameters as well as some fit results for ten data runs, five at 2,000 volts, five at 1,900 volts. These runs are shown in Figures 3.4 and 3.5. Recall μ is the average

number of pes per event (Poisson mean); μ is seen increasing in the table.

Light Level	Run	Voltage (-V)	χ^2 per NDF	Gain	μ
20	2647 / 2206	2000 / 1900	0.754 / 1.415	969,200 / 820,300	0.0264 / 0.0228
30	2193 / 2671	2000 / 1900	0.864 / 0.717	970,800 / 792,300	0.1284 / 0.1254
35	2194 / 2205	2000 / 1900	1.793 / 1.228	968,900 / 789,900	0.2833 / 0.2826
40	2195 / 2207	2000 / 1900	2.031 / 1.925	971,800 / 790,800	0.6355 / 0.6335
45	2196 / 2208	2000 / 1900	3.269 / 3.561	969,600 / 785,800	1.417 / 1.411
Average:				970,000 / 795,800	
Std. Dev:				1,200 / 12,400	

Table 3.1: Here are two sets of gain measurements for PMT 1. The values on the left/right are -2,000 V/-1,900 V data.

These runs are all great fits with low error and similar measurements. The values for μ should be the same for the same tube and light level at different voltages. It is reassuring to see the fit producing very similar μ values for the same light level settings and the same photo-cathode. It looks like anywhere from 0.01 to around 2.0 are good values for μ in this measurement because these values produce consistent results with low χ^2 . Figuring out exactly which light level produces the best fits takes many data runs and is investigated later in this chapter. All of these light levels are acceptable since they all produce similar gain measurements and low error.

The fact that the fitting algorithm produces very similar gain measurements for a variety of low light levels indicates that the model is accurate and produces high-precision results, at least within this regime. For high gain with PMT 1, all the measurement results are falling within around 0.2% of one another. For a lower gain, there is a larger spread. Already at a gain of 800,000, the spread is around 2%, an order of magnitude higher. This method won't give low-error results for gains much lower than 10^5 because the Gaussian peaks begin to fall into the same ADC bin.⁵

The 1,900 volt data doesn't look quite as good as the 2,000 volt data because all the signals are overlapping with each other more; they are squeezed into the pedestal. The effect of this is larger χ^2 values and gain deviation as seen in Table 3.1. This data is still pretty

⁵With higher resolution in the ADC, lower gains can be characterized.

good, however, with a gain of around 800,000. This is higher than the maximum gain of PMT 4 (around 650,000).

Taking Good Data with PMTs 4 and 5

Next, compare the same data taken at 2,000 volts for PMT 4 (refer to Table 3.2 and Figure 3.6). The maximum gain of this tube is quite low but still measurable ($\approx 600,000$). The deviation in the fit results is getting larger, over 3% now, larger than the error predicted by Root (1.5%). It is interesting how close the quantum efficiency seems to be for PMTs 1 and 4⁶.

Light Level	Run	Voltage	χ^2 per NDF	Gain	μ
20	2835	2000	0.782	594,000	0.0207
30	2836	2000	0.468	560,100	0.1194
40	2837	2000	1.284	550,500	0.6181
Average:			568,200		
Std. Dev:			18,700		

Table 3.2: Run parameters and some fit results of good data taken at the maximum high voltage for PMT 4.

Finally, here is some data from PMT 5, one of the ET tubes, at its maximum voltage of 1,350 volts. This tube has a very high gain which makes the measurement quite easy. Refer to Table 3.3 and Figure 3.7. The spread in the fit results is about 1% here. There is a different light level measured for this tube. This could be a difference in QE, collection area, and/or window size. Assuming the same number of photons are hitting this cathode as with the Hamamatsu tubes, this PMT has a QE twice that of PMTs 1 and 4.

The values for α and W_α are highly variable and sometimes unreasonable. The real values of these parameters are largely unknown, but don't seem to matter very much in very low-light fits. This is discussed more later in the chapter.

⁶The same QE and the same PMT model should produce the same μ values, and those are seen here.

Light Level	Run	Voltage	χ^2 per NDF	Gain	μ
20	3191	1350	2.660	2,219,200	0.0544
30	3192	1350	2.939	2,215,200	0.2773
40	3193	1350	1.954	2,265,300	1.377
Average:			2,233,200		
Std. Dev:			22,700		

Table 3.3: Run parameters and some fit results of good data taken at the maximum high voltage for PMT 5.

Taking Bad Data

Over a thousand data runs were collected with these six PMTs over the last few years, with accompanying analyses being performed in an attempt to understand the PMT spectrum. The fitting algorithm doesn't always produce good results, and sometimes it won't produce any results at all. At times like this, it is hard to know if the data is bad or if the model parameters are bad, or if the model doesn't apply to this situation. This section summarizes investigations into the various experimental parameters that affect the gain measurement.

Gain is Too Low

When measuring the gain of a PMT over its entire voltage range, some gains will necessarily be too low for the Poisson model to reliably work. The results of a voltage scan for PMT 1, taken at light level 40, are shown in Figure 3.8. Table 3.4 gives the run parameters and some results for the data.

Voltage	Run	χ^2 per NDF	Gain	% Error	μ
1900	2207	1.925	790,800	0.3	0.6335
1800	2219	2.205	624,100	0.7	0.6575
1700	2231	1.756	492,300	1.5	0.6414
1600	2243	1.786	385,500	4.8	0.5991
1500	2255	1.720	289,700	20.5	0.6028
1400	2267	0.992	193,400	15.5	0.635
1300	2279	2.074	148,700	5.5	0.5558

Table 3.4: Run parameters and some fit results for PMT 1 voltage scan at light level 40. The percent error shown is calculated by Root during the fit. All the light levels (μ) should be the same value.

These fits all look great again, but they are artificially good, to some degree. If Root is asked to check too large a range on too many parameters, it will likely find a local minimum somewhere in the parameter-space that is not the global minimum and therefore not the best result. Because of this, bounds are placed on the parameters to force Root to search a small space with finer precision. If the correct results are within the interval, the fitter will likely find the best fit parameter values, but it is up to the researcher to make an educated guess as to how to bound the algorithm. This educated guess is usually based on results from fits to data in regimes where the Gaussians are clearly distinguishable; trends are identified and assumed to continue into lower and lower voltages.

Even with appropriate bounds on the parameters, once all the Gaussian peaks have become very close together on the x-axis due to low gain, it becomes very difficult to tell how the Poisson distributions and the Gaussians each individually contribute to the overall mean of the data. This is because increasing the gain parameter has the same effect as decreasing the light level parameter on the shape of the fitting function. In this regime, the fitter has to choose between many different pairs of values for gain and light level which produce very similar χ^2 values. With low enough gain, Root will simply be selecting a pair of random values from within the chosen intervals (either high gain and low light level or vice versa).

Table 3.5 gives the results of light level scans for each of the voltages shown in the previous figures (1,900 - 1,300 volts) for PMT 1. The table lists the average gain measurement, standard deviation of measurements, and the ratio of the two values (RMS / Mean).

Light Level is Too High

Turning up the light level raises a very interesting question: does the low-light model work at high light? If the light level is unknown, the fitting algorithm will not be able to extract the gain or the light level for light levels above $\mu \approx 5$. When $0 < \mu < 2$, great fits are achieved that extract gain and light level information, assuming the gain is high enough.

Voltage	# of fits	Average Gain	Std. Dev.	% Deviation
2000	5	967,524	5,571	0.58
1900	5	784,093	11,597	1.48
1800	3	627,328	6,527	1.99
1700	5	489,112	2,267	0.46
1600	5	390,171	10,636	2.73
1500	2	318,867	7,620	2.39
1400	3	223,972	4,034	1.80
1300	3	145,880	15,867	10.88
1200	1	103,236	N/A	N/A

Table 3.5: Average gain, std. dev., and relative error for a range of low light levels and voltages for PMT 1. The number of fits considered is given. Below 1,600 volts, it becomes very difficult to obtain any believable fits at all. When fits are achieved, they are often very variable.

The fit results become inconsistent quickly as the light level goes up. Higher light level peaks inherently have more noise, as can be seen by Equation 2.7. More photo-electrons ejected from the cathode means a larger number of electrons in the amplification cascade and consequently more variation in the number of electrons seen at the anode. Besides this, the Poisson distribution becomes Gaussian for large means.

In order to get any reasonable fits, it is necessary to force the fit to converge on a known, measured light level. This is because all the different Gaussian signals are piling up together again, but this time far away from the pedestal. Like with low-gain, when the signals pile up, turning up the light level parameter gives very similar results to turning down gain. It is therefore important to put tight bounds on either the light level parameter or the gain parameter. Calibrating the light level is discussed in Chapter 4, but for now, the light levels used will be assumed correct. For some fits, the upper bound allowed for the light level parameter is 10% higher or lower than the best-guess value; for other fits, only a 1% variation is allowed by the parameter bounds chosen. Either way, the model is highly dependent on best-guess inputs for high light levels. Figure 3.9 and Table 3.6 show a series of high-gain fits with increasing light levels.

The number of photons increases exponentially as the light level increases by units of

Light level	Gain	μ	χ^2	% Gain Error (estimated by Root)
30	970,500	0.1279	2.866	0.5
35	969,000	0.2836	4.853	0.5
40	972,300	0.6363	3.378	0.3
45	971,600	1.421	3.873	0.4
50	969,700	3.149	3.026	0.6
60	936,900	14.57	12.189	0.2
70	983,700	51.72	17.376	0.5
Ave	967,700			
RMS	13,400			

Table 3.6: Increasing light levels for PMT 1 @ 2,000 volts. The gain is more variable at higher light levels. The measured light level, μ , is also included here; recall μ is the average number of PEs per event.

10; this means that the minimum light level (0) should be on the order of 10^{-3} , and the maximum light level (100) on the order of 10^3 . This is a very large range, and it would be highly beneficial to understand and model this entire range with high precision. There is more information present in the low-light spectrum. Changing the gain and light level parameters do NOT produce the same effect on the shape of the fitting function in this regime; therefore, Root can correctly disentangle these two parameters. This information results in low fit error. The results from low-light measurements are used to bound the high-light measurements, and the error must be propagated accordingly.

Statistics are Too Low

The time it takes to record enough data for a PMT to completely characterize its gain depends on the data collection frequency and the required statistics. CODA run control program acted as a bottleneck for the data rate. The readout controller takes 6 μs to query the ADC for its events, and then takes another 150 μs or more to send this information to CODA. At 3,000 Hz, it takes around three minutes to gather a distribution containing 500,000 events for a single voltage and light level setting. Depending on how many voltages and light levels are in question, it should take anywhere from an hour to a day to characterize the gain of a PMT.

The requirement on statistics usually comes from error considerations; sufficient events must be recorded such that the statistical error is negligible compared to other error sources. Over 100,000 events offers around 1% statistical error; most of the data used in this analysis contains at least 500,000 events. The model needs sufficient detail in the distribution (e.g. sharp curves in the data points) to rule out different parameter values. Table 3.7 and Figure 3.10 show plots of five different levels of statistical precision. The runs increase in number of events, but show consistent gain and light level measurements. 1,000 events is too few, resulting in high fit error. 10,000,000 events gives a high χ^2 due to the unaccounted for artifact right of the signal and/or drift in pedestal values or light intensity of LED over time.

# of events	Gain	μ	χ^2	% Error from fit
1,000	1,022,800	0.1597	1.088	5.6
10,000	1,060,700	0.2037	0.637	1.3
100,000	1,026,600	0.1875	0.643	0.5
1,000,000	1,033,000	0.1873	7.364	0.4
10,000,000	1,020,400	0.1854	67.29	0.4
Ave	1,032,700			
RMS	14,600			

Table 3.7: Gain results for PMT 1 using light level 50 with filter 8 and various number of events.

One big problem using this model on the current PMTs is the high-energy noise tail is absent in the model. Of course, there is an exponentially decaying tail in the model, but the Hamamatsu PMTs have a nearly-Gaussian bump larger (in charge) than the entire signal. At low statistics, the bump is ill-defined and easily mistaken for exponential decay; however, at high statistics (over a million events), the bump takes on a well-defined curve to its shape, clearly not decaying exponentially. This feature is shown in Figure 3.11. The three images in this figure show increasing number of events per run to the right.

All three images show a log scale to bring the tiny noise tail into view. This high-energy bump is always present, as is a low-energy tail that is not as obvious when looking at the distribution. These features can perhaps be avoided or at least changed by using a

different type of PMT or base, but it is essentially unavoidable and must be dealt with in the numerical analysis.

This small high-energy bump is dealt with in three ways in this thesis: the data is fit without assuming any exponential distribution, the bump is cut out of the fit, or the bump is included in the exponential decay distribution. These are a few of the many choices required in fitting to the chosen model. The next section goes into depth about the procedure taken to fit the model and extract parameters with error estimations.

Producing a Great Fit

Choosing the left and right bounds for the fit range is very important input to the algorithm. The very low and high signal sizes are the ones that are not included in the model. To be specific, the pedestal is assumed to be Gaussian, but in reality it is only approximately Gaussian, and it is the data to the left of the pedestal peak that cause large χ^2 values. Also, the high energy bump mentioned in the previous section is not part of the model from Chapter 2. Trying to fit the model to these points draws the minimization software away from the correct answer, and the result is a higher perceived fit uncertainty.

Cutting these points out of the fit is a cheap, easy, and effective way of dealing with outliers. A few possible changes to the model are mentioned below that could account for these artifacts rather than disregarding them completely.

High-Energy Bump

Many additional changes to the model were tested to account for the bump right of the signal in Figure 3.11. A single Gaussian of large RMS and small amplitude was attempted, but the results were not good, probably because 500,000 events aren't enough events to reveal the information needed to fit to this bump.

Another model was attempted, provoked by the correlation between the signal and the noise bump. Assuming that the bump is actually a manifestation of double-PE ejection that

is characteristic of bi-alkali photo-cathodes. If each photon has some probability of ejecting two electrons, some high-energy bump would be expected. This double-PE model is nothing more than the low-light model ran again on the data, but this time with some initial values twice that of the main fit, and smaller amplitudes. More time could be spent on this model and produce results, but that would require an in-depth study.

Non-Gaussian ADC Distribution

The CAEN ADC distribution is not a perfect Gaussian. Unfortunately, this affects every PE peak, but modeling it would add too many additional parameters; each Gaussian would need to become a triple-Gaussian distribution, as seen in Figure 3.12. Fortunately, adjusting the mean of the ADC distribution⁷ results in a much more Gaussian pedestal.

An alternative to increasing the model's complexity is simply cutting out the troublesome data points (if possible). The pedestal seems to either be symmetric or else it has extra events to the left side (depending on the run). This is fortunate, because cutting the events to the left of the pedestal mean leaves behind a portion of the pedestal that is very nearly Gaussian for all runs. This cut is made on almost every fit shown in this document.

Making cuts on the data is only the beginning of tuning the fit inputs. The next section discusses in detail all the necessary inputs to Root in order to correctly fit the model to data.

Fit Inputs: Constraints

Another recap of the model is appropriate here. A Gaussian "dark current" pedestal (Q_0 , σ_0) is some distance away from a signal Gaussian with a different width(Q_1 , σ_1). There are a series of other Gaussians that are defined by the signal, and whose amplitudes are scaled by the light level exhibiting Poisson statistics (μ). Each Gaussian peak is shifted or modified by a decaying exponential (α , W_α). An initial value is required for each of these

⁷The pedestal mean is a programmable parameter via the CAEN drivers.

seven parameters, and some of them require bounds.

In addition to these seven parameters, there are two more "pedestal injection" parameters, W_{ped} and W_{real} , that can be fixed to the exact known values or allowed to vary between 0 and 1. W_{ped} represents the proportion of pedestal events that were "injected" into the data. Some extra pedestal events are injected into the data by acquiring data WITHOUT pulsing the light source. This ensures that the pedestal will be visible in all data runs regardless of light level or filtering. W_{real} represents the proportion of pedestal events acquired in the presence of a pulse of light.

The number of PE peaks to consider is another unseen parameter. On the low-light fits, two or three PE peaks can be seen in some plots. For log scale plots or high light levels, sometimes up to twenty PE peaks can be seen. The fitting algorithm considers 10 - 20 PE peaks for low light levels, and chooses which and how many peaks to consider based on a best guess of the peaks relevant at this light level. For the highest light levels observable on the ADC range, the estimated average event is a 770-PE event. These fits attempt to include over a hundred PE peaks in their computations. This sometimes results in Root crashing.

Another input is the choice of minimization algorithm for finding the best fit. χ^2 minimization has been chosen here over log-likelihood method because χ^2 gives believable results more often. The low light fits have no empty bins in the fit range and should not have problems with this method. Besides this, Root accepts other flags for triggering behaviors such as increased computation time on minimization and increased error predictions; both of these behaviors are used to produce fits in this analysis. Table 3.8 summarizes and categorizes the fit inputs.

For any given data run collected at some light level and voltage, there are thousands of different combinations of values for the fit inputs to choose from. With these thousands of different input starting conditions come many noticeably different output fit shapes, errors, and measurements. Many of these outputs are often good, low-error measurements that

Param. type	Parameter name						
	Q_0	σ_0	Q_1	σ_1	μ	α	W_α
Initial	$(Q_0)_0$	$(\sigma_0)_0$	$(Q_1)_0$	$(\sigma_1)_0$	μ_0	α_0	$(W_\alpha)_0$
Low bound	Q_{0min}	σ_{0min}	Q_{1min}	σ_{1min}	μ_{min}	α_{min}	$W_{\alpha min}$
High bound	Q_{0max}	σ_{0max}	Q_{1max}	σ_{1max}	μ_{max}	α_{max}	$W_{\alpha max}$
Additional Model	$(W_{ped})_0$	$(W_{ped})_{min}$	$(W_{ped})_{max}$	$(W_{real})_0$	$(W_{real})_{min}$	$(W_{real})_{max}$	Minimization technique
	n_{min}	n_{max}	x_{min}	x_{max}			

Table 3.8: This table includes all information input into the fitting algorithm by the user that affects the output fit results (32 parameters). The initial parameters are all required as input if a high success rate is desired. Bounding parameters are used to force the fit to converge to physical quantities, especially on parameters with range $[0, 1]$. Model settings are also necessary inputs. In the model settings, n represents the number of PE peaks to consider, while x represents the fitting range.

do not seem to agree with one another; this indicates that the fit error estimations are not always reliable.

In order to make and report a measurement of the gain of any PMTs, the varied outputs must be considered and sorted through, either to be used and explained or cut out of the analysis (and perhaps still explained). Even in the low-light regime where the problem of identifying the peak separation is relatively easy, questions remain. This will be discussed further in this chapter after the fitting algorithm is fully explained.

Fit Outputs: Gain and Light Level

Throughout this document, the gain and light level results of the model have been referenced repeatedly. With these parameters come error estimations. There has been some discussion about the gain error, but nothing has been said about the light level error. Sometimes, Root returns 0.1% error prediction, sometimes 1000%. This error estimation depends on the initial conditions and bounds as well as the data itself. Sometimes, the error estimation is accurate and precise, but this must be assessed through analysis of many fits to many data runs, and sufficient knowledge of the setup is required. This is only achievable at the low-light level for a non-calibrated light source.

χ^2 and the number of degrees of freedom are two fit outputs that are very useful in

determining which fits will have useful, believable results. These parameters characterize the amount that the data seems to deviate from the model used. With a combination of good data and accurate models, low χ^2 can be achieved. Of course, this parameter can be low even when the measurement is bad, so of course, decisions must be made about which results to believe and use.

There are essentially seven parameters in the model that come with seven error estimates. Sometimes, the pedestal injection parameters are not constrained during the fit, so this leads to two more output parameters with errors. Considering χ^2 per d.o.f. as a single output parameter brings the total to 17. These outputs are listed in Table 3.9 for convenience and completeness. Besides these outputs, Root offers a correlation matrix for the parameters; this matrix is not considered in this analysis.

Parameters	$(Q_0)_{out}$	$(\sigma_0)_{out}$	$(Q_1)_{out}$	$(\sigma_1)_{out}$	μ_{out}	α_{out}	$(W_\alpha)_{out}$
Errors	$(Q_0)_{err}$	$(\sigma_0)_{err}$	$(Q_1)_{err}$	$(\sigma_1)_{err}$	μ_{err}	α_{err}	$(W_\alpha)_{err}$
Additional	χ^2/NDF	$(W_{ped})_{out}$	$(W_{ped})_{err}$	$(W_{real})_{out}$	$(W_{real})_{err}$		

Table 3.9: The fit outputs consist of the parameter values, their respective error estimates, and the fit "goodness" parameter.

Another very important output produced by the fit is the graph. The algorithm plots the data histogram on the range chosen by the user and draws in different colors the pedestal and signal peaks. This graph can be shown on a linear or log scale, and different parts of the model are visible in these different depictions. These images are indispensable tools for the human to visualize the data and model.

Measurement Error

The error in the low-light gain measurement begins with the CAEN ADC. Calibration of the charge sensitivity of the ADC used was not performed, so the manufacturer spec must be used. According to the V965 user manual [7], each channel of ADC output represents 25 femtocoulombs of charge, and there is a $\pm 4\%$ variation in this factor among the 16 input channels. This quoted 4% will be the starting point (and therefore minimum) for the error

in this measurement. After the ADC comes the voltage supply. The voltage applied to the PMT was monitored through the power supply itself, and reported at most a variation of 1% from the set point value.

Besides these two experimental errors, the error from the statistical model is all that remains. The parameter error reported by Root was scaled up by $\sqrt{\frac{\chi^2}{NDF}}$ in order to keep error estimates conservative⁸. The error on the gain is simply the error on Q_1 scaled by $\frac{25.0}{0.000160217}$, where 25.0 is the number of fC of charge per ADC channel and 0.000160217 is number of fC per electron (resulting in unitless gain). Typical values for the percent error on the gain measurement after this scaling range from 0.1% to around 5%. The final error estimate on a single low-light gain measurement is then⁹:

$$\begin{aligned} \%error &= \sqrt{0.04^2 + 0.01^2 + 0.001^2 (0.05^2)} \\ &= \sqrt{0.001701 (0.0042)} \\ &= 0.0412 (0.0648) \end{aligned} \tag{3.1}$$

This 0.1% - 5% fit output error is just a best estimate. Performing many fits to the same data file can produce a spread in results larger *or* smaller than the average Root error estimate. If a set of fits are gathered for a single data file, and the results of those fits predict gain values in a range larger than any individual fit error predicts, then this range is used to estimate the error rather than Root's reported error. This will be discussed more in the next section.

MySQL For Managing Many Fit Results

Many of the 32 different input parameters are very important for producing a good fit with low error. Without a tuned set of input parameters for the fit, chances are good that Root

⁸This scaling was only performed on fits where $\frac{\chi^2}{NDF} > 1$.

⁹If the ADC error were reduced to 1%, then the gain % error would be reduced to 0.0142 (0.0520).

will converge on a non-physical result. Producing a hundred fits to a single data run would only probe a tiny fraction of the available phase space here; then these hundred runs must be analyzed and compared to one another. Then, this analysis must be performed for several other data runs to investigate the same results at a different gain or light level. The number of results to be analyzed quickly reaches into the thousands. A database is required to manage all this information.

Two MySQL tables were created in a database for the analysis of all data in this experiment. One table called *run_params* stored the experimental run parameters of the data files such as voltage, PMT, ADC channel, filter, data rate, etc. The other table, called *fit_results*, stored all the inputs and outputs to the fitting algorithm. The *run_params* table makes automation of the fitting algorithm possible; through a series of shell commands, thousands of different fits can be performed for different groups of data. For instance, all PMT 1 data taken with filter 8 and light level 50 can be selected and analyzed. The selected runs can easily be analyzed repeatedly with different sets of input parameters. The MySQL tables also store data file names and locations as well as fit output png locations.

Filling the Database

Filling the database with results is as easy as writing shell scripts. Shell scripts are very versatile; from the shell, it is possible to perform logic, access MySQL database values, and execute the Root fitting algorithm. Some shell scripts written and used for filling the database are described in Table 3.10. Through the use of some combination of these scripts, a group of runs can be selected and fit to the model using several different input fit parameters.

Figure 3.13 gives an example of using the scripts via command line to run the fitting algorithm on some runs from PMT 1 with 2,000 volts and light level 30 and filter 7. The output from the fit are viewed from the command line (also shown in the figure), and the average gain and light level are measured for the fits performed.

Running the `run_batch.sh` script results in creating 3 - 6 fits per data run for a predefined

Name	Description
<code>sql_select_runs.sh</code>	Selects all run_id's for runs matching input criteria and stores the list in selected_runs.csv
<code>sql_remove.fits.sh</code>	Removes all selected fits from database and deletes associated files
<code>run_fit_pmt.sh</code>	Runs the fitting algorithm with user input about initial conditions and constraints for all selected runs
<code>run_batch.sh</code>	Runs <code>run_fit_pmt.sh</code> repeatedly with some different settings for different PMTs based on user input

Table 3.10: Description of some shell scripts written for searching and selecting data runs based on user input and executing the fit algorithm on selected runs. Some scripts write output to .csv or .txt files, some scripts may read these results. The scripts call Root macros (C++ algorithms) to perform complex computations and graphing.

group of great data runs for PMTs 1 - 6. These batches of fits show the performance of the fitting algorithm on the given data in highly-constrained and unconstrained conditions with respect to multiple parameters. The output from the shell script is hundreds of lines from Root reporting PNG files are being created. After running at full speed on multiple cores for a few hours, there are abundant results to sort through and interpret.

It is necessary to either fill the database with tens of thousands of fits that analyze all the data for all the PMTs over their ranges, or to repeatedly fill and empty the database with results from specific studies one at a time. Trying to handle over a thousand output PNG files and trying to use MySQL queries to single out groups of fits both become more difficult as numbers increase. This, among other things, may mean filling the database with runs from a single PMT at a time is more practical. Once the database is full of fit results, it is time to look for trends in the data.

Analyzing a Full Database

With a database full of data files and fit results, macros and shell scripts (or some other program) are necessary for making many plots quickly and efficiently. There are many plots

that could be made; it is important to know how to visualize the data to bring to light all the intricacies present. Systematic errors could be uncovered here as well as clues as to what is good or bad about the model.

Besides additional data analysis, the MySQL tables allow for quick and easy representation and documentation of fit results. Vast results can be produced depending on the number of PMTs. Table 3.11 describes shell scripts used to aid statistical analysis of the fit results. These scripts form MySQL queries to find averages and deviations of parameters found in the tables as well as plot these values against each other in scatter plots. The shell scripts embody the logic that decides how the data is represented in the graphs.

Name	Description
sql_select_fits.sh	Selects all fit_id's for fit results matching input criteria and stores the list in selected.fits.csv
sql_average.sh	Finds the average value of the chosen fit parameter from all the currently selected fit results
sql_view_fits.sh	Displays the PNG results for all selected fits
sql_make_plots.sh	Plots the chosen results on a 2D plot with 8 different colors to use for a third dimension

Table 3.11: These shell scripts perform functions such as calculating the average and variance of parameter values and making plots of one parameter vs. another.

The most important plot to be made from the many fit results is the Gain Vs. Voltage curve. This curve was mentioned in Chapter 2, Equation 3.1. Figure 3.14 shows a scatter plot of gain measurements for all six PMTs.

Looking at a single PMT means that the 3rd axis of the plot (color) is free to express another parameter. All of the following plots show fit results with χ^2 per NDF of at most 10 and relative error on the gain measurement of less than 10%. The largest amount of data has been collected with PMT 1. A large spread in voltage and light level was taken with PMT 6 with multiple filter setting (0.3%, 6%, 100% transmission). Figure 3.15 shows gain measurement results for PMTs 1 and 6. The black dots show results from fits where

the exponential decay was included in the fits as described [6]; the red dots show fit results where the exponential distribution only modified the signals, and the blue dots show the result of completely removing exponential decay from the model ($\alpha = 0$ and $W_\alpha = 0$). It has been mentioned throughout the document that the exponential distribution plays little to no role in modeling the data collected with these PMTs.

When trying to fit the data with an exponential decay in the pedestal and signal with identical amplitude and decay constant, the fitter runs into problems if the signal bump is well-separated from the pedestal. This is because the exponential decay must drop quickly to zero after the pedestal. When removing exponential decay from the model altogether, the fitter struggles because there is clearly some high-energy noise to the right of the signal that can be fit with exponential decay, especially at high light levels. Only using exponential decay in the signal and not in the pedestal gives the fitter flexibility and often results in fits with low error and χ^2 , but this also leads to a large spread in gain results; due to this inconsistency, it is unclear as to whether this makes the model more or less accurate.

The MySQL database also allows for the investigation of how the gain depends on other experimental factors. The plots in Figure 3.16 seem to suggest that the gain is dependent on light level. This is either real and physical, or it is an indication that the calibrated gain value or light level value is wrong. It is certainly possible that at high light levels, the PE ejection events are no longer independent but become correlated. Some sort of saturation effects at the cathode or anode could change the gain. Saturation effects are seen when the cathode or anode become depleted of electrons, resulting in smaller signals.

Figure 3.17 shows the results obtained when the fitting algorithm is allowed to vary by different amounts. When allowed to vary 50%, Root can try values between 50% and 150% of the best guess value. By default, the fitting algorithm is allowed to vary 20% from the best-guess input parameter. This is a fairly small window to examine, but iterative fits and analysis give confidence that the true values lie in this range. When allowed to vary more, the gain measurements still often fall very close to the input values.

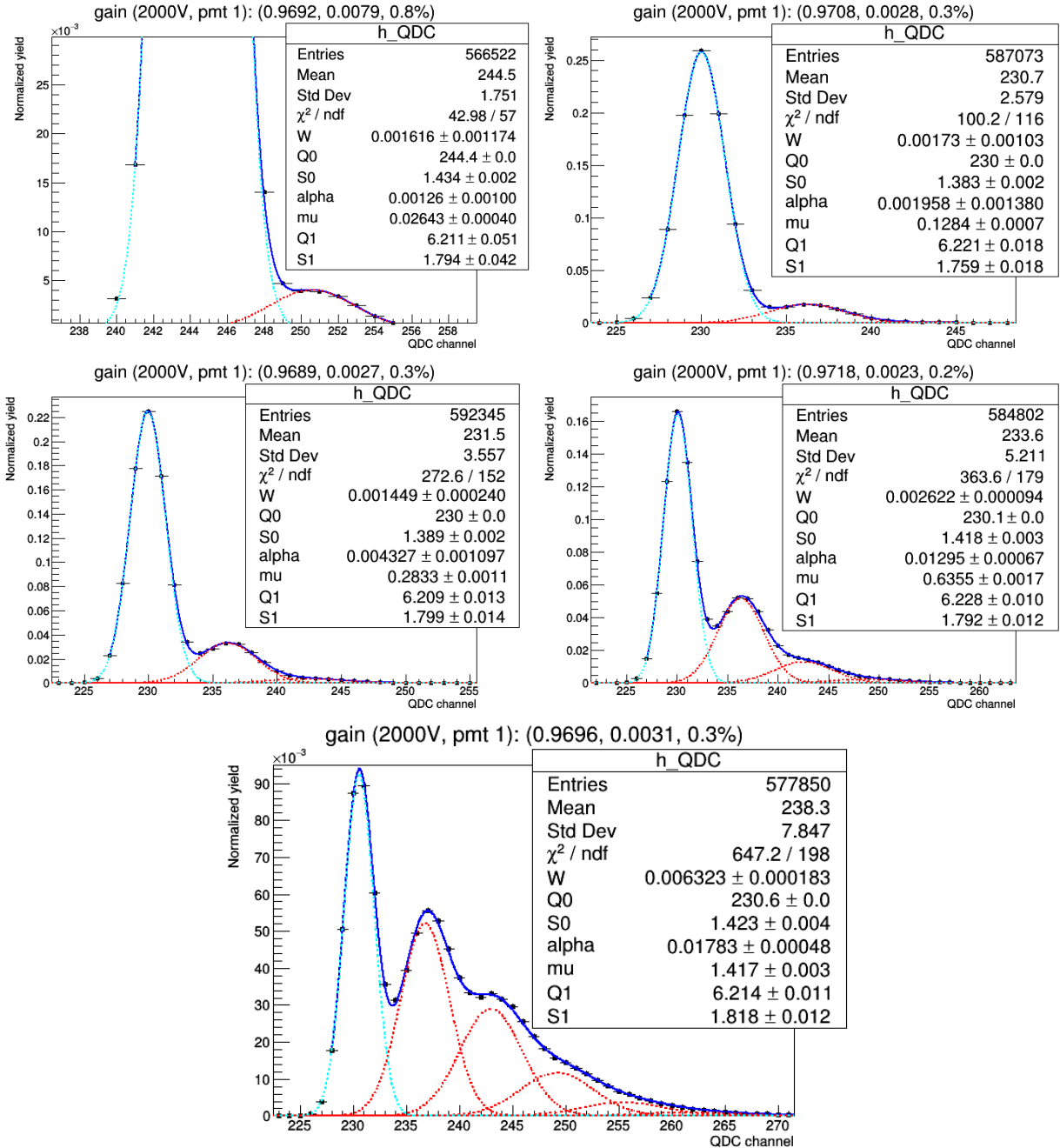


Figure 3.4: Runs taken at the maximum voltage for a few different light levels with PMT 1. The cyan line is the pedestal, the red lines are PE peaks, and the blue line is the overall fit.

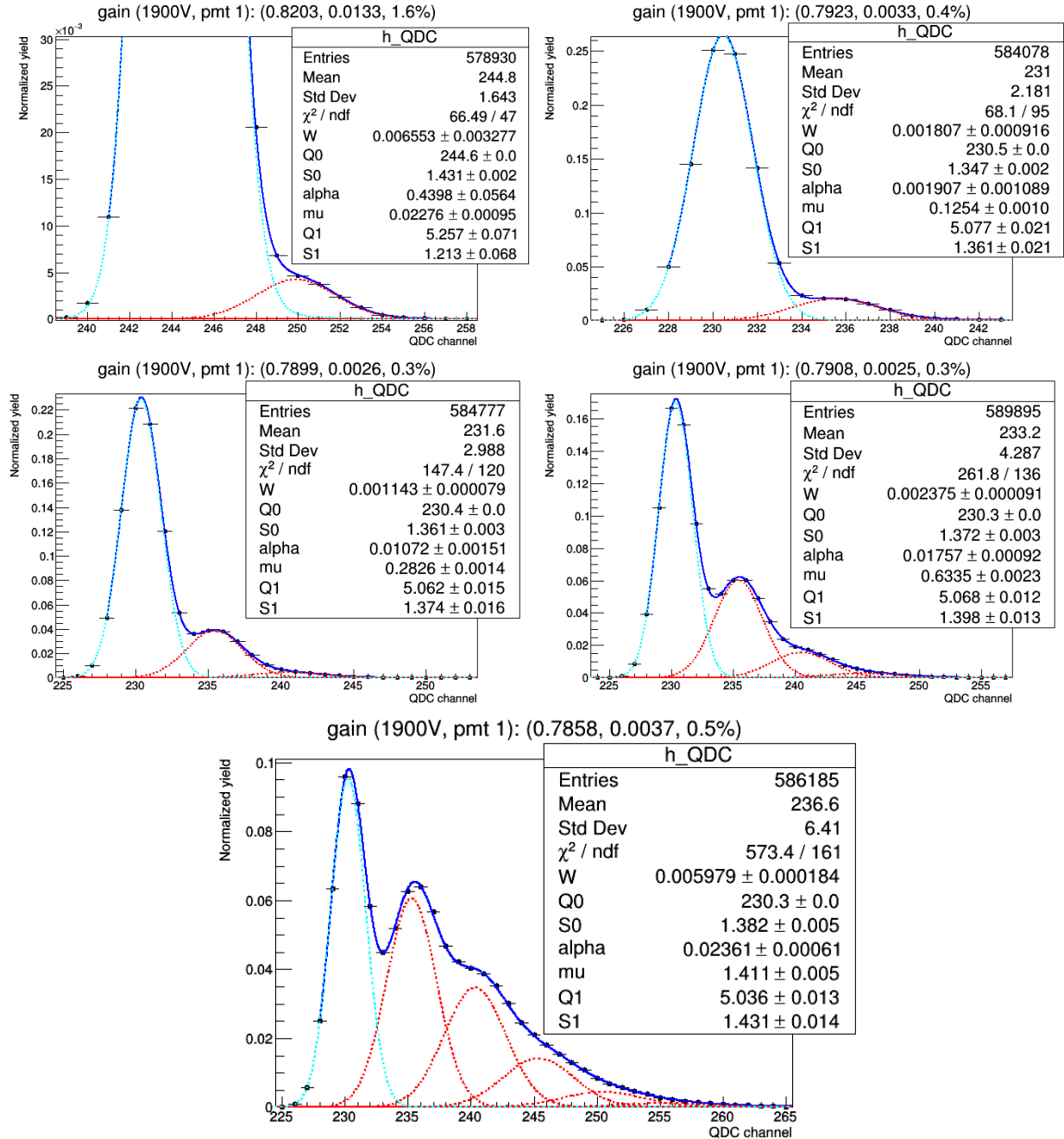


Figure 3.5: Runs taken below the maximum voltage for a few different light levels with PMT 1.

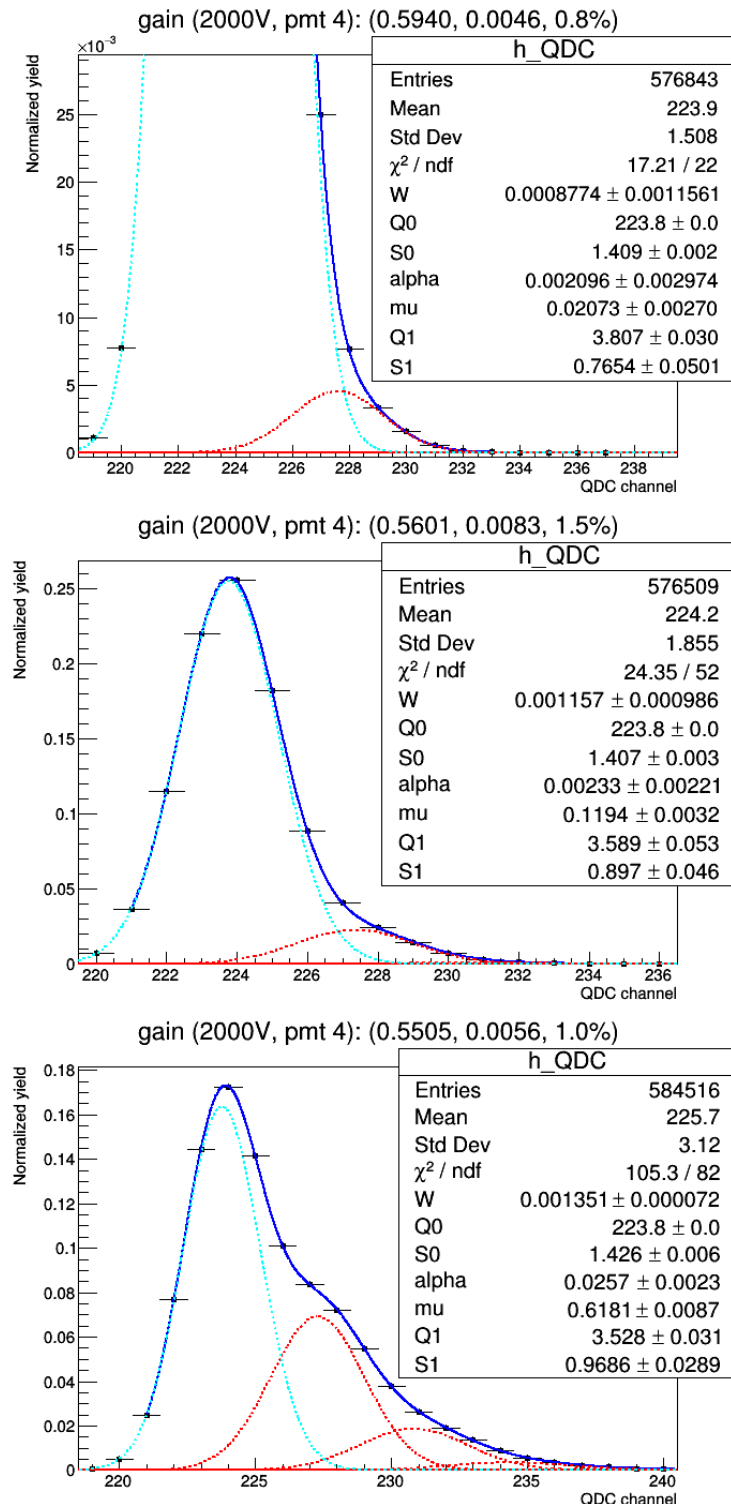


Figure 3.6: Runs taken at the maximum voltage for a few different light levels with PMT 4.

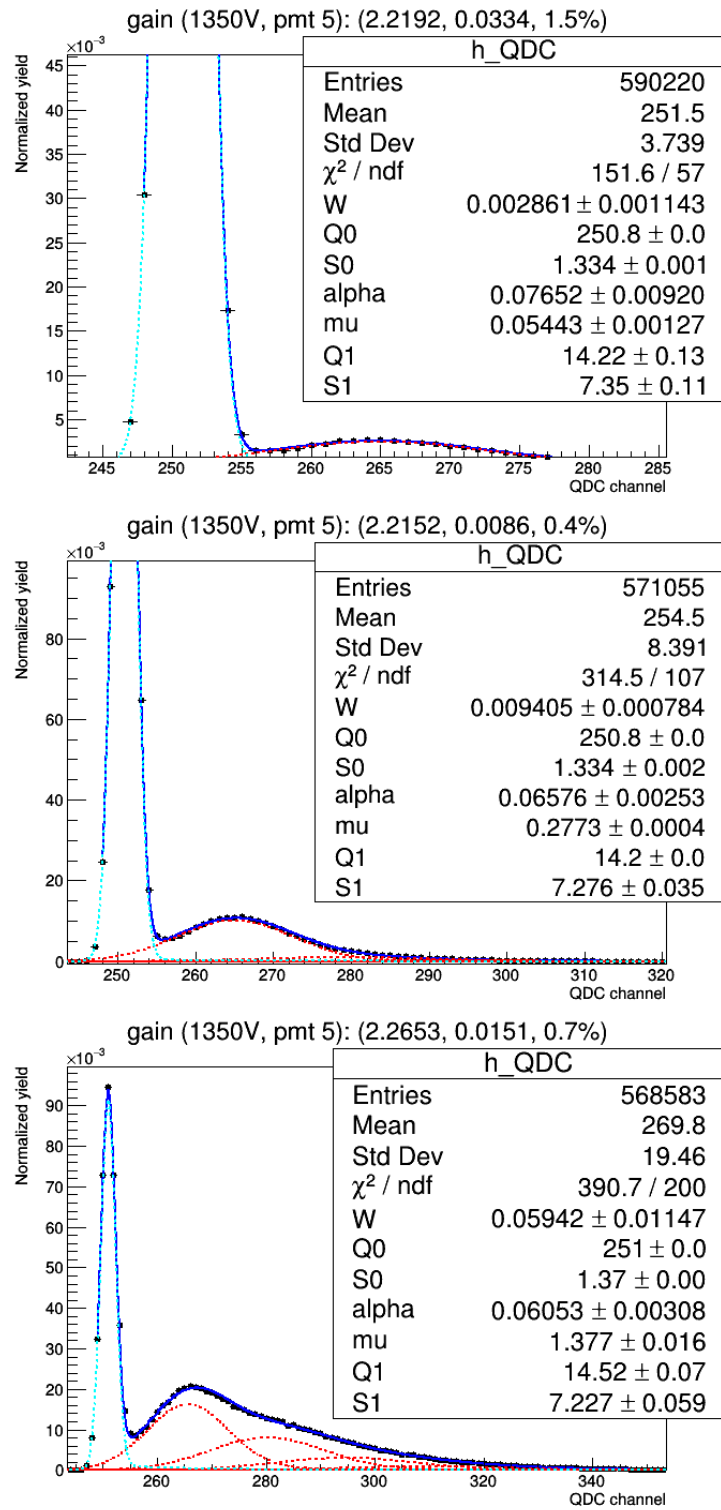


Figure 3.7: Runs taken at the maximum voltage for a few different light levels with PMT 5.

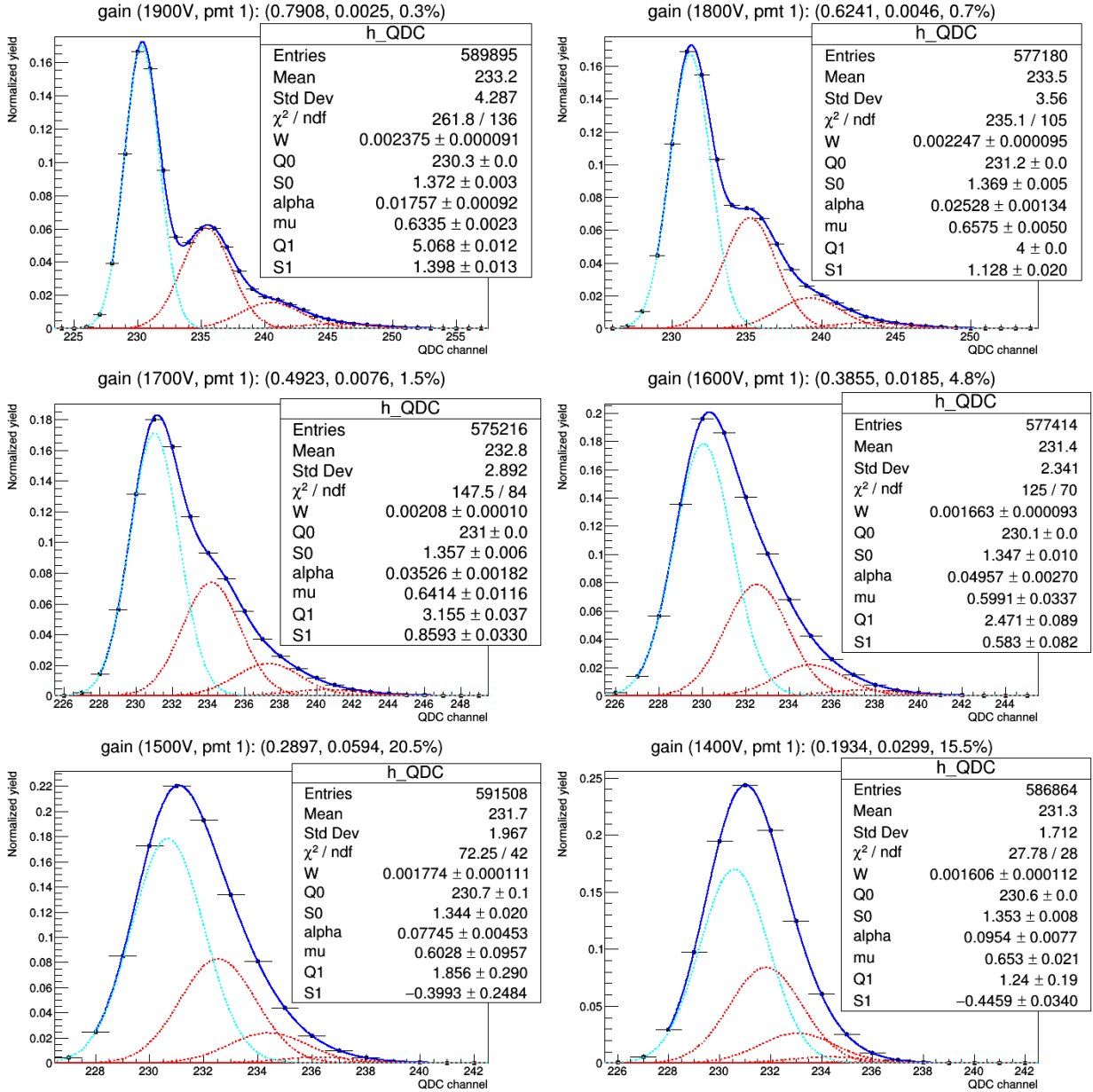


Figure 3.8: PMT 1 voltage scan from 1,900 V to 1,400 V at light level 40. These fits are produced with intelligent starting parameters and bounds. Voltage is decreasing from top left to bottom right in these images.

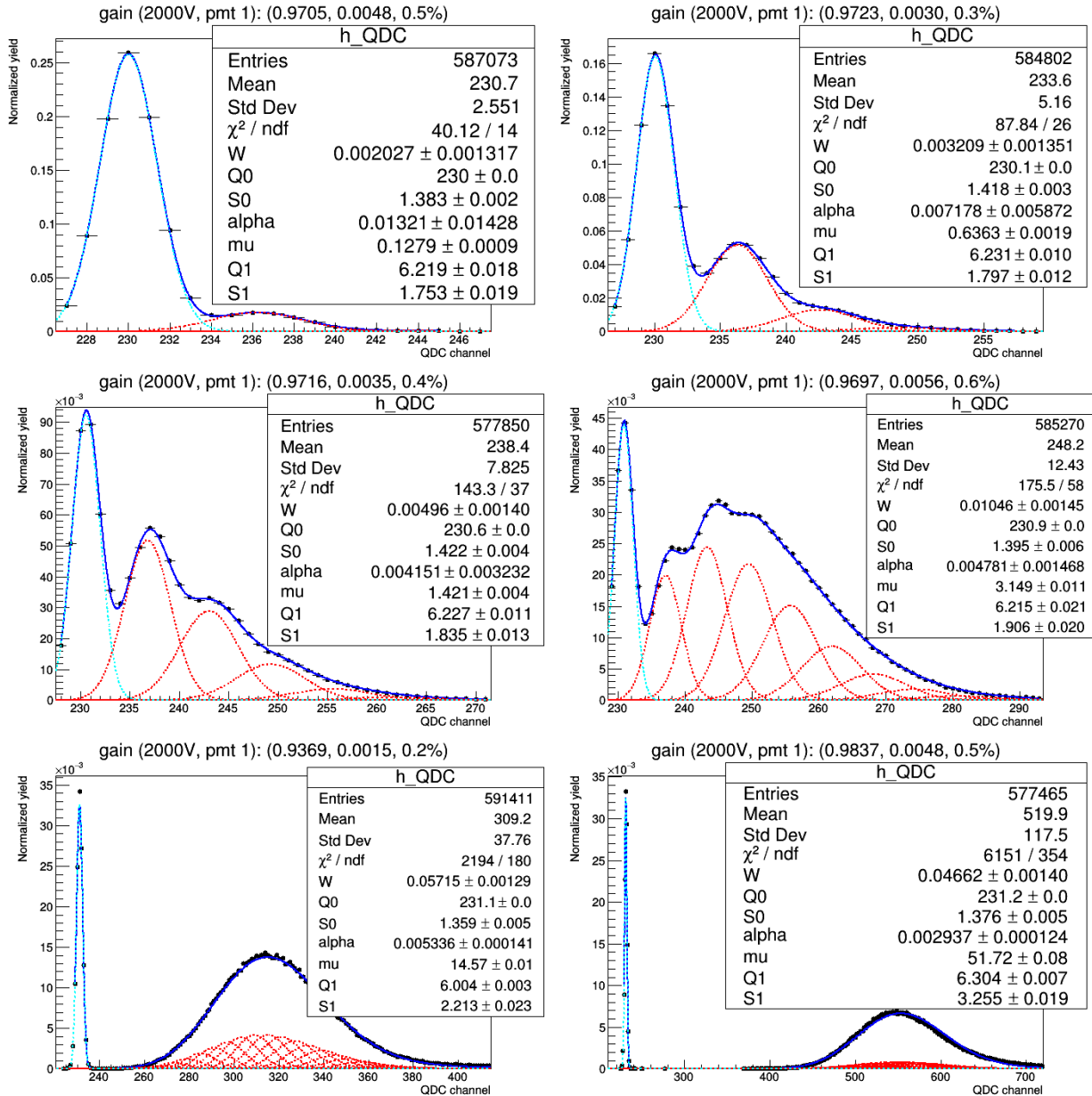


Figure 3.9: These plots show the PMT 1 response at 2,000 volts. The light level increases from top left to bottom right as follows: 30, 40, 45, 50, 60, 70.

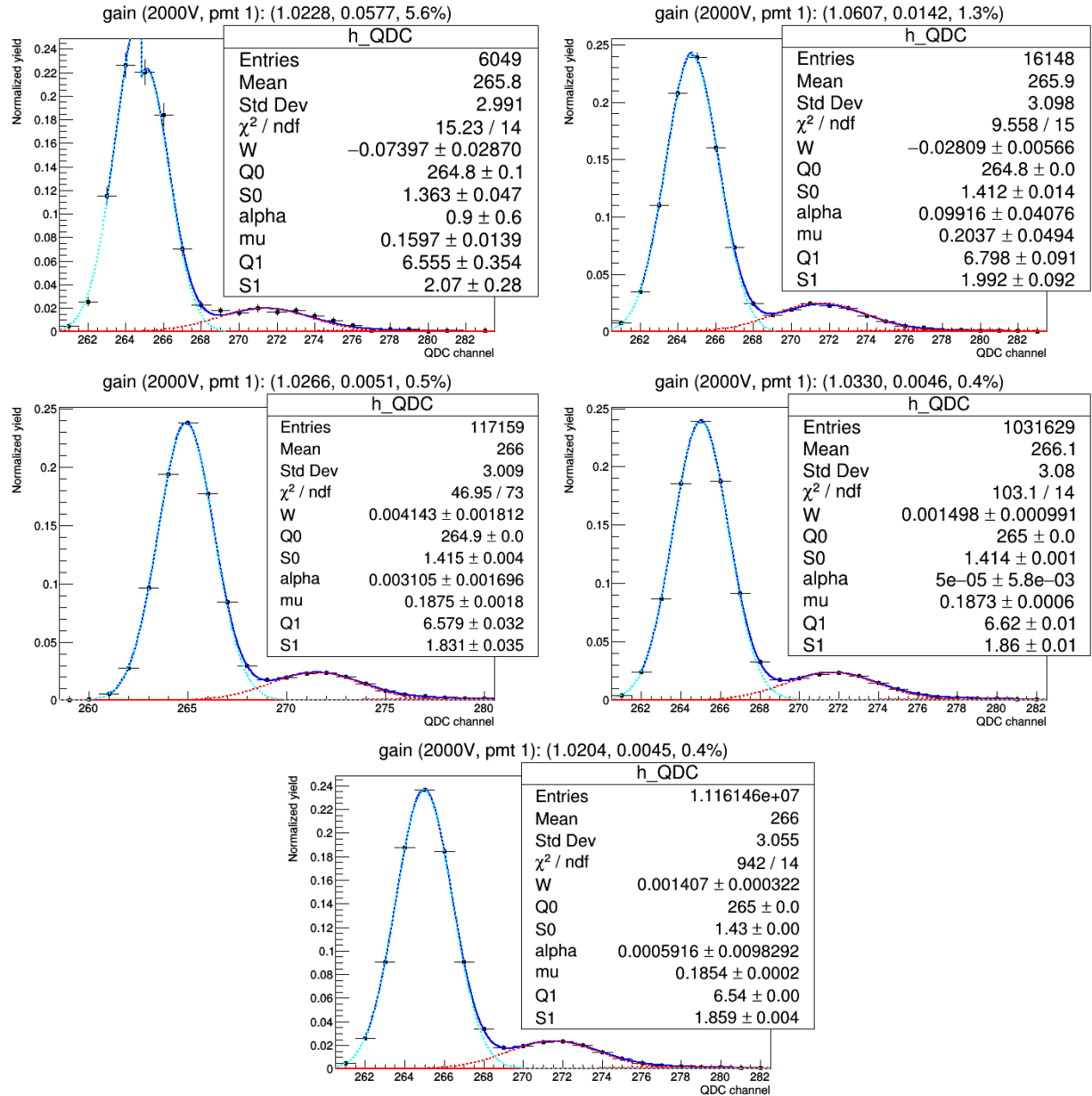


Figure 3.10: These fits are increasing in number of events by factors of 10 from left to right, top to bottom, starting with 10^3 and going up to 10^7 events in the last run.

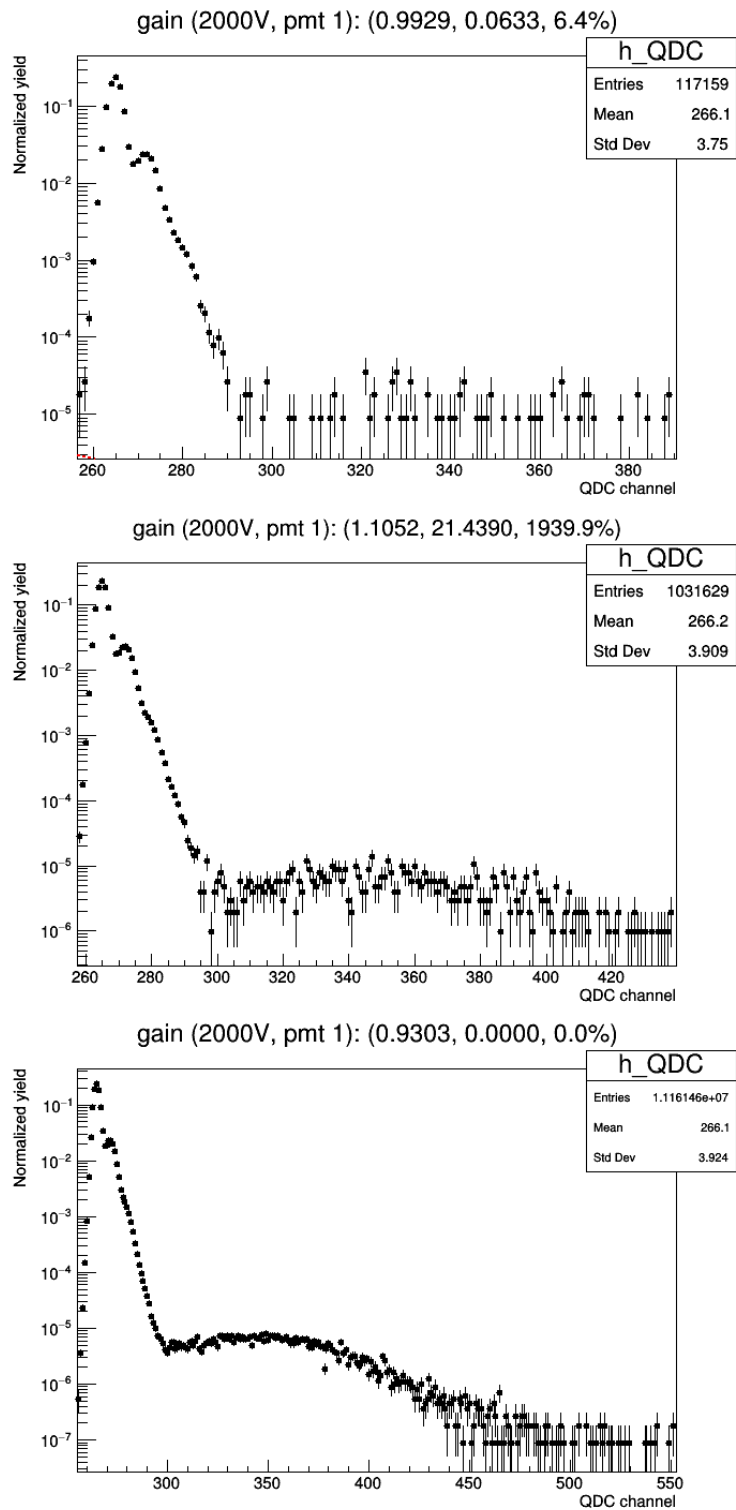


Figure 3.11: The events shown here are the last three runs from Figure 3.10. All these plots are log-scale in order to make the high-energy bump visible in the graphs.

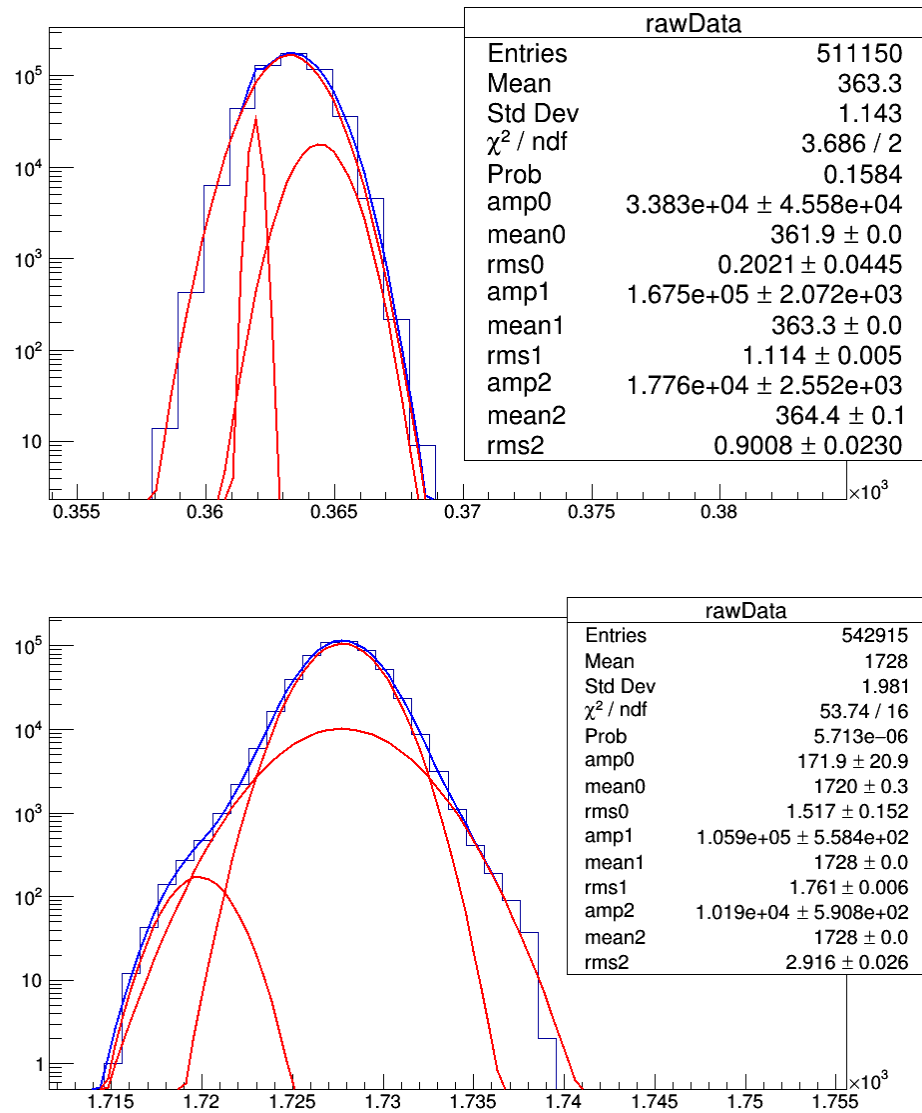


Figure 3.12: CAEN ADC pedestal distributions (Counts vs ADC channels). The left image has a low pedestal mean, the right image has high pedestal mean. Three independent Gaussian distributions are used to model this shape; the dominant Gaussian is normalized. Shown in log scale.

```

brady@brady-Predator-PH300:~/Projects/Low-Light-PMT-Data-Root-Fit$ ./sql_select_runs.sh hv=2000 pmt=1 ll=30 filter=7
6 run_ids selected
brady@brady-Predator-PH300:~/Projects/Low-Light-PMT-Data-Root-Fit$ head selected_runs.csv
51,63,98,109,543,770
brady@brady-Predator-PH300:~/Projects/Low-Light-PMT-Data-Root-Fit$ ./run_fit_pmt.sh conGain=100 conLL=20
Warning in <TCanvas::Constructor>: Deleting canvas with same name: canvas
Info in <TCanvas::Print>: png file fit_pmt_fitID1024_runID51_chi4_log0.png has been created
Info in <TCanvas::Print>: png file fit_pmt_fitID1024_runID51_chi4_log1.png has been created
Warning in <TCanvas::Constructor>: Deleting canvas with same name: canvas
Info in <TCanvas::Print>: png file fit_pmt_fitID1025_runID63_chi1_log0.png has been created
Info in <TCanvas::Print>: png file fit_pmt_fitID1025_runID63_chi1_log1.png has been created
Warning in <TCanvas::Constructor>: Deleting canvas with same name: canvas
Info in <TCanvas::Print>: png file fit_pmt_fitID1026_runID98_chi2_log0.png has been created
Info in <TCanvas::Print>: png file fit_pmt_fitID1026_runID98_chi2_log1.png has been created
Warning in <TCanvas::Constructor>: Deleting canvas with same name: canvas
Info in <TCanvas::Print>: png file fit_pmt_fitID1027_runID109_chi0_log0.png has been created
Info in <TCanvas::Print>: png file fit_pmt_fitID1027_runID109_chi0_log1.png has been created
Warning in <TCanvas::Constructor>: Deleting canvas with same name: canvas
Info in <TCanvas::Print>: png file fit_pmt_fitID1028_runID543_chi0_log0.png has been created
Info in <TCanvas::Print>: png file fit_pmt_fitID1028_runID543_chi0_log1.png has been created
Warning in <TCanvas::Constructor>: Deleting canvas with same name: canvas
Info in <TCanvas::Print>: png file fit_pmt_fitID1029_runID770_chi1_log0.png has been created
Info in <TCanvas::Print>: png file fit_pmt_fitID1029_runID770_chi1_log1.png has been created
brady@brady-Predator-PH300:~/Projects/Low-Light-PMT-Data-Root-Fit$ ./sql_select_fits.sh fit_cond="fit_id>=1024"
6 fit_ids selected
brady@brady-Predator-PH300:~/Projects/Low-Light-PMT-Data-Root-Fit$ ./sql_view_fits.sh
^Cbrady@brady-Predator-PH300:~/Projects/Low-Light-PMT-Data-Root-Fit$ ./sql_average.sh col=gain
gain (avg, std): (0.7427906666666666, 0.2734367725652292)
brady@brady-Predator-PH300:~/Projects/Low-Light-PMT-Data-Root-Fit$ ./sql_average.sh col=mu_out
mu_out (avg, std): (0.13599400000000003, 0.005720351067315129)
brady@brady-Predator-PH300:~/Projects/Low-Light-PMT-Data-Root-Fit$ ./sql_average.sh col=h_QDC
brady@brady-Predator-PH300:~/Projects/Low-Light-PMT-Data-Root-Fit$
```

fit_pmt_fitID1025_runID63_chi1_logX.png

Figure 3.13: Output from shell scripts from Tables 3.10 and 3.11. First, some runs are selected with PMT 1, filter 7, light level 30, and 2,000 volts. Then, the matching run_id's are shown, and the fitting algorithm is run on these fits. Next, the images are viewed (as seen in the bottom image here). Finally, the average gain and light level are computed and shown. The output images produced by the fit are the concatenation of a linear and log scale of the fitted data.

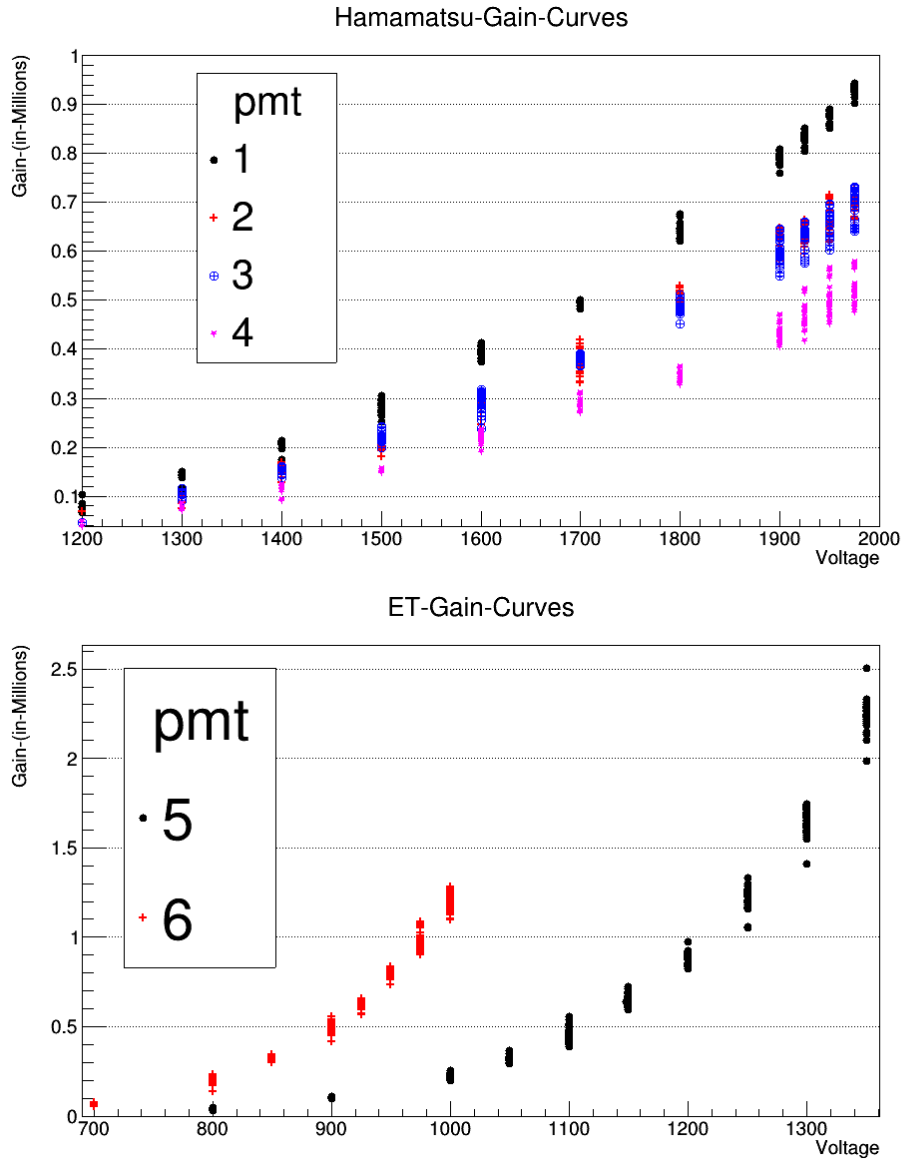


Figure 3.14: The gain measurements for all six PMTs over a large range of voltages. All of these plots have a χ^2 per NDF of at most 4 and relative error on the gain measurement of less than 5%. The lowest gains that produce fits this good are around 10^5 .

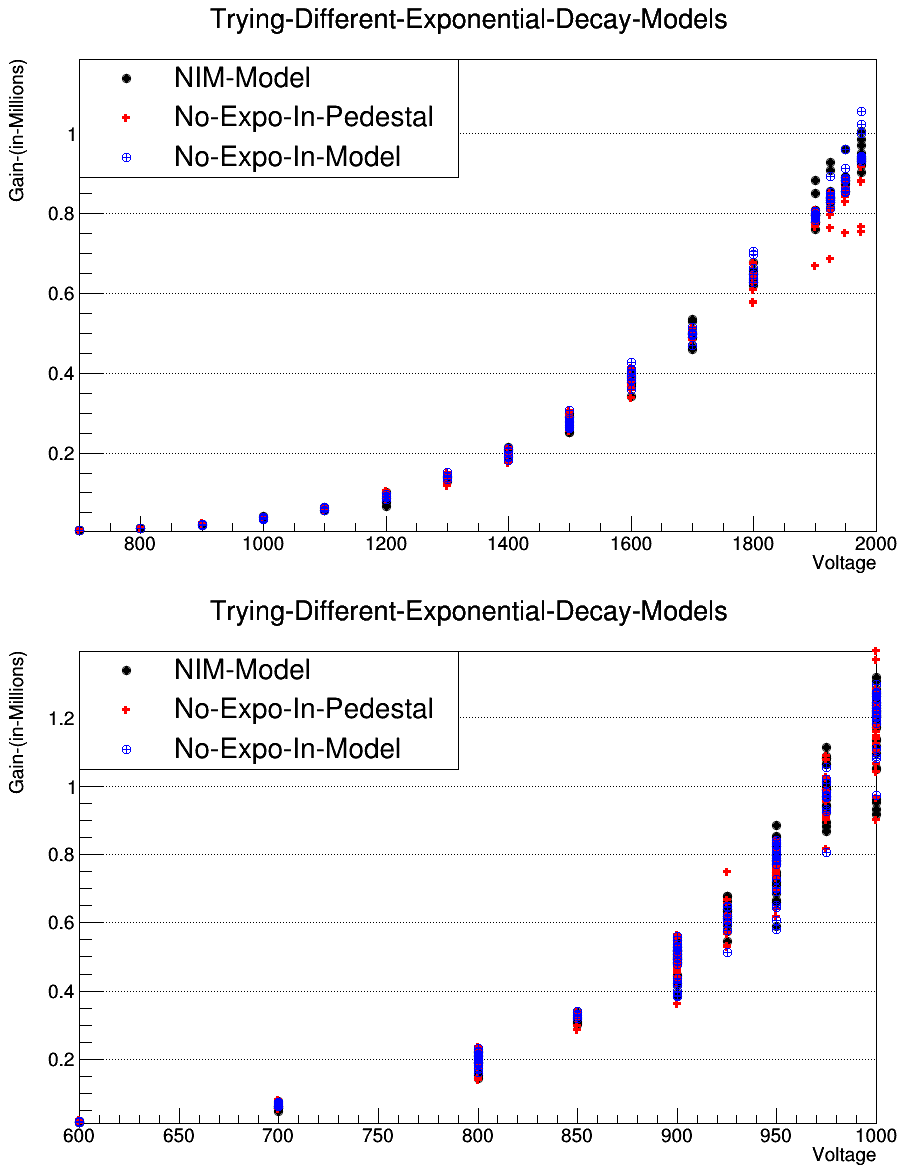


Figure 3.15: The gain measurements for PMTs 1 and 6. The colors show fit results from assuming different roles for the exponential decay in the model. All of these plots have a χ^2 per NDF of at most 4 and relative error on the gain measurement of less than 5%.

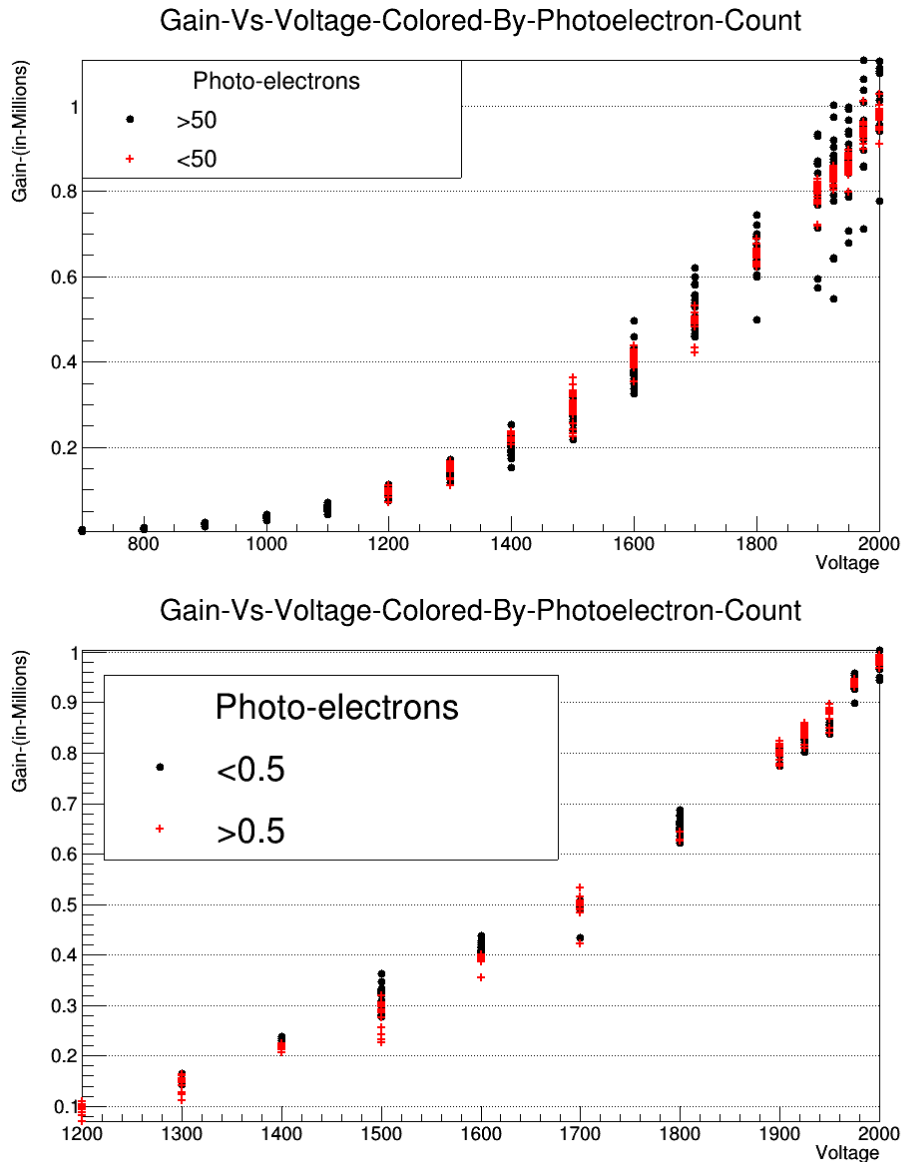


Figure 3.16: The gain measurements for different light levels (PMT 1). The left image shows the gain results including very high light data. The right image shows only low light results.

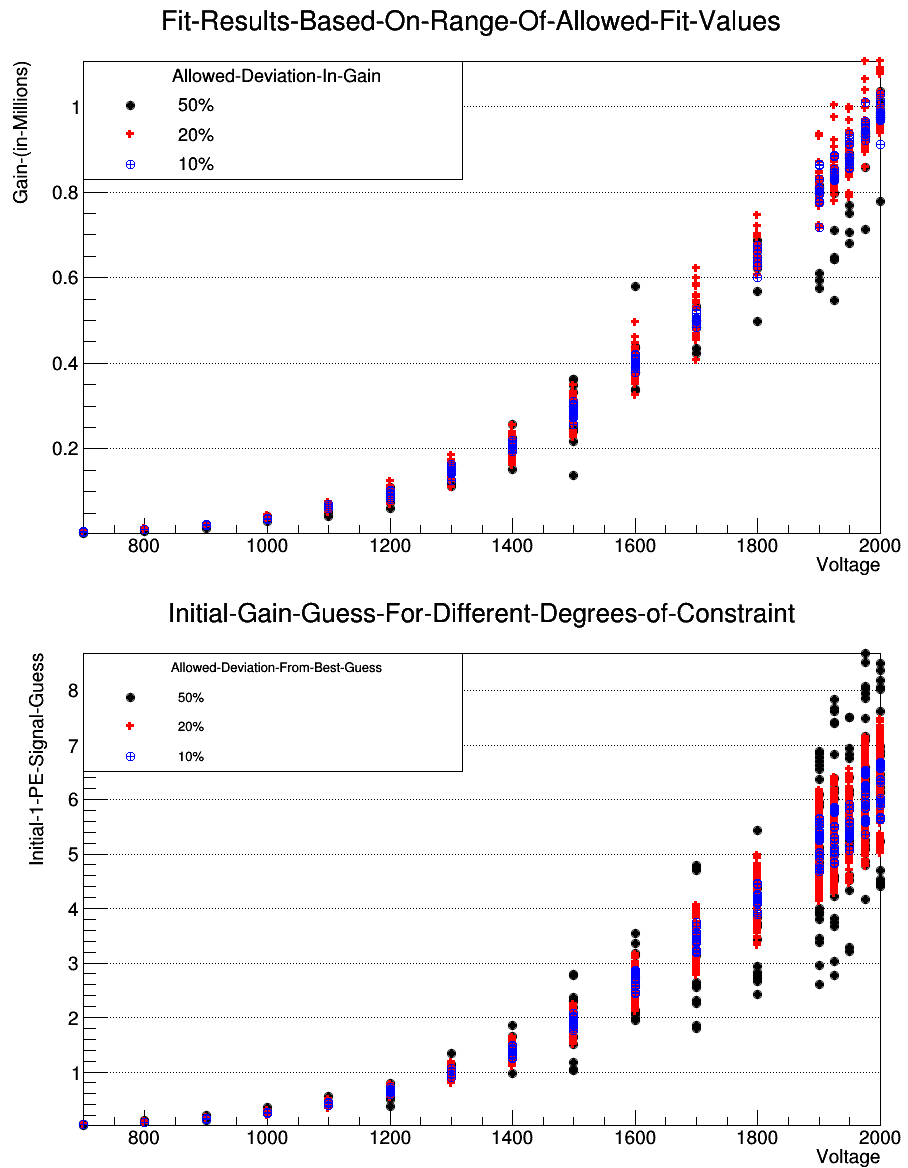


Figure 3.17: The varied results obtained when letting the fitter choose values far from the "correct" value (PMT 1). The left plot shows the location of convergence while the right plot shows the starting guesses of the gain parameter.

Chapter 4

Light Level Calibration

A calibrated gain at any voltage allows for the calibration of a certain range of light levels. For a gain on the order of 10^6 , single PE light levels can be calibrated. In this regime, the maximum light level resolvable depends on the cathode and anode maximum currents; too much light will break the PMT. For lower gain, single PE light levels are indistinguishable from pedestal events; the range of usable light levels here is larger, and 1-PE light levels are not included in this range.

This chapter goes over the results from the full range light level calibration as well as a filter calibration. This calibration is used to perform the gain measurement at low gain values for all the tubes.

Calibrating Light Levels With the Gain Data

Calibrating single PE light levels is very straight-forward given the previous work. As mentioned, fitting the model to the data characterizes the gain and the light level simultaneously. Root can perform this task with minimal knowledge of the actual values at 1-PE levels (given sufficient gain). The MySQL database with gain measurement results also contains the low-light calibration results.

The light source produces photons with exponentially increasing intensity as the knob is turned up at a constant rate. Table 4.1 shows the average observed light level for a given value on the dial. The table also gives information about the average error on the measurement as well as standard deviation in the results considered. These fits are considered to be mostly believable, but with a few outliers still that perhaps should be cut out.

Table 4.2 is just like Table 4.1, except for tighter selection criteria for usable fits. All the fits in this table are also present in Table 4.1, but only the fits with the lowest values for χ^2 and error are shown. This table is less conservative, but gives a more reasonable error

Light Level		Stats		
On Dial	Observed Avg. (μ)	Std. Dev. (μ)	Avg. Fit Error	# of Fits
20	0.02518	0.00159 (6%)	0.00084 (3%)	59
30	0.12068	0.01054 (9%)	0.00548 (5%)	90
40	0.63218	0.02887 (5%)	0.01000 (2%)	74
50	3.0592	0.1611 (5%)	0.0292 (1%)	122

Table 4.1: Average values and standard deviations of the light intensity (μ) from different dial settings. Only fits with χ^2 per NDF less than 10 and gain relative error less than 10% were used. The average value of the error on μ returned from Root is also shown.

estimate, assuming the model is correct¹. These tables give a full set of results of a low light calibration for a single PMT. These results must be obtained for each PMT in order to measure its low-voltage gain values; recall that the quantum efficiency of the photo-cathode is embedded in the results shown in the tables.

Light Level		Stats		
On Dial	Observed Avg. (μ)	Std. Dev. (μ)	Avg. Fit Error	# of Fits
20	0.02528	0.00157 (6%)	0.00082 (3%)	54
30	0.12250	0.00853 (7%)	0.00300 (2%)	44
40	0.63153	0.02613 (4%)	0.00956 (2%)	10
50	3.0439	0.1851 (6%)	0.0664 (2%)	20

Table 4.2: Average values and standard deviations of light intensity (μ) from different dial settings. Only fits with χ^2 per NDF less than 2 and gain relative error less than 3% were used. The average value of the error on μ returned from Root is also shown.

The best fit table suggests that the relative error in the low light measurement is around 6%. This is pretty high, unfortunately, but at least in the same ballpark as the minimum 4% error arising from the ADC itself. Table 4.3 gives the light level calibration results with relative error for all six PMTs. The Hamamatsu tubes all have similar quantum efficiencies as well as identical collection areas. The ET tubes are similar to one another as well. All of these plots have a χ^2 per NDF of at most 2 and relative error on the gain measurement of less than 3%.

These calibrations are sensitive not only to specific PMT cathode, but also distance from PMT to fiber optic, filter setting, diffuser, etc. If the experimental setup changes,

¹If the model is not correct, fits with high χ^2 values could have more accurate results.

PMT	Light Level (% Error)			
	20	30	40	50
1	0.0253 (6%)	0.1225 (7%)	0.6315 (4%)	3.044 (6%)
2	0.0217 (6%)	0.1123 (7%)	0.5841 (5%)	NO FITS
3	0.0241 (3%)	0.1211 (5%)	0.6426 (4%)	3.0570 (5%)
4	0.0202 (9%)	0.1143 (8%)	0.5939 (8%)	NO FITS
5	0.0571 (2%)	0.3099 (1%)	1.4530 (7%)	7.2425 (4%)
6	0.0503 (5%)	0.2598 (4%)	1.3236 (2%)	6.0437 (4%)

Table 4.3: Average values and relative error of light intensity measurements for all PMTs. Only fits with χ^2 per NDF less than 2 and gain relative error less than 3% were used. The average value of the error on μ returned from Root is also shown. The relative error shown is from the larger of the std. dev. of fit results and the average Root error.

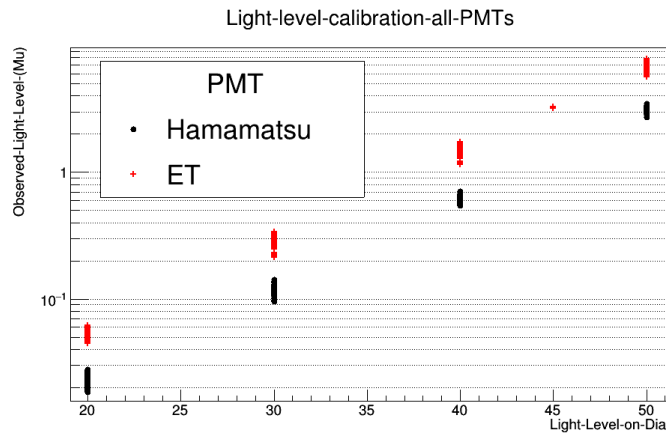


Figure 4.1: Light level curve for all six PMTs.

the calibration needs to be done again². By performing the light level calibration with and without a filter, the transmission coefficient of the filter can be characterized.

The values listed in the last three tables represent the average number of PEs ejected from the respective cathode given the incoming light pulse. Clearly, the quantum efficiencies vary by no more than 10% between tubes of the same model³. Figure 4.1 shows the results of Table 4.3 plotted. The log scale shows a very linear function of intensity vs. dial setting at the low light levels.

²Thanks to the PMT holders, the light level remains constant to within the error bars when swapping out the tubes.

³It is hard to compare QE between different model tubes because the light collection areas are different.

Calibrating Filter Transparency

In order to calibrate the high light levels, filters must be used. This is because there is no knowledge of the amount of light present, and there is no knowledge of the PMT gains at these light levels. The gain could be higher or lower for higher light levels, but normally the gain decreases with light level due to PMT saturation effects (at high enough light). By reducing the light level a known amount with a calibrated filter, the high light level regime can be characterized while fitting to low light data where the gain is known.

The filter calibration at low light was performed using PMT 6 since it has high gain. Figure 4.2 shows the results of measurements of the light level curve with filter 8, filter 1, and no filter. The black points show the light level curve over the whole usable dial range with no filtering. All results were obtained using the low-light Poisson model. The fact that the light level curve falls off at the high light end of the graph may indicate that the PMT is becoming saturated, or it may simply be that the light source itself outputs light with this diminishing intensity. It could also be that the starting values given to the fitter are too low. It is shown later that this is NOT due to PMT saturation.

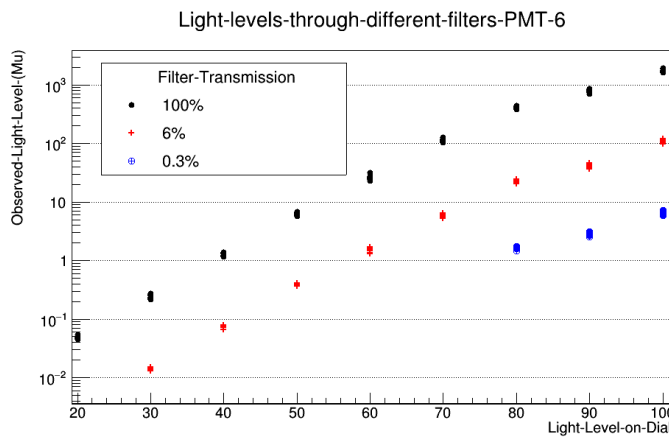


Figure 4.2: Best fit results for light level measurement using PMT 6 at multiple high voltage setting and light levels with and without a filter.

If the PMT were experiencing saturation near light level 80 as it appears to be in Figure 4.2, then one would expect this PMT to show saturation signs with around 500 PEs per

pulse no matter the filter. The decreased slope in the light level curve shows up at the same light level for each filter rather than the same cathode current; this means that it is certainly not PMT saturation effects producing this curve⁴. This is great news; the filters do not necessarily have to be used to measure gain at high light levels. From now on, it will be assumed that it is safe to use high light levels without filtering⁵.

Table 4.4 shows the average and std. deviation of the different light level measurements for filter 8. Whether or not this information will be used, it is here and should be documented. A similar table could be made for filter 1 (also shown on the graph) and would show a transmission coefficient of around 0.32%.

Light Level	μ (no filter)		μ (filtered)		Filter Transmission
	Average	Std. Dev.	Average	Std. Dev.	Average
30	0.255	0.013	0.014	0.001	5.32%
40	1.307	0.059	0.073	0.002	5.58%
50	6.043	0.321	0.375	0.018	6.20%
60	25.86	1.563	1.581	0.142	6.11%
70	117.5	12.82	5.929	0.313	5.05%
80	456.2	85.65	19.58	2.093	4.29%
90	717.1	71.11	41.83	4.054	5.83%
100	1,695	158.7	107.2	13.27	6.32%
			Avg:		5.59%
			Std:		0.64%

Table 4.4: This table lists the results of a light level calibration for PMT 6 with and without filter 8. This filter is found to have a transmission coefficient close to 6%.

The calibration of the filter results in a range of possible values from 4.5-6.5%. The minimum error achievable in a gain measurement using this filter is at least 12%. It is certainly preferable to take low-gain data at light levels 60-80 with no filter; unfortunately, this was not known during the data acquisition portion of the project, so for PMTs 2-5, there is no data for light levels 60-80. The results of the data taken will be presented in this thesis, but further analysis will take place to extend the data set and minimize the error on these PMTs. Figure 4.3 is a great representation of the optimal light levels for data taking.

⁴There is some independent evidence shown in Section 6.3 from Cerenkov data that this is the case.

⁵These results must, of course, be checked for every PMT.

Light levels 90 and 100 are off the ADC range for the highest gains with no filtering, so they are out of the question. Notice the bunching of the data points; for a range of light levels (30-50 without filter), the data points have much better bunching. Too low of light level makes for a difficult deconvolution because the signal has fallen into the noise floor; too much light is too difficult because the individual PE contributions become smashed tightly together into one signal.

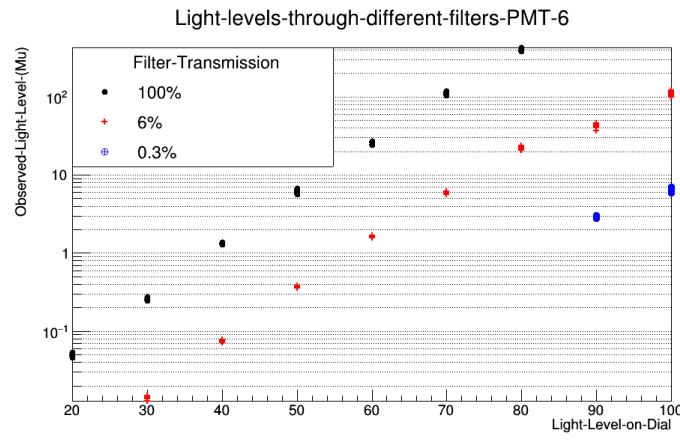


Figure 4.3: Full light level calibration for PMT 6 with and without filters. All the data shown here was taken with gain of around a million, so the results have minimal noise and error. The points with the tightest bunching are the optimal light levels for making measurements.

Chapter 5

High-Light Gain Measurement at Low Voltages

The Poissonian (low-light) model can be used to characterize the gain at low voltages using high light levels, but this process is very computationally expensive. At high light, there is no need to deconvolute the signal; in fact, it is nearly impossible. The deconvolution happening in the low-light model is guided using the previous knowledge of the light level in the code itself. The fitting algorithm reads the best guess values for gain and light level from CSV (comma-separated value) files during each fit, so even using the low-light model doesn't get around using the light level calibration.

A much quicker and simpler model was described in Chapter 2; at high light, the individual PE signals merge into a single Gaussian peak (with some exponential decay), well separated from the pedestal. This model has 5 parameters rather than the 7 of the NIM model. The pedestal and signal Gaussians each have a mean and RMS, and the exponential decay has a decay rate. This chapter compares the high-light model results with the low-light model.

Gain measurement at low voltage

Measuring the number of ADC channels between the pedestal and the signal gives some large amount of charge, Q . This charge is equal to the average number of PEs per flash for this data run (μ) times the charge of 1-PE; therefore, the separation of the means of these Gaussians divided by μ gives the gain measurement for high-light data ($q = \frac{Q}{\mu}$).

The plots for the low gain measurements are a bit different than the low-light model. The high light model shows three plot panels; the first shows the entire raw data histogram, the second shows just the pedestal with a Gaussian fit, and the third shows just the signal with a Gaussian fit convoluted with a decaying exponential. The code used is shown in Appendix A. The goal of the high light model is simply to deconvolute the Gaussian signal

from its high-energy tail so that the Gaussian mean can be used in the gain measurement along with μ from the light level calibration.

Examples of individual results

Figures 5.1 and 5.2 show PMT 1 results using the high light model at 2,000 volts for the whole light level range. Most are great fits with low error. This method of measuring the gain is very fast and easy and does not produce the wide range of results that come from the low-light model; however, this method does depend on the low-light model for calibrating the light levels and filters with minimal error.

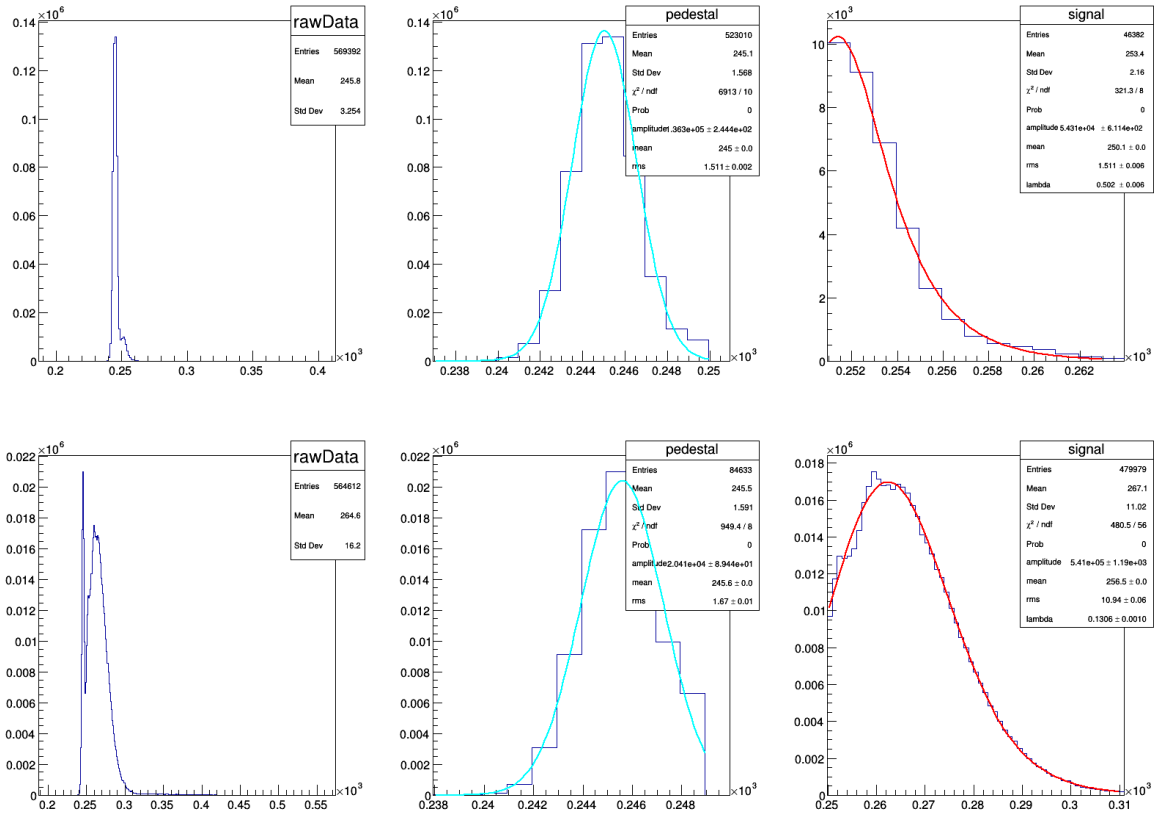


Figure 5.1: The first panel in each image shows the entire raw data histogram for the run (counts vs channels), the second panel shows just the pedestal with a Gaussian fit, and the third panel shows the signal with a modified Gaussian fit including exponential decay.

This method will never produce a smaller error than the low-light method. The low-

light model contains this simple model within it and includes an extra parameter; the extra parameters in the low-light model allow it to make a more detailed fit to the data. If a good enough light level calibration is achieved, however, then this method can allow for fast and easy characterization of the voltage and light level ranges of the PMT outside of the low-light, high-gain regime. Figure 5.1 also shows how the high-light model responds to single-PE levels. The simple model tries to slice the two distributions apart even if they spill into one another; in this regime, there are bound to be larger errors in the results. It is nice to see these results blend smoothly, though, from great and usable to nonsense.

Trends in the results

Figure 5.3 shows a couple plots made from the MySQL database of fit results. The gain curve is shown for the high-light measurements; these points have incorporated in them the light level calibration. Unfortunately, the results from the high-light analysis vary and can be interpreted to agree or disagree with the low-light model, depending on the assumptions made.

For instance, the top-right image in Figure 5.3 shows that the gain at light level 100 is higher than at light level 90 for PMT 2; this is unintuitive. PMTs 3 and 4 show a curve very similar to that shown for PMT 2. For PMTs 1, 5, and 6, however, the gain seems to be higher for light level 90 as seen in the other three images. This is very troubling, and likely implies that something is wrong with the light level calibration for all of the PMTs. There is not enough data over the light level and filter ranges to reach a sure conclusion on this point in this thesis; more data must be taken to resolve this issue. For now, it will be assumed that the light level calibrations for all PMTs are valid, and their error terms will be carefully accounted for.

It could be that the gain is the same over all the light levels used as discussed in the light level calibration chapter. As mentioned in that chapter, the light level curves for PMT 6 seem to indicate that there is no saturation happening, but this could be a false result

reached through the iterative process of trying to calibrate the light levels using results from known regimes. There could be an inherent flaw in the process used that shifts the gains or light levels one way or another.

Another possible issue is brought to light in the top-left and bottom-left images in Figure 5.3. For some gain and light level, the ADC will eventually saturate, and this value is different for each PMT. This phenomenon is very easy to identify by examining the raw data histograms, but it could be that near this high end of the spectrum, the ADC no longer has a linear response. It must be assumed that the ADC itself provides a linear response, but this is just one more thing to be aware of and keep an eye on for big signals.

To complicate matters further while trying to clear up questions in the results, filters can be considered. Only two filters were used in this analysis, and one of them barely lets any light through. Filter 8 allows for about 6% transmission of incident light and can thus be used in the high-light analysis for light levels greater than about 80. The filter calibration adds another source of error, but could be used to bridge low- and high-light regimes. Figure 5.4 shows how the gain measurement changes if the 6% filter is used. If the gain changes, it is expected to increase when a filter is introduced due to less saturation, but there could be other effects in the cathode at high light levels that actually increase the gain. It is clear that something isn't calibrated right, either light level 90, light level 100, filter 8, or some combination of these parameters for all PMTs.

Oddly enough, when a filter is introduced, exactly the same result is observed that is questioned in the last section: PMTs 1, 5, and 6 seem to have higher gain for higher incident light levels while PMTs 2, 3, and 4 have lower gain for higher incident light levels (consistent with saturation). Perhaps the analysis is accurate and the different tubes have these different responses to incident light. It should be noted that PMTs 1, 5, and 6 are the highest gain tubes and could all be experiencing bad light level calibrations at high light. It is also suspicious that the filter 8 results agree the best with unfiltered results for PMT 6 than any other PMT because PMT 6 was used for the filter 8 calibration. It is expected that if more

data were taken with filter 8 using the Hamamatsu tubes and the calibration redone, the filter 8 results would agree with PMTs 1-4 rather than PMT 6.

Comparison to Poisson Results

It is very important to compare the high-light measurements to the low-light measurements. Although it should be expected that these models may disagree in their respective regimes, one would hope for the models to predict results that blend well from one regime to another in order to bridge the gap accurately and precisely. Whether or not these results agree depend largely on which measurements are trusted and which are not. Figure 5.5 shows results from different models and regimes.

Due to the large variation in results from the low-light model, assuming that there is no saturation and the gain is constant over the whole light level range results in a large percent error for the gain measurement (over 10%). This percent error can be reduced to around 6% if those high light level results are not used. The low-light results form a pretty tight band; the high-light results are a looser band with lower gain. This indicates that the gain is indeed light-level dependent. However, it is possible that this discrepancy comes from a bad light level measurement. For some PMTs, the results from light level 90 agree with the low-light band of the Poisson model while the results at light level 100 agree with the high-light band. For other PMTs the situation is reversed. There is some evidence for saturation effects, and there is some evidence for gain linearity across the light levels. This conflicting evidence means that the light level calibration is not good enough yet to trust. Both bands must be considered viable options for the low-gain measurements until more data is acquired.

Because all of the results found using the simple high-light model fall within the results found using the low-light model, all of the gain measurements found in Chapter 3 will be used to characterize the gain of all the PMTs over their respective voltage and light level ranges. Although it is more computationally intensive, the low-light model is also better

understood and more supported in the code at this point in the analysis.

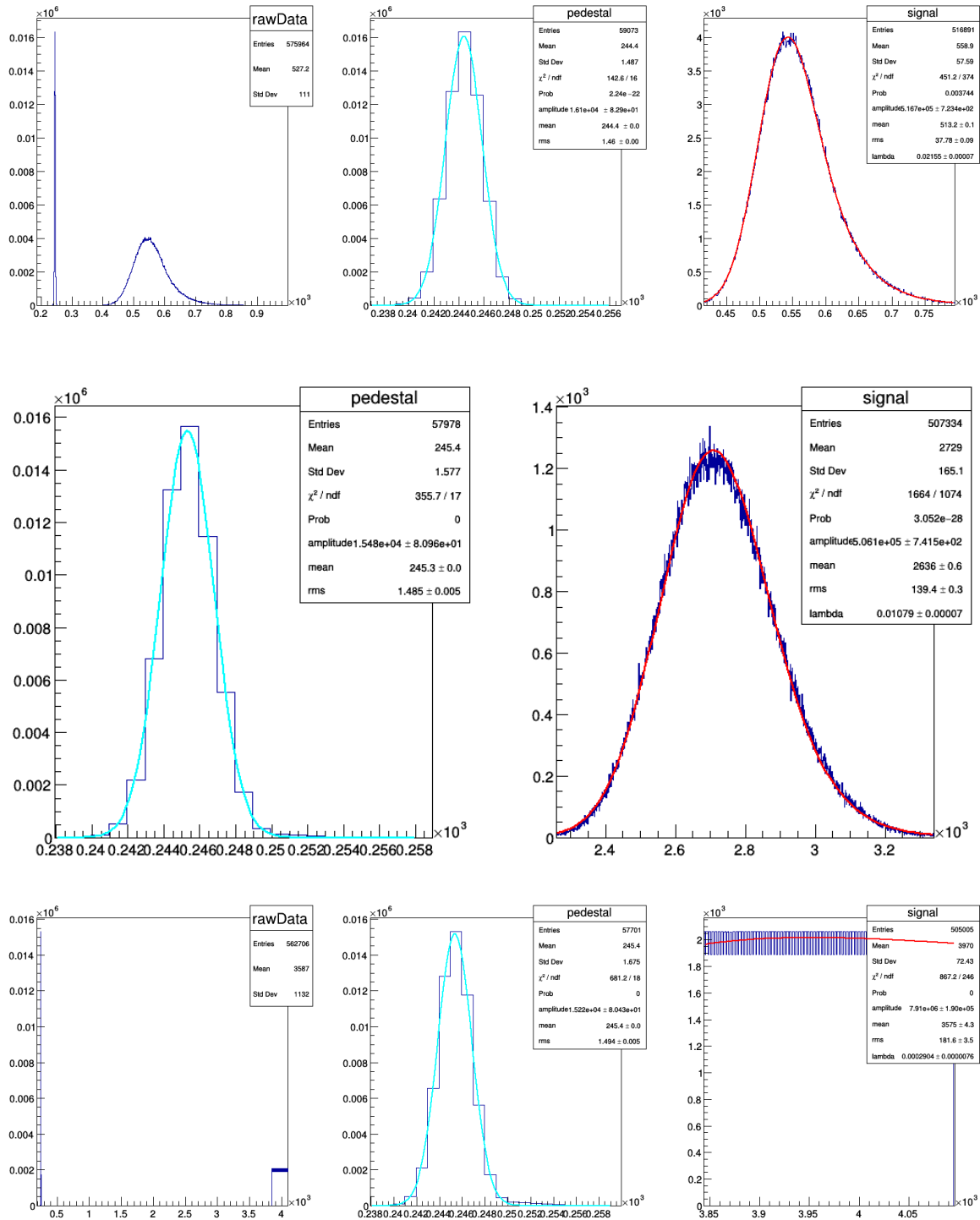


Figure 5.2: The first and second images are $\mu = 50$ and $\mu = 400$, and the fifth image shows ADC overflow around $\mu = 1,000$. Vertical axis represents counts. Horizontal axis gives signal size in units of ADC channels.

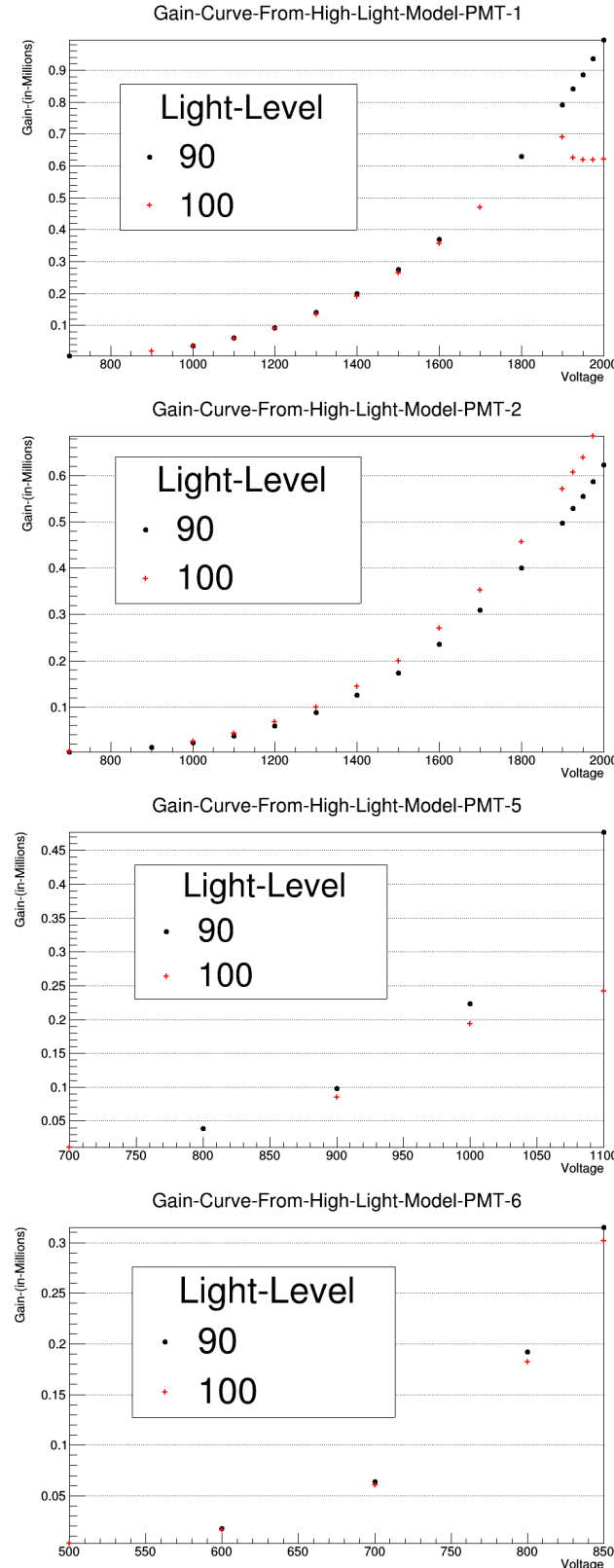


Figure 5.3: Gain curves from the high-light model for PMTs 1, 2, 5, and 6 (left to right starting on top). These results incorporate the light level calibrations for all PMTs at light level 90 and 100. No filtered runs are shown.

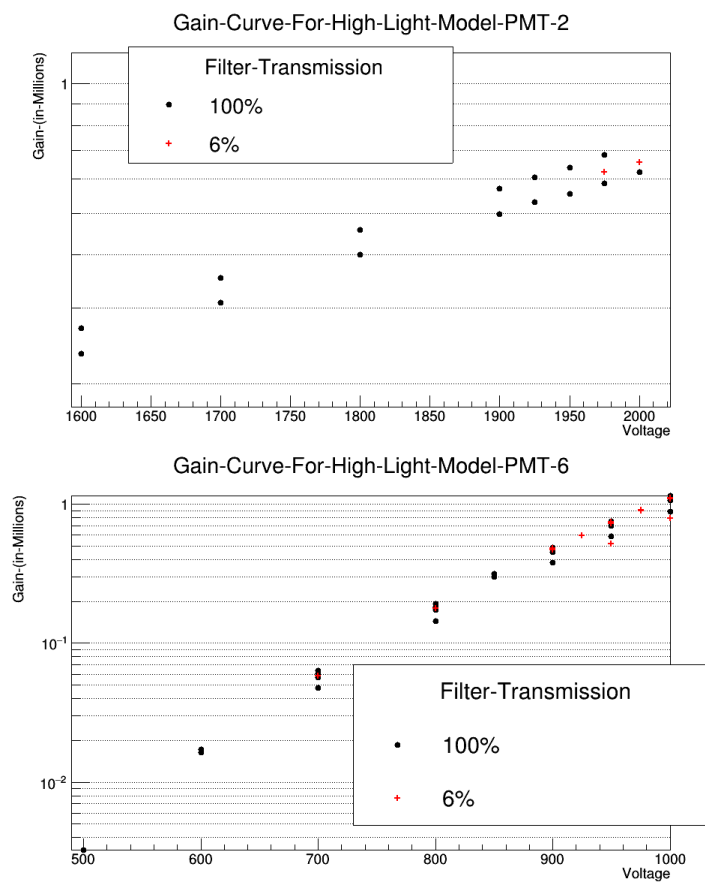


Figure 5.4: Results for the high-light model compared to the unfiltered results.

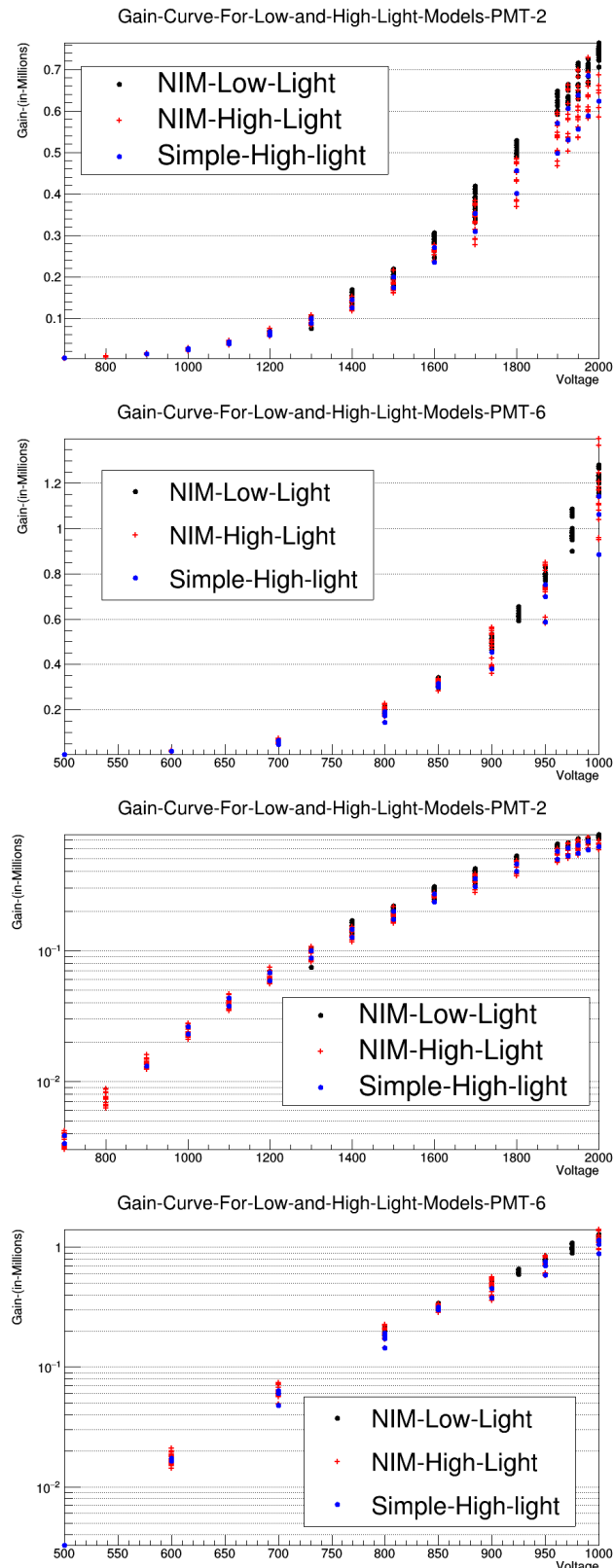


Figure 5.5: Gain curves resulting from one of three scenarios: the low-light model was used on low-light data, the low-light model was used on high-light data, or the high-light model was used on high-light data.

Chapter 6

Characterizing Cerenkov Detectors with PMTs

The work discussed in this thesis was performed to achieve the goals of PREx [1], CREx [2], MOLLER [3], and other future experiments exploiting the parity-violating asymmetry of the weak interaction. As discussed in Chapter 1, with a polarized target, the polarization of the incoming electron will affect the weak scattering cross-section whereas the electromagnetic scattering cross-section will be independent of polarization. Counting charged particles very precisely allows for the measurement of the asymmetry between the scattering cross-sections for the two polarization directions. This asymmetry, A_{PV} , then gives an indirect measurement of the neutron distribution of the target.

This chapter discusses the theory behind Cerenkov detectors, the design considerations, and final models used in this experiment. Results of the analysis of data acquired at Stanford Linear Accelerator Center (SLAC) is shown and discussed. The results are compared with Monte Carlo simulations.

Intro to Cerenkov Detectors

Cerenkov radiation is a type of braking radiation emitted when a charged particle travels through a medium, but in contrast to bremmstrahlung, this radiation is emitted continuously as the particle travels through the medium due to the vicinity of nuclei and bound electrons. Cerenkov radiation, like a sonic blast, is a pile-up of waves on a cone-shaped front due to some source traveling faster than the waves it is producing. Due to interactions with charged particles in the quartz, light can only travel through about two-thirds as fast as it can in vacuum. In contrast, massive particles continue through the quartz unimpeded, unless of course they scatter.

Cerenkov radiation, like a sonic blast, travels outward from the source at an angle determined by the particle's mass and momentum and the index of refraction of the medium.

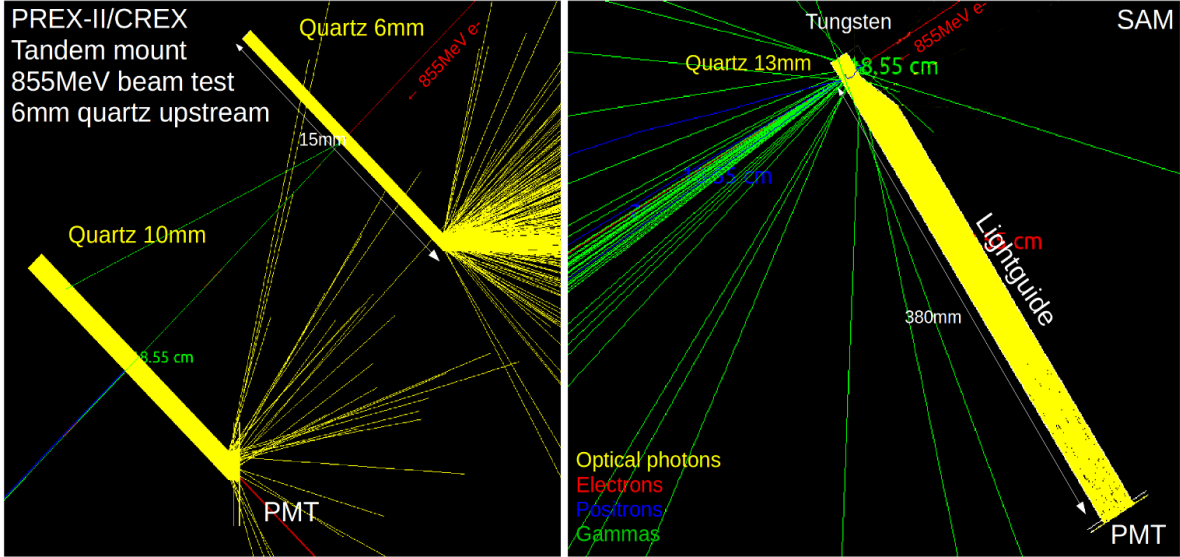


Figure 6.1: The left image shows the quartz pieces in the tandem detector with a single incident electron. The right image shows another quartz detector called the small angle monitor (SAM) which has a small piece of tungsten, a small piece of quartz, and a long light guide. The tandem simulation shows very little creation of secondary electrons and positrons from gamma production. All the light remains inside the quartz until it reaches the 45 degree bevel. The SAM image shows a large amount of gammas emerging from the thin piece of tungsten. Many photons are absorbed in the long light guide.

Figure 6.1 shows a particle traveling through a piece of quartz as well as the resulting radiation front. The 2 - 8 GeV scattered electrons expected in PREx and CREx will have a Cerenkov angle of about 45° . Thanks to the index of refraction of quartz, light traveling at 45° will be totally internally reflected and remain inside the rectangular quartz prism, as can be seen in the figure. A 45° bevel on one end of the quartz piece allows the Cerenkov radiation to exit normal to the quartz surface and head toward the PMT window. Approximately the same number of photons is produced every time a relativistic charged particle traverses a quartz piece; this makes counting charged particles easy¹.

Angle Dependence

Because Cerenkov radiation is emitted continuously as the electron travels, a longer path means more photons will be created in the quartz. A decrease in light is seen at the PMT.

¹Of course, it's never *that* easy; hadronic and photonic noise among other things must be accounted for.

Even with small angle changes, light will be lost out the sides of the quartz, and light that does exit the appropriate quartz face will be refracted away from the center of the PMT. Figure 6.2 shows the signal falling very quickly to zero, more quickly in one direction than the other. An angle of 5° is enough to drop the signal by 20%.

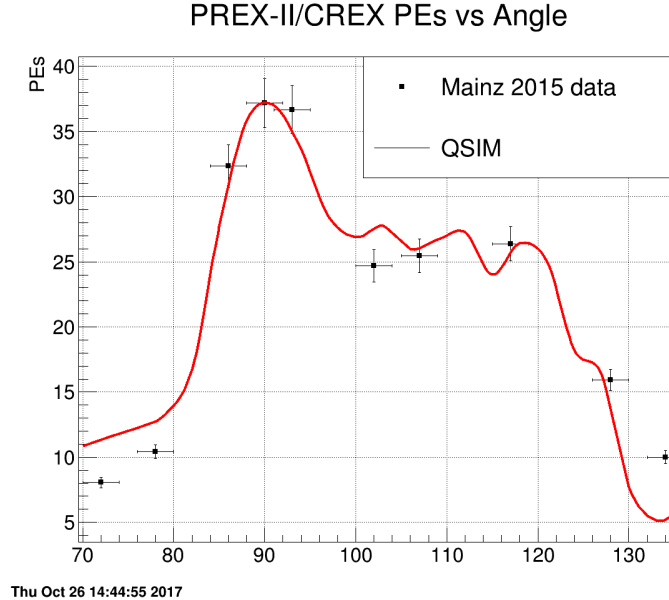


Figure 6.2: Angle dependence of the thin quartz detector response. The solid line shows results from a Monte Carlo simulation. The data points shown were collected at the Mainz Microtron beam in Germany [8, p. 69].

Quartz Requirements

The quartz crystals used in Cerenkov detectors must be nearly perfect. They are grown in a lab impurity-free, machine cut to size, and the sides are all polished. The polish must be very good to ensure total internal reflection of the entire signal. The polish on each piece of quartz is unique and must have its own value tuned in the Monte Carlo simulation for the detector. The polish parameter is near 99.9%, meaning that 0.1% light losses are expected for each reflection of a photon while traveling inside the quartz.

Thin Quartz

Thin quartz detectors are thin because any interactions that happen inside the quartz other than Cerenkov produce a large amount of noise. This includes interactions happening upstream of the quartz. The amount of material in the beam line is always minimized. The frame required to hold the quartz and PMT together will need to have a window for the beam to pass through. If the beam hits something upstream of the quartz, a shower will be produced, and more particles will go through the quartz at odd angles and speeds. For this same reason, the thin quartz detectors are placed upstream of the other detectors in the experiment.

Tandem Design

One thin quartz detector design, named the Tandem detector, is shown in figure 6.3. This detector has two pieces of thin quartz; the upstream quartz is 6 mm thick, and the downstream quartz is 10 mm thick. These two slabs each have their own 2" PMT receiving their photons. This gives two very clean signals for counting.

Because the photons come out of a 45° bevel, the detector body must mount the PMT in this way with respect to the quartz. The detector has a metal face plate that acts like a base for the detector body. The PMT attaches to one side of the face plate via 3D printed attachment mechanism. To the other side of the face plate mounts some aluminum rails with a clamping system for holding the quartz in place. A 3D printed custom plastic shell was made that surrounds the quartz and rails, and is mounted to the face plate. This shell protects the quartz from any damage while also blocking stray light. Because the radiation hardness of our plastic is unknown, a window is printed into our shell for the beam to pass through; this window is covered with Kapton which is often used in beam.

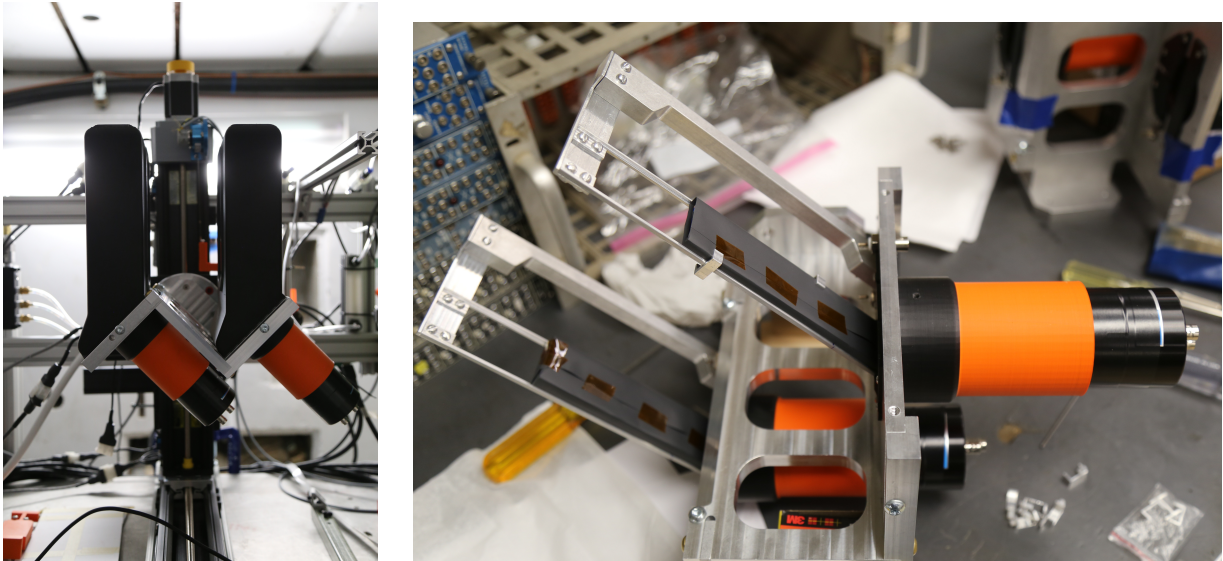


Figure 6.3: Pictured here is the Tandem detector. On the left, the detector is mounted on a rotary stage mounted to horizontal and vertical mobile platforms in the beam line. On the right, the inside of the detector is shown with quartz clamped into place and wrapped with kapton.

Tandem Data

Figure 6.4 gives an example of the PMT response from single electron data taken at SLAC. The electron beam was filtered through a copper slug from hundreds of electrons per bunch to 1-5 electrons per bunch. The filtering process used gives rise to a Poisson distribution, but this time the distribution describes the number of electrons incident on the quartz. This means that the 1-electron, 2-electron, 3-electron, etc. peaks are correlated. This makes it easy to incorporate all of the peaks in the fit rather than just considering the first peak.

The fit in Figure 6.4 is very similar to the low-light data, but now, μ refers to the average number of incident electrons hitting the quartz and Q_1 now represents the "gain" of the quartz detector. Q_1 still gives the fixed separation between the peaks. Each electron that travels through the quartz produces some number of photons on average, and some portion of those photons make it to the photo-cathode. The photons that make it to the photo-cathode kick out some photo-electrons according to the quantum efficiency of the PMT. These PEs will then be amplified inside the PMT according to the gain of the tube.

The millions of electrons that come out of the PMT go into the ADC and are recorded as hundreds or thousands of channels. Equation 6.1 puts this chain of events into a single statement:

$$Q_1(\text{channels}) = 1(\text{electron}) * N_\gamma * QE * G_{PMT} * F_{ADC}, \quad (6.1)$$

where N_γ is the average number of photons per incident electron, QE is the quantum efficiency, G_{PMT} is the gain of the PMT, and F_{ADC} is the ADC conversion factor (channels per unit charge).

The average number of photo-electrons created per incident electron is then calculated by:

$$n_\gamma = N_\gamma * QE = \frac{Q_1}{G_{PMT} * F_{ADC}} \quad (6.2)$$

ShowerMax Detector

While the thin quartz detector wants a single electron and a very clean signal, the ShowerMax detector embraces the shower. The term "shower" refers to the electromagnetic cascade of particles that is produced when an energetic charged lepton plows through dense matter. All ShowerMax discussions will be in reference to Daniel Sluder's thesis [8]. This detector is shown in Figure 6.5.

The ShowerMax detector consists of repeated stacks of tungsten and quartz. The tungsten slabs act as radiators; when one electron enters the tungsten, tens or hundreds of electrons and positrons come out the back. Each of these hundreds of charged particles will then travel through a piece of quartz and emit Cerenkov radiation. The ShowerMax 1A design uses 6 mm quartz pieces while the 1B design uses 10 mm thick quartz. Both designs use 8mm thick tungsten pieces. The vertical and horizontal dimensions of the detectors are referred to as the radial and azimuthal directions, radial meaning the radial distance from

the beam line. In the radial dimension, the quartz and tungsten pieces are 105 mm tall.² In the azimuthal direction, the material is 246 mm wide. The light guides are very important in these designs; even with them, the photon yields are low due to the distance from PMT to quartz.

The electromagnetic shower is most regular and predictable when allowed to grow to a maximum; showers resulting from sending electrons through a thin piece of tungsten are highly variable. The ShowerMax places multiple stacks of tungsten and quartz in a row to allow the shower to grow to its maximum radius, hence the detector name. The Cerenkov radiation leaves these pieces of quartz and must be reflected to the PMT by a light guide due to the orientation of the quartz. Figure 6.6 shows a simulation of a ShowerMax event as well as the expected signal sizes and resolutions from incident electrons with different energies. Higher energy electrons create more light and give a sharper peak, resulting in better detector resolution at those energies. The term 'resolution' here means the RMS divided by the mean of the distribution observed with a single incident electron. This resolution can be calculated very easily from simulated results, but the distributions gathered at SLAC include responses from 0-, 2-, 3-, etc. incident electrons. The resolution can only be estimated from this data.

ShowerMax Data

The ShowerMax is a calorimeter; unlike thin quartz, the light yield increases with particle energy in the ShowerMax. This means it is less susceptible to hadronic backgrounds than thin quartz [8, p. 8]. These two detectors, among others, will provide the ability to count precisely while accurately identifying background sources. Data from ShowerMax prototypes 1A and 1B is shown in Figure 6.7. The plots in this figure seem to imply that the same amount of light is produced by an electron of 5.5 GeV as one of 8 GeV. This is not expected and could indicate an error in electron energy, voltage, or perhaps a design flaw. Whatever the reason, the simulated results differ from the real data. The photo-electron yield and

²The bevel of the quartz pieces begin at 105 mm and extend out as far as they need to.

resolution estimates can be compared to Figure 6.6 above.

The average number of photo-electrons observed for an electron incident on the ShowerMax is also different from the simulation prediction. The observed number of PEs for configuration 1A is about 308 for both 5.5 GeV and 8 GeV electrons. The simulation predicts over 800 PEs for ShowerMax 1A with 5.5 GeV electrons, and it predicts over 1,000 PEs for 8 GeV electrons! This could be due to an error in the simulated light guide geometries, a flaw in the bending and assembling of the light guide, or even a non-homogeneous quantum efficiency near the edges of the PMT. Recall that each of the 4 pieces of quartz are sampling the shower at different stages in its development. The last quartz piece samples the shower at its maximum. If the light from the last piece of quartz does not make it to the PMT, then the signal would be significantly smaller and noisier. This would especially be true for the higher energy electrons which reach their shower maximum in the last piece of tungsten.

Benchmarking Apparatus

In order to measure what is happening to the signal as the amount of tungsten and quartz is increased, another apparatus was designed and 3D printed, called the benchmarking apparatus, and is shown in Figure 6.8. The benchmarking apparatus places the quartz much closer to the PMT window resulting in much more light yield than the full-scale ShowerMax. The benchmarking design allows for quick and easy loading and unloading of quartz and tungsten slabs.

Using this detector, electron beam data was collected using a single piece of quartz with no tungsten (effectively a thin quartz measurement) as well as with a single piece of quartz AND tungsten, two pieces of quartz and tungsten, three pieces of each, and four pieces of each. Four stacks of tungsten and quartz is considered a "full" stack, where the shower will grow to its maximum. Simulations have shown that this is where the resolution of the detector should reach a minimum. Like the ShowerMax, the benchmarking 1A and 1B use 10 mm and 6 mm thick quartz pieces, respectively, and 8 mm thick tungsten pieces. Unlike

the full-scale detector, though, the benchmarking material is only 80 mm tall by 40 mm wide (radial and azimuthal).

Benchmarking Data Using Gain Measurements

Data was collected for at least one voltage setting for each of the 1A and 1B benchmarking configurations. Figure 6.9 compares data collected with the benchmark 1A detector without (left) and with (right) tungsten. Without tungsten, approximately 80 photo-electrons are observed for all three voltages shown. Without tungsten, the signal resolution is good (around 13%). With a single piece of tungsten, the resolution skyrockets to around 70%; this is due to the high variation of an under-developed shower. Recall that the 1A detector uses 6 mm thick quartz pieces.

Notice that the x -axis on these plots are in photo-electrons instead of channels; this transformation was made using the gain measurements from earlier chapters. It would be better to know the absolute number of photons coming out of the quartz, but this would require a measurement of the quantum efficiency. The quartz simulation can assume the quantum efficiency reported by the PMT manufacturer in order to estimate the number of expected photo-electrons, and this can be directly compared to plots such as these.

Also notice that the 1,100 volt data seems to differ from the others; this could be a statistical fluctuation of the data or positioning of the detector, but it could also be a problem with the gain of the PMT at that voltage. This is exactly why it is so important to know the gain precisely and to know the error on the gain measurement. The right plot shows again that the 1,100 volt data gives about a 7% larger PE yield than the 1,200 volt data. This is right around the uncertainty of the gain measurement. Taking a look at data from the 1B benchmarking configurations with 2 and 3 stacks in Figure 6.10, the same trend is not seen. For two stacks, the 1,200 volt measurements are in near-perfect agreement with the 1,100 volt data. The three stack data also shows great agreement down to 1,000 volts. The gain is around 200,000 for 1,000 volts and around 900,000 for 1,200 volts. The resolution

of these data runs is much better than for a single stack; two stacks gives resolution around 30% while three stacks drops to 20%. Recall that the 1B detector uses 10 mm thick quartz pieces.

Now, look at the 1B data with 3 stacks again in Figure 6.10. The first peak represents all events corresponding to a single electron going through the stack. The second peak represents the 2-electron events. The fact that this peak lies right at 4,700 PEs (twice the value in the 1-electron peak) proves that the PMT is not experiencing any saturation effects for at least up to 5,000 PEs for up to 1,100 volts. The 2 stack data shows the same thing for up to 1,200 volts.

Figure 6.11 compares the benchmarking detector response using a full stack for 3.0 GeV, 5.5 GeV, and 8.0 GeV electrons. These plots show a clear energy dependence on the signal; these benchmarking detectors can easily differentiate 3 and 6 GeV electrons. Looking at the 8 GeV data shows that the PMT gain measurement is valid for up to 12,000 PEs at 900 V where the gain is around 100,000. The resolution estimate (Sigma / Mean) is decreasing with higher energy electrons as predicted by simulation. These plots also give confidence that there is no PMT saturation for over 10,000 PEs at around 200,000 gain for PMT 5.

Comparison With Simulation

The data seen in 6.9 can be compared to the blue curve in 6.12. Unfortunately, the simulation was performed using 5 GeV while the data was taken with 5.5 GeV electrons. The real data should be slightly higher than what was predicted for 5 GeV. Coincidentally, the number of PEs predicted and observed are very close for both the thin quartz and the quartz with radiator plots. Without a radiator, the PMT generates around 85 PEs, and with a radiator, around 950 PEs are generated. The estimated resolution on the thin quartz measurement is too low to be correct. The other resolution estimate seems too high, but may actually be too low as well. This gives more confidence in the hypothesis that the light guide (simulated or real) may have some misunderstood or unknown issue.

Figure 6.13 shows the expected result of using 2, 3, and 4 stacks of quartz and tungsten. The signal size grows while the resolution decreases in the simulated results. The plot showing the full 4-stack configuration can be compared to Figure 6.11 (the left plot). Again, be aware that the simulated energies are NOT the exact energies used while collecting data. Distributions were simulated for 2, 5, and 8 GeV incident electrons while the real data show 3, 5.5, and 8 GeV results. Notice again that the 5 GeV prediction matches quite well with the 5.5 GeV data. The yield from 8 GeV electrons falls a couple hundred PEs short of what was predicted for that energy.

Future Studies

The gain calibrations discussed in the previous chapters is sufficient for characterizing these Cerenkov detectors, but it could be improved upon. As discussed in Chapter 4, the light level calibration has conflicting evidence of the behavior of the tubes at high light levels. This problem could be solved by using Cerenkov detectors themselves as the light source instead of an LED with filters. Alternatively, precisely calibrated filters could also solve the issue (or any other calibrated light source). The Cerenkov detectors deliver a predictable amount of light relative to the 1-electron signal. This means that once the light level from a single piece of quartz with a single incident electron is calibrated with high precision, the higher light levels observed with more incident electrons can be used to characterize the PMT gains at lower voltages. Decreasing the error in the light level calibration decreases the error in the subsequent low-voltage gain measurements.

The wavelength of the incident light was not considered in this work. PMTs behave differently with different wavelengths of light incident upon the photo-cathode. The quantum efficiency can change if the incident light causes double PE ejection too frequently. The light source used to perform the gain measurement was all visible light near the violet end of the spectrum while the light emitted from the quartz pieces contains a significant amount of UV radiation. The spectrum of the light emitted from the quartz could be measured, and the

observed light level of the PMTs could be calibrated for different colors of incident light.

The angle of incidence of light upon the photo-cathode was also not studied here. Small angles were used in the gain calibrations. The light was directed straight at the cathode, and a diffuser was used which introduced some distribution of angles. The incident angle of photons can affect the quantum efficiency of the cathode which will affect the observed light level. The Tandem detector sees light of predominantly normal incidence, the benchmarking sees mainly light incident at an angle of 45° , and the full-scale ShowerMax sees predominantly angles between normal and 45° . Measuring observed light level for different distributions of incident angles would quantify differences in detector responses.

The quantum efficiency itself was also not studied in this work. The quantum efficiency is assumed to be equal for all tubes of the same model. The value used for quantum efficiency is that delivered by the tube manufacturer. Of course, the quantum efficiency of each tube is unique. It is unknown what the percent deviation is between these different QE values. Using the quartz Cerenkov detectors with different PMTs allows for the comparision of relative QE values. This study would give a quantifiable estimate of the error introduced from QE differences.

Further investigation into the feature observed in the high-energy tail of the PMT distribution could result in certainty of one model over another. Discovering how to fit this artifact would reduce the uncertainty in all of the gain measurements and light level calibrations, and it would also decrease the error in fitting the Cerenkov detector responses. This may be especially important for fitting the electron beam data from the Cerenkov detectors since this data also exhibits a Landau tail at the high-energy end of the spectrum. This Landau tail, characteristic of particle interactions, should be incorporated into the model in order to reduce uncertainty in detector response and resoultion estimates.

The full-scale ShowerMax detector disagrees with simulation significantly more than any of the other detectors. This discrepancy is believed to be caused by misunderstanding the light guide. Trying different light guide designs and materials could shine light on this

misunderstanding. If there is some mechanical error in the light guide construction or mounting, then this could be verified by trying different bends, positioning, etc. Creating a small light guide for the benchmarking apparatus would give the ability to study small, simple light guides. The dark box apparatus used to measure gain could also be used to perform light level tests of the light guides in the lab without requiring electron beam.

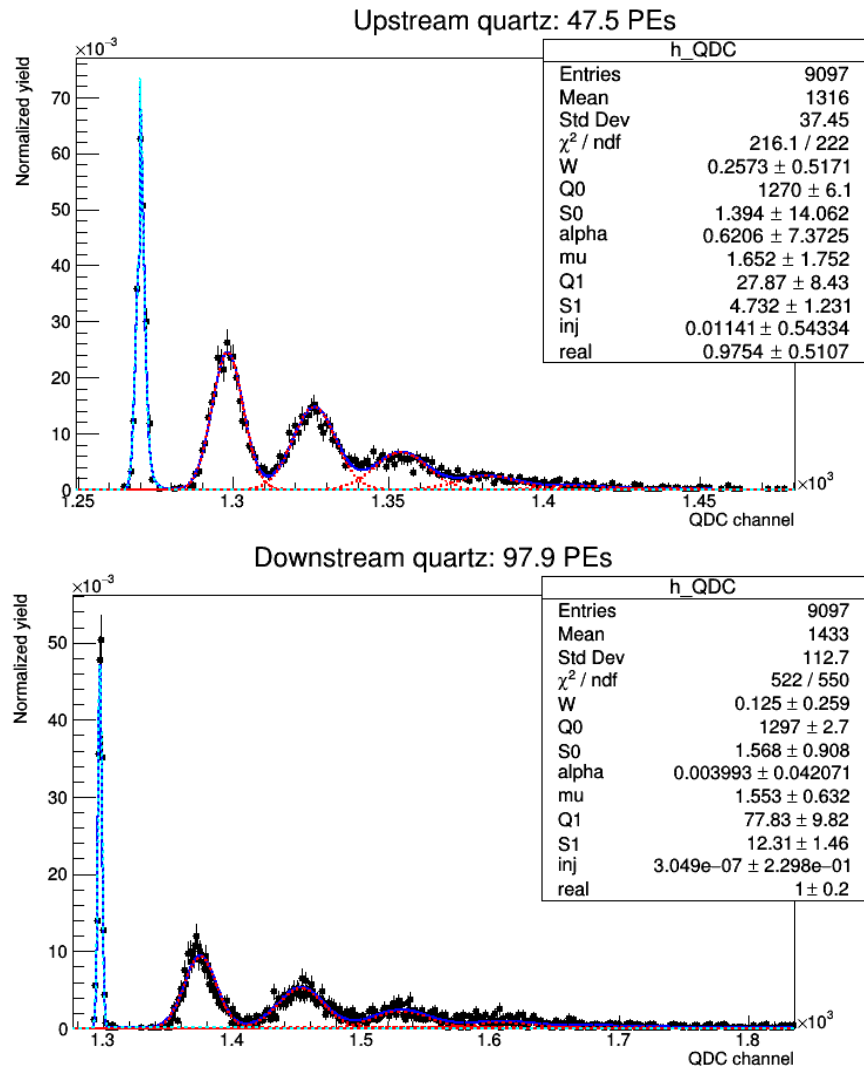


Figure 6.4: Tandem detector data. PMT 2 was used for the upstream signal, PMT 1 for the downstream, both at 2,000 volts. The average number of photo-electrons per electron is shown in the plot title; this number is calculated using the gain of the PMTs measured earlier in the thesis.



Figure 6.5: ShowerMax stack of tungsten and quartz (left) and the fully-assembled 1A and 1B ShowerMax prototypes (right). The quartz is wrapped in kapton, like in the Tandem detector.

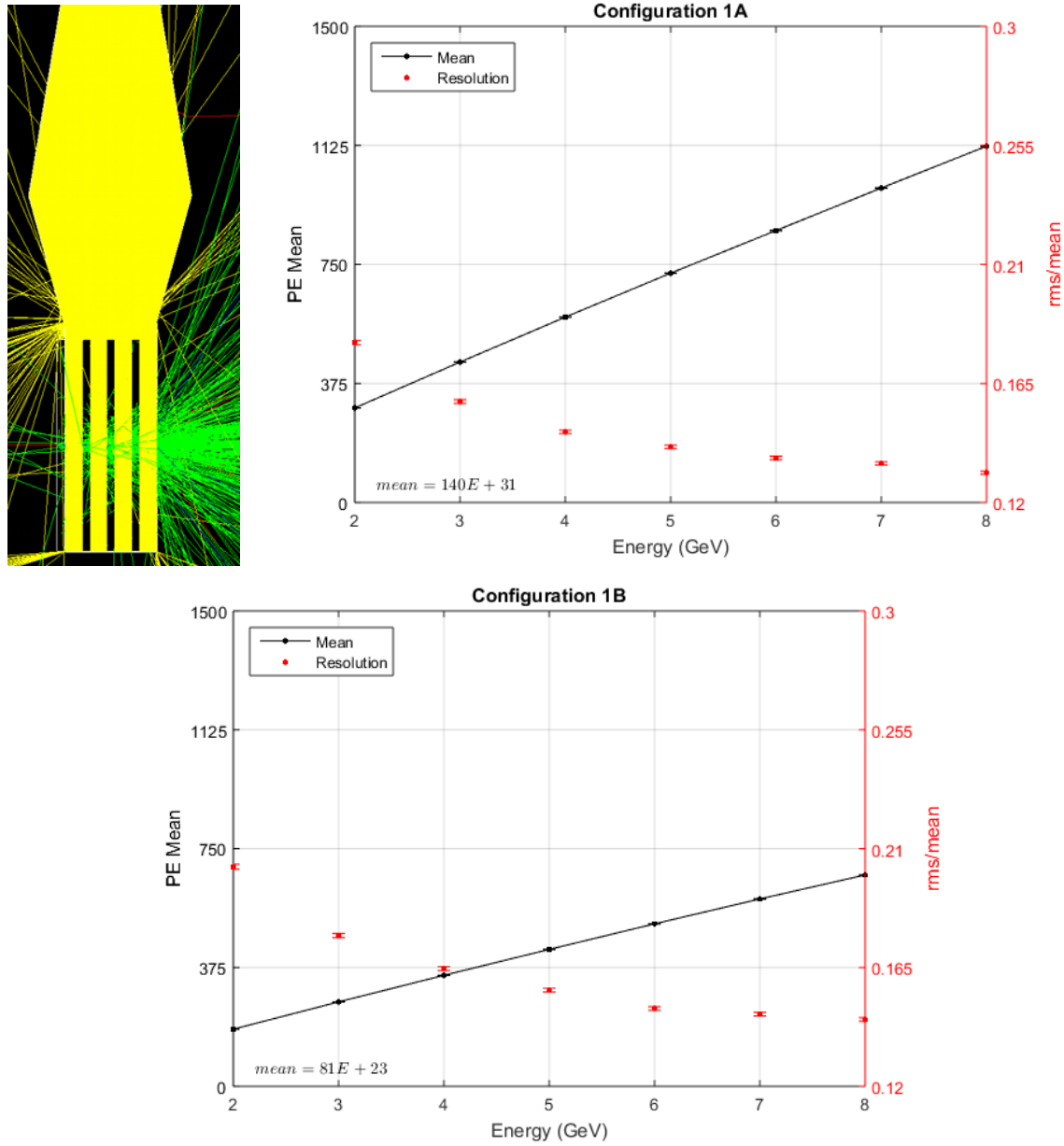


Figure 6.6: The image shown here is a simulation of an electron incident on the ShowerMax resulting in gammas (green) and photons (yellow). The plots show the PMT response (in PEs) as well as the detector resolution as a function of incident electron energy [8, p. 49].

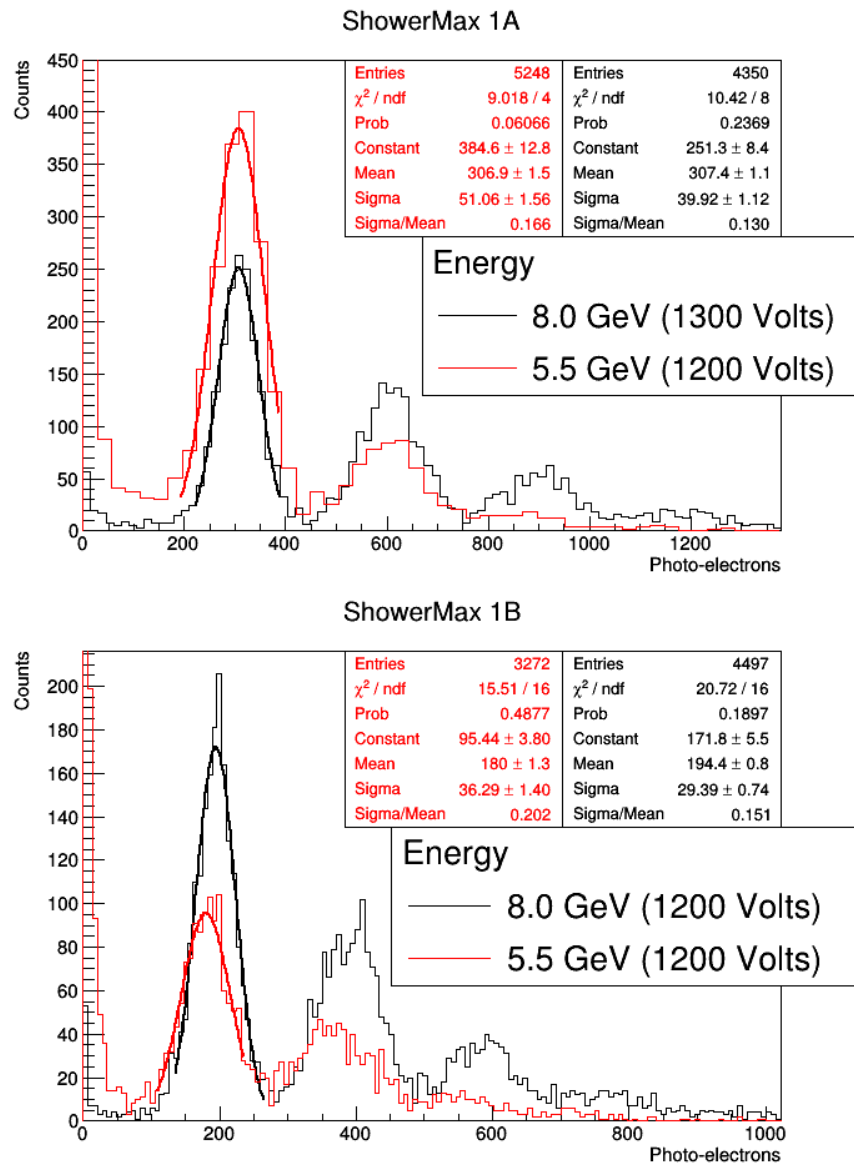


Figure 6.7: These plots show the PE yield from electron beam data with the ShowerMax full-scale prototypes 1A and 1B. The plots x-axes have been converted from ADC channels to PEs using the gain measurements performed earlier.

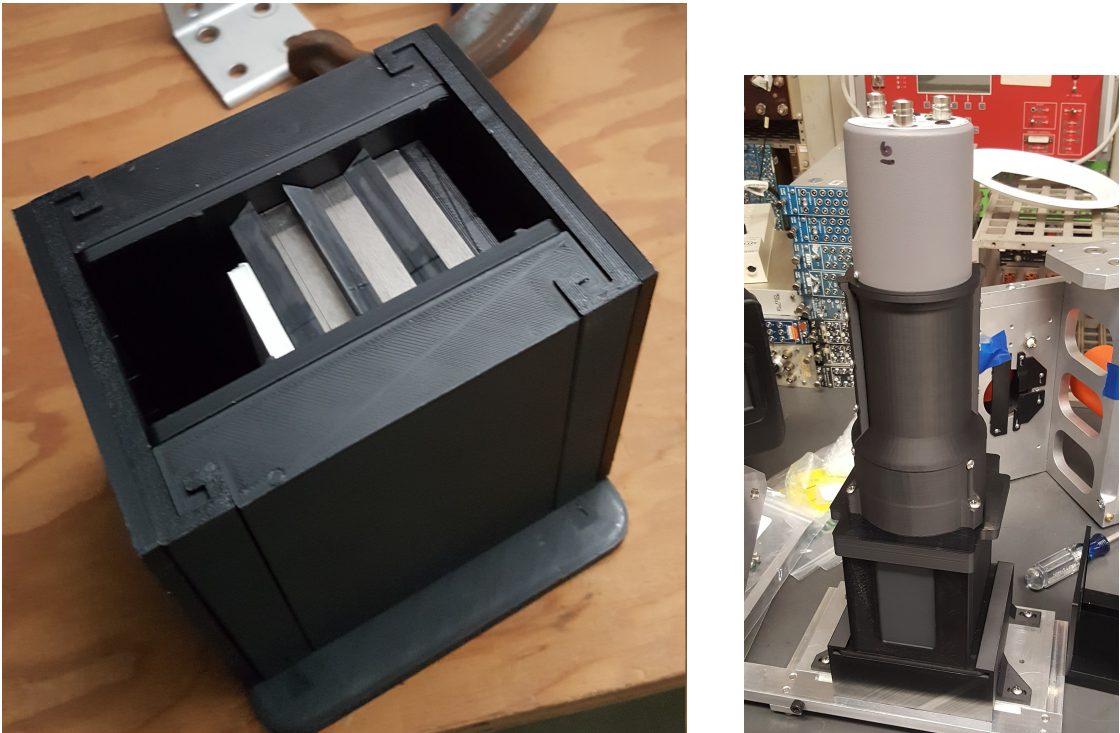
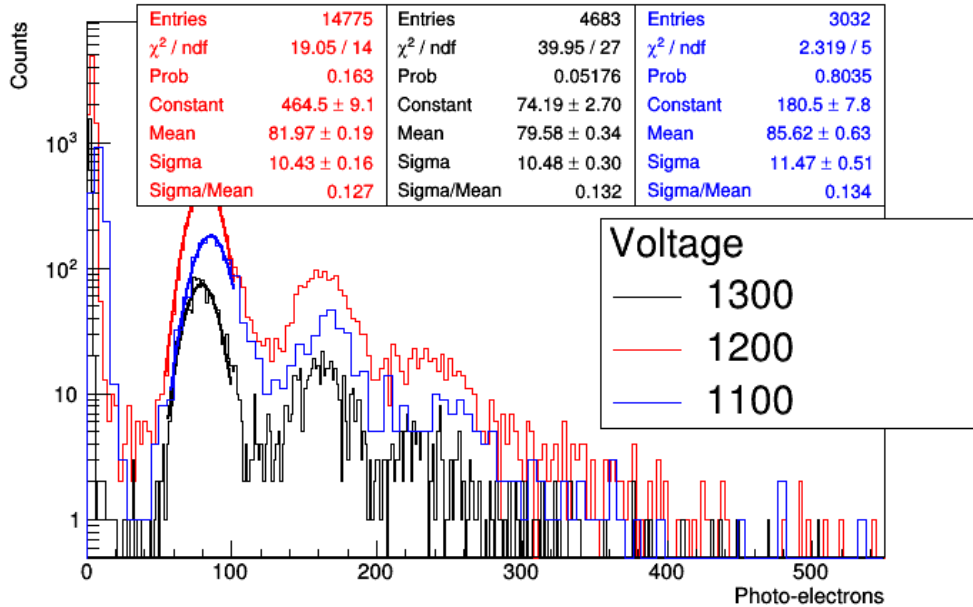


Figure 6.8: The left image shows the stacks inside the benchmarking apparatus. The right image shows a 3" PMT in its 3D printed sleeve attached to the apparatus.

Benchmarking 1A (5.5 GeV): no tungsten



Benchmarking 1A (5.5 GeV): 1 tungsten

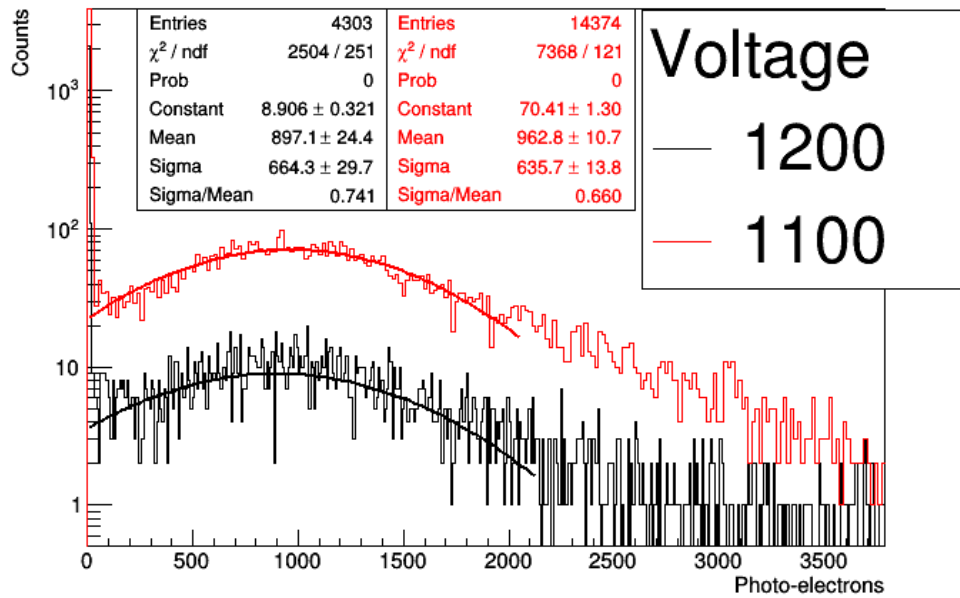
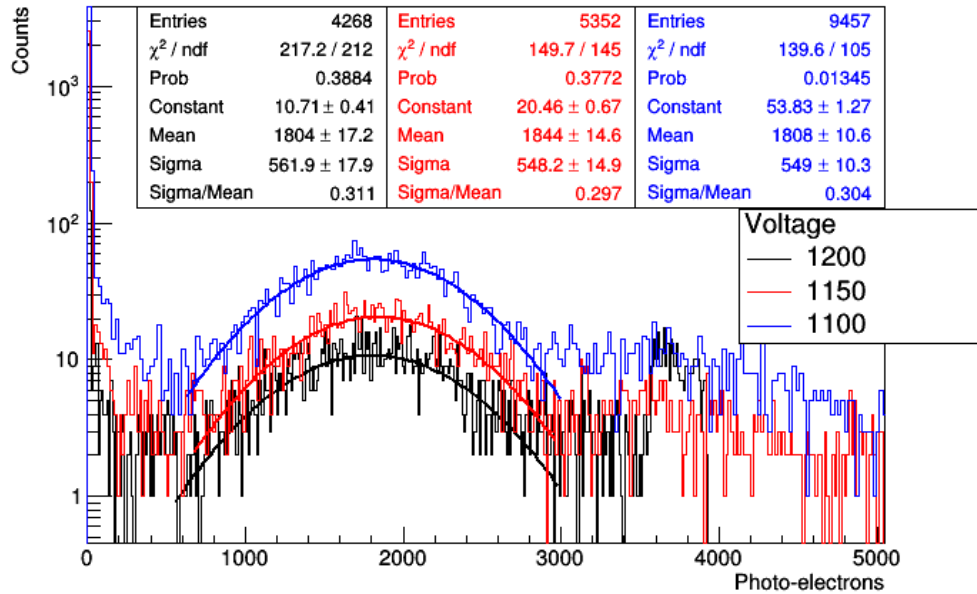


Figure 6.9: These plots compare the PE yield from a single piece of quartz without/with a tungsten piece.

Benchmarking 1B (5.5 GeV): 2 tungsten



Benchmarking 1B (5.5 GeV): 3 tungsten

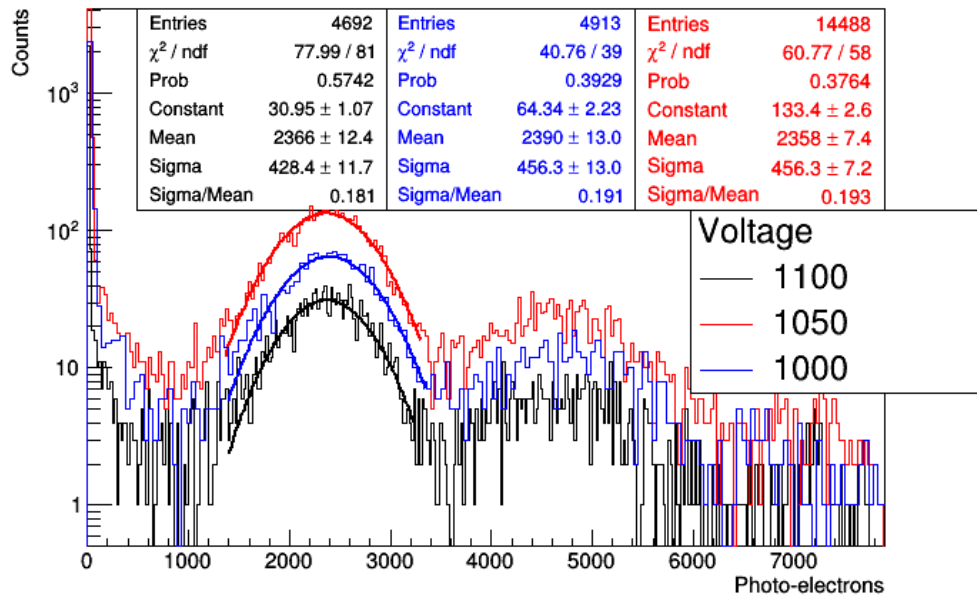
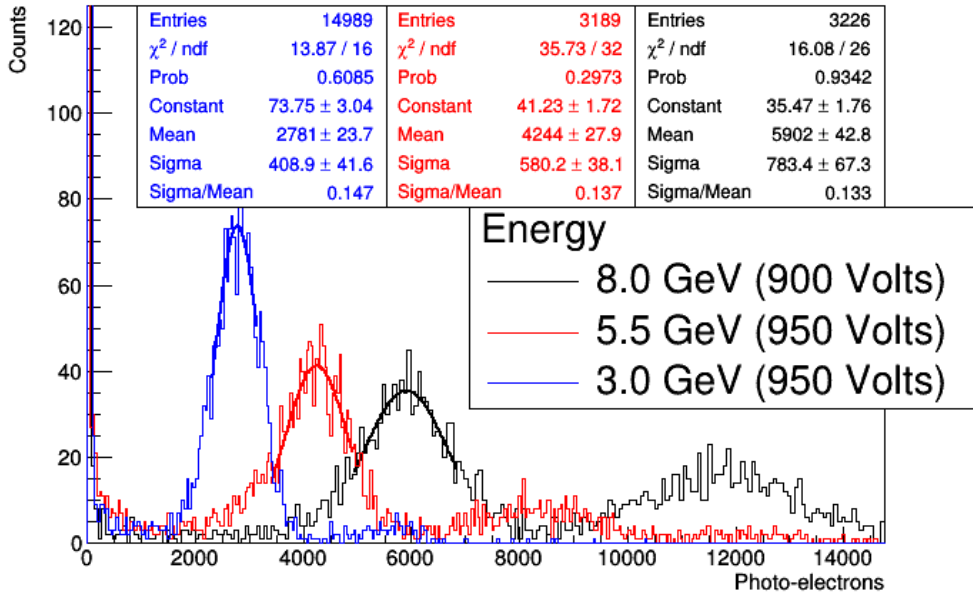


Figure 6.10: These plots compare the PE yield from two and three stacks of quartz and tungsten.

Benchmarking 1A: Full stack



Benchmarking 1B: Full stack

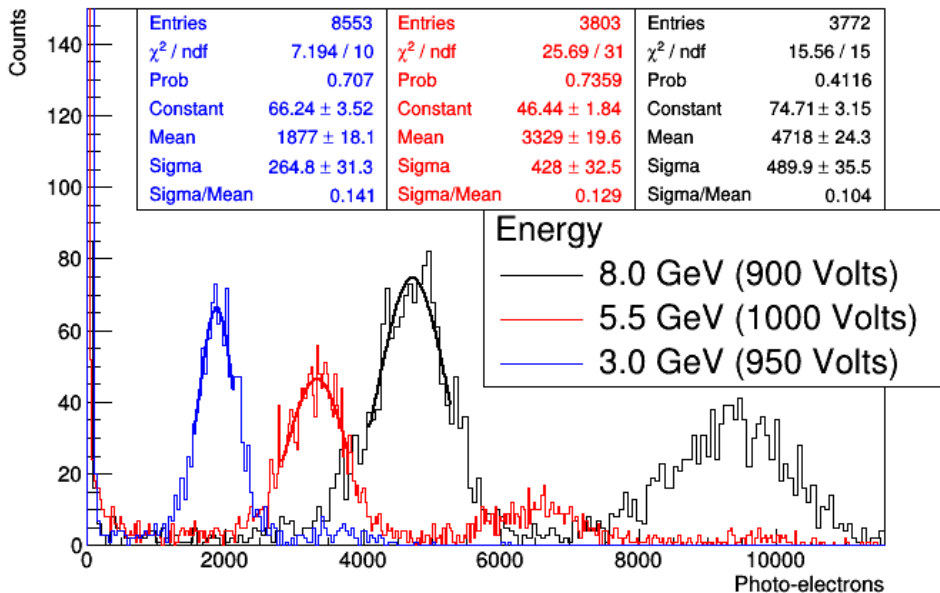
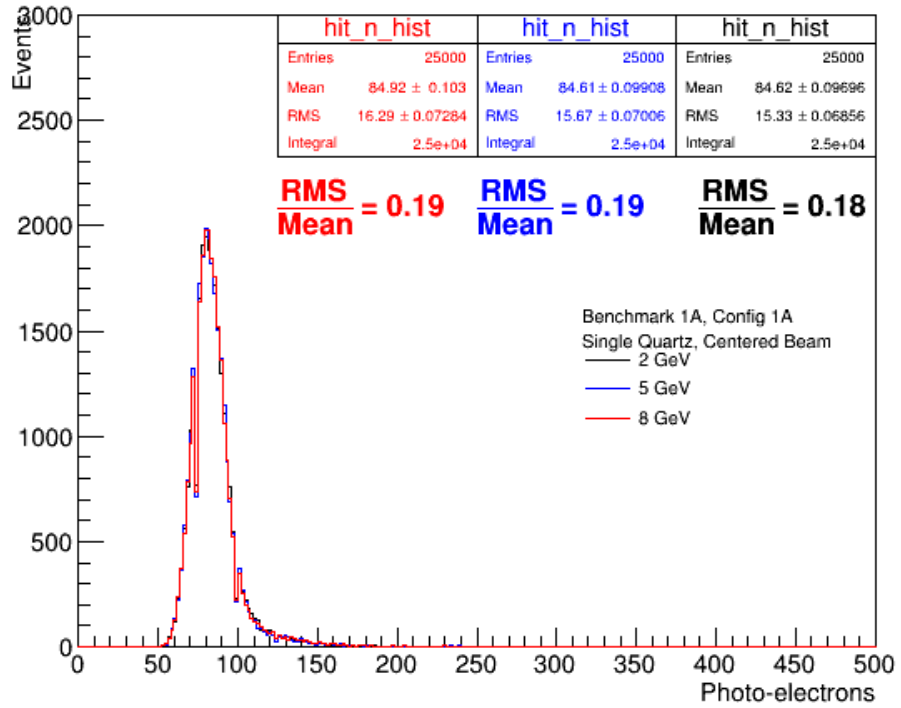


Figure 6.11: These plots show the energy dependence of the signal obtained by the ShowerMax design; more energetic electrons create more secondary particles. In each of the runs shown, the beam was near the middle of the quartz in both directions. Notice that the resolution of the detectors decrease as energy increases.

Benchmark 1A: Single Quartz



Benchmark 1A: n=1

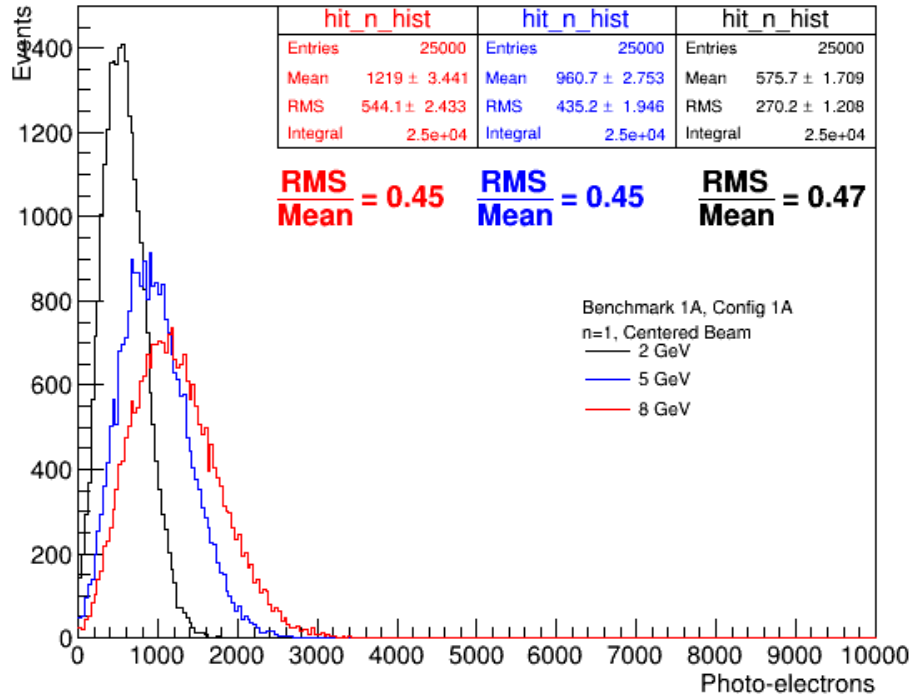


Figure 6.12: The left plot shows the signal distribution using only a piece of quartz and no tungsten (thin quartz). The right plot shows how the signal changes when introducing a single tungsten radiator (1 stack). The number of photons is greatly increased with a radiator, as is the resolution.

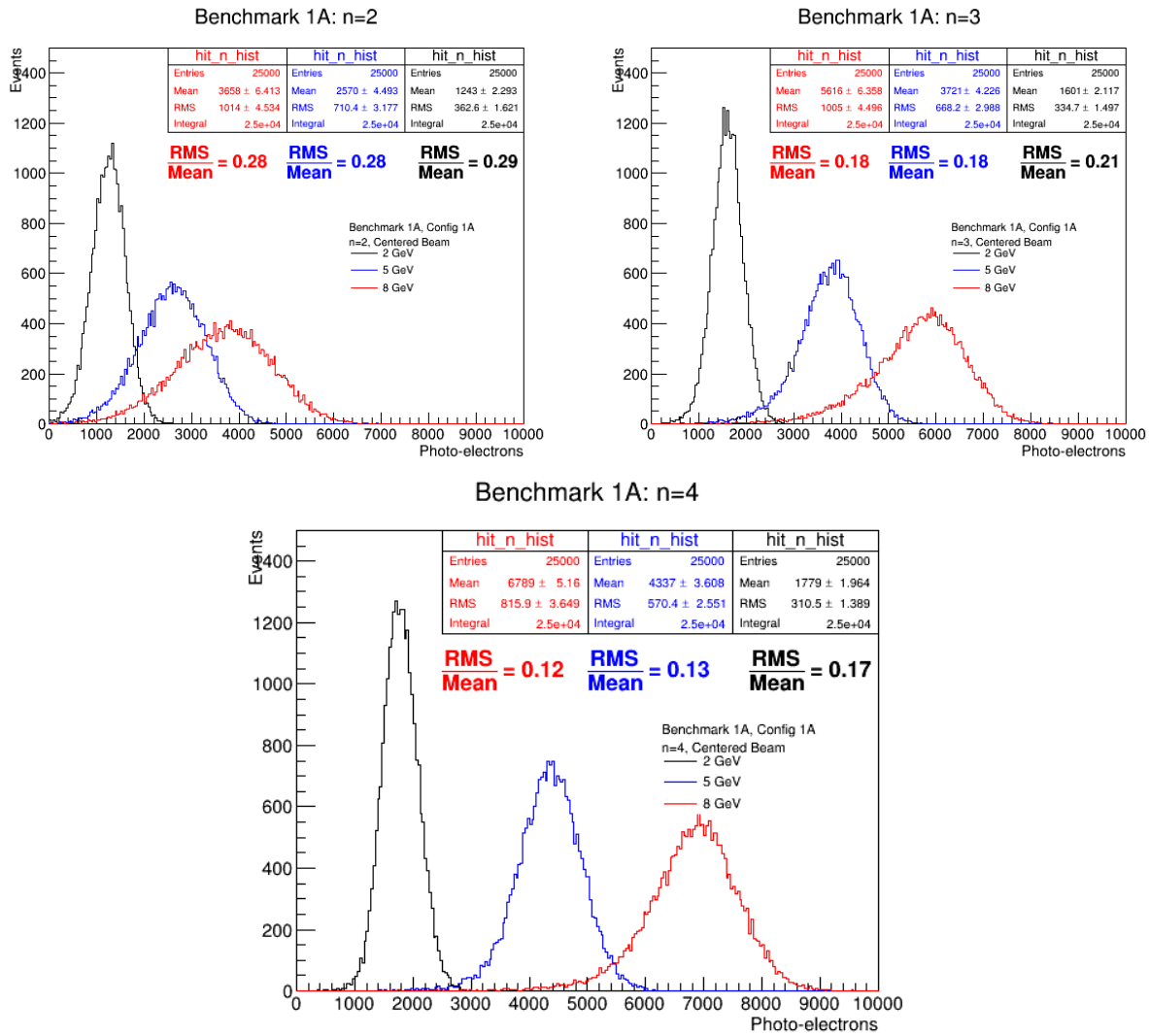


Figure 6.13: These three plots show the PMT response using 2 stacks, 3 stacks, and 4 stacks.

Bibliography

- [1] K. Paschke et al. “PREX-II: Precision Parity-Violating Measurement of the Neutron Skin of Lead”. In: *Proposal to Jefferson Lab PAC 38* (2011).
- [2] J. Mammei et al. “CREX: Parity-Violating Measurement of the Weak Charge Distribution of ^{48}Ca to 0.02 fm Accuracy”. In: *Proposal to Jefferson Lab PAC 40* (2013).
- [3] J. Benesch et al. “The MOLLER Experiment, An Ultra-precise Measurement of the Weak Mixing Angle using Moller Scattering”. In: *Proposal to Jefferson Lab PAC 37* E12-09-005 (2010).
- [4] Wikipedia. *Photomultiplier tube*. 2019. URL: https://en.wikipedia.org/wiki/Photomultiplier_tube.
- [5] Jake Bobowski. *Monte Carlo PMT Simulation*. 2012. URL: <https://people.ok.ubc.ca/jbobowsk/Maple/Monte%20Carlo%20PMT%20simulation.pdf>.
- [6] E.H. Bellamy et al. “Absolute calibration and monitoring of a spectrometric channel using a photomultiplier”. In: *Nucl. Instrum. Meth.* A339 (1994), pp. 468–476.
- [7] CAEN. *Technical Information Manual: Mod. V965/V965A*. technical manual. 2005.
- [8] Daniel Sluder. *ShowerMax: An Electromagnetic Calorimeter for Independent Measurement of the Parity-Violating Asymmetry in Møller Scattering*. Master’s Thesis. 2018.

Appendix A

Gain Measurement Software

Most of the mathematics used in this work was computed in Cern's Root C++ interpreter (version 6.15). Root uses C++ to define objects such as histograms, graphs, functions, canvases, trees, etc. which are used to structure, preprocess, and analyze data. Table A.1 lists the names of the objects used along with some other information.

Name	Object Type	Description of Use
TTree	Ordered set of sets	Used to store all information of all events in one data run
TLeaf	Numeric type	Single ADC value from a single channel)
TF1	1-D Function	Arbitrary function of 1 independent variable and N parameters
TH1F	1-D Histogram	The ADC events are sorted by size into 4096 bins
TCanvas	Window object	For drawing and interacting with histograms and functions

Table A.1

Each data run consists of some number of events; those events are recorded as a single number between 0 and 4095 by the ADC. These numbers are put into bins in a histogram based on their ADC value. This forms the distribution with Gaussian peaks, exponential tails, etc.

Some mathematical model is defined as a function with some number of parameters (Chapter 2). That model is drawn on the same axes as the histogram, and the parameters in the function are incrementally changed until the shape of the function matches the shape of the distribution as well as possible. The degree to which the shapes match is determined by calculating the distance between the distribution and function at each point in the fit range. This iterative minimization algorithm is built into the TH1F histogram object in Root. A given 1-D histogram can be fit with a given TF1 function object. Built into this minimization algorithm is statistical functions for calculating correlations between parameters as well as estimating the error on the predicted parameters.

Several fitting functions were defined and tested, but only a few were used to create the final results. Table A.2 lists the fitting functions defined and what they were used for.

Low-Light model is the main model for measuring gain in this thesis. It has some variants which allow for investigation into whether or not the distribution shows exponential decay. The triple-Gaussian pedestal function is a simple sum of three different Gaussians which models three separate Gaussian processes feeding the ADC value. The high-light model uses a simple Gaussian for the pedestal and a modified Gaussian for the signal; the signal Gaussian is convoluted with a decaying exponential starting at the Gaussian mean.

Model	# Par.	Description
Low-Light (no expo)	5	Measures the gain and light level of low-light PMT data
Low-Light	7	Same as above, but also measures exponential decay
Low-Light (sig expo)	7	Same as above, but the pedestal has no exponential decay
Pedestal	2	Simple Gaussian mean and RMS fit is sufficient for pedestal
Pedestal (triple)	8	Sum of three Gaussians gives a better pedestal fit
High-Light	5	Gaussian pedestal and a modified Gaussian signal

Table A.2

The most important fitting function in this analysis is the Low-Light model. Some screenshots are included to show examples of parts of this algorithm. This algorithm is broken up into a few parts. First, the data must be loaded along with the experimental run parameters, initial conditions, range to be considered, and minimization engine (Figure A.1). Then, when fitting the model, the contributions from each Gaussian peak are computed separately and then summed, and must be drawn individually (Figure A.2). The pedestal Gaussian is slightly different from the rest, so it is computed in its own function (Figure A.3). The signal Gaussians are computed in a loop with their own function (Figure A.4).

```

fit_func->SetLineColor(4); // Dark blue
fit_func->SetNpx(2000);
fit_func->SetLineWidth(2);
// 11 parameters
fit_func->SetParName(0, "W");
fit_func->SetParName(1, "Q0");
fit_func->SetParName(2, "S0");
fit_func->SetParName(3, "alpha");
fit_func->SetParName(4, "mu");
fit_func->SetParName(5, "Q1");
fit_func->SetParName(6, "S1");
fit_func->SetParName(7, "inj");
fit_func->SetParName(8, "real");
fit_func->SetParName(9, "MIN_PE");
fit_func->SetParName(10, "MAX_PE");

// Set initial parameters
fit_func->SetParameters(initial);

// Constrain the parameters that need to be constrained
for (int i = 0; i < N_FIT_PARAMS; i++) {
    // Check if there is restraint on this param
    if (min[i] >= 0.0 && max[i] >= 0.0) {
        // Check if param needs to be fixed
        if (min[i] == max[i]) fit_func->FixParameter(i, initial[i]);
        // Otherwise, just bound the param
        else fit_func->SetParLimits(i, min[i], max[i]);
    }
}

// Define results pointer
TFitResultPtr res;
// Select fitting technique (chi, likelihood, etc.)
// Perform fit
switch (fitEngine) {
    case 0:
        // user range, return fit results, use improved fitter
        res = h_QDC->Fit(fit_func, "RSM", "", low, high);
        break;

    case 1:
        // Log likelihood, user range, return fit results, use improved fitter
        res = h_QDC->Fit(fit_func, "LRSM", "", low, high);
        break;

    case 2:
        // return fit results, use improved fitter
        res = h_QDC->Fit(fit_func, "SM", "");
        break;

    case 3:
        // Log likelihood, return fit results, use improved fitter
        res = h_QDC->Fit(fit_func, "LSM", "");
        break;

    case 4:
        // Better errors w/minos, return fit results, use improved fitter, user range
        res = h_QDC->Fit(fit_func, "ESMR", "");
        break;

    case 5:
        // Better errors, likelihood, return fit results, use improved fitter, user range
        res = h_QDC->Fit(fit_func, "ESMRL", "");
        break;
}

```

Figure A.1: Here, the parameters are given meaningful names, and the initial values are set for the parameters as well as the min and max for each parameter. The fit is performed in the bottom screenshot. The minimization engine is chosen by sending in different flags to the function "Fit". Default engine is χ^2 minimization, but "L" flag will use a log-likelihood computation instead. Flag "M" triggers more accurate error estimations.

```

// Create vector and grab return parameters
legend->AddEntry(fit_func, "Total fit", "l");
Double_t back[N_FIT_PARAMS];
fit_func->GetParameters(back);

// Make signal distribution functions for showing deconvolution in image
TF1 *fis_from_fit_pe[nPE];
// Make one for each PE contribution considered
for ( int bb = minPE; bb < maxPE; bb++) {
    // Set current PE peak in consideration
    fit_func->GetParameters(back);
    back[0] = (double)(bb);
    fis_from_fit_pe[bb] = new TF1(Form("pe_fit_%d", bb), low_light_model_pe, 0, MAX_BIN, N_FIT_PARAMS);
    fis_from_fit_pe[bb]->SetParameters(back);
    fis_from_fit_pe[bb]->SetLineStyle(2);
    fis_from_fit_pe[bb]->SetLineColor(2);
    fis_from_fit_pe[bb]->SetNpx(2000);
    fis_from_fit_pe[bb]->Draw("same");
    if (bb == minPE) legend->AddEntry(fis_from_fit_pe[bb], "PE distributions", "l");
}

// Make background distribution function for printing for user
TF1 *fis_from_fit_bg;
if (noExpo < 2) {
    fis_from_fit_bg = new TF1("fis_from_fit_bg", low_light_model_bg, 0, MAX_BIN, N_FIT_PARAMS);
} else {
    fis_from_fit_bg = new TF1("fis_from_fit_bg", low_light_model_bg_no_expo, 0, MAX_BIN, N_FIT_PARAMS);
}
fis_from_fit_bg->SetParameters(back);
fis_from_fit_bg->SetLineStyle(2);
fis_from_fit_bg->SetLineColor(7); // Cyan
fis_from_fit_bg->SetNpx(2000);
fis_from_fit_bg->Draw("same");
legend->AddEntry(fis_from_fit_bg, "Pedestal", "l");
if (draw_Legend > 0) legend->Draw();

/////////////////////////////////////////////////////////////////
// DONE FITTING
/////////////////////////////////////////////////////////////////

```

Figure A.2: The fit functions (background and signal) are used to draw the individual contributions together on a plot. The signal distributions are created in a loop.

```

// The model used here is described in a NIM publication in the "docs" directory.
Double_t low_light_model(Double_t *x, Double_t *par){
    Double_t s_real_sum = 0.;
    Double_t initial_par9 = par[9];
    for (int i = (int)(par[9]); i < (int)(par[10]); i++) {
        par[9] = (double)(i);
        s_real_sum += low_light_model_pe(x, par);
    }
    par[9] = initial_par9;
    Double_t s_bg = low_light_model_bg(x, par);
    return s_real_sum + s_bg;
}

// This is the same as the above model, except the exponential decay
// is not included in the background
Double_t low_light_pmt_model_without_expo_in_pedestal(Double_t *x, Double_t *par) {
    Double_t s_real_sum = 0.;
    Double_t initial_par9 = par[9];
    for (int i = (int)(par[9]); i < (int)(par[10]); i++) {
        par[9] = (double)(i);
        s_real_sum += low_light_model_pe(x, par);
    }
    par[9] = initial_par9;
    Double_t s_bg = low_light_model_bg_no_expo(x, par);
    return s_real_sum + s_bg;
}

// This function returns the background (pedestal) distribution
// which includes real 0-pe events, injected 0-pe events, as
// well as exponential decay distribution of discrete background events.
Double_t low_light_model_bg(Double_t *, Double_t *par){

    // Initialize variables, grab current x value
    Double_t qn, sigma_n, term_1, term_2, term_3, igne, igne_is;
    Double_t poisson_ls = exp(-par[4]);
    Double_t gaus_is = exp(-pow(x[0] - par[1], 2) / 2.0 / pow(par[2], 2)) / par[2] / sqrt(twopi);

    // If we are to the right of the pedestal, include the exponential.
    if(x[0] >= par[1]){
        // Use this line to use noExpoPed fit model
        //if(false){
        igne_is = par[3] * exp(-par[3] * (x[0] - par[1]));
        //} else {
        //    igne_is = 0.;

        // Calculate background portion
        Double_t s_bg = poisson_ls * par[8] * ((1 - par[0]) * gaus_is + par[0] * igne_is);

        // Add in clock contribution
        Double_t s_clock = par[7] * ((1-par[0]) * gaus_is + par[0] * igne_is);

        // Sum and return
        return s_bg + s_clock;
    }

    Double_t low_light_model_bg_no_expo(Double_t *x, Double_t *par){

        // Initialize variables, grab current x value
        Double_t poisson_ls = exp(-par[4]);
        Double_t gaus_is = exp(-pow(x[0] - par[1], 2) / 2.0 / pow(par[2], 2)) / par[2] / sqrt(twopi);

        // Calculate background portion
        Double_t s_bg = poisson_ls * par[8] * gaus_is;

        // Add in clock contribution
        Double_t s_clock = par[7] * gaus_is;

        // Sum and return
        return s_bg + s_clock;
    }
}

```

Figure A.3: In the top screenshot, the full fit function is defined as well as a variant of the fit function. The full function calls two helper functions to calculate background and signal portions separately. They are slightly different, and the signal function must be called in a loop. The bottom screenshot shows the background fit function definition. The modified version of the background is also shown which does not include any exponential decay. This algorithm comes from [6].

```

// This function takes in the same parameters from the above fit (+1 extra), and returns
// the signal value from ONLY A SINGLE pe contribution (par[9] = n).
// This will allow us to draw a deconvoluted picture of the fit.
Double_t low_light_model_pe(Double_t *x, Double_t *par){

    // Grab current x value, current pe, and prepare variables
    Int_t n = (Int)(par[9]);
    Double_t qn, sigma_n, term_1, term_11, term_2, term_3, igne, gn, igne_is;

    // Calculate values to be used for this PE
    qn = par[1] + n * par[5];                                // mean of this PE dist
    sigma_n = sqrt(pow(par[2],2) + n * pow(par[6],2));      // sigma of this PE dist
    term_1 = x[0] - qn - par[3] * pow(sigma_n,2);           // expo and erf argument
    term_11 = x[0] - qn - par[3] * pow(sigma_n,2) / 2.0;    // Error or correction
    term_2 = par[1] - qn - par[3] * pow(sigma_n,2);          // Erf argument
    term_3 = x[0] - qn;                                       // x[0] shifted by PE mean

    // Calculate igne
    // Depending on which side of the PE distribution we are on, add or subtract in parentheses
    if (term_1 >= 0.) {
        igne = par[3] / 2.0 * exp(-par[3] * term_11) *
        (
            TMath::Erf(fabs(term_2) / sqrt(2.0) / sigma_n) +
            TMath::Erf(fabs(term_1) / sqrt(2.0) / sigma_n)
        );
    } else {
        igne = par[3] / 2.0 * exp(-par[3] * term_11) *
        (
            TMath::Erf(fabs(term_2) / sqrt(2.0) / sigma_n) -
            TMath::Erf(fabs(term_1) / sqrt(2.0) / sigma_n)
        );
    }

    // Calculate gn
    gn = exp(-pow(term_3, 2) / 2.0 / pow(sigma_n, 2)) / (sqrt(twopi) * sigma_n);

    // Put it all together and return
    return TMath::PoissonI(n, par[4]) * par[8] * ((1 - par[0]) * gn + par[0] * igne);
}

Double_t low_light_model_pe_no_expo(Double_t *x, Double_t *par){

    // Grab current x value, current pe, and prepare variables
    Int_t n = (Int)(par[9]);
    Double_t qn, sigma_n, gn;

    // Calculate values to be used for this PE
    qn = par[1] + n * par[5];                                // mean of this PE dist
    sigma_n = sqrt(pow(par[2],2) + n * pow(par[6],2));      // sigma of this PE dist
    gn = exp(-pow(x[0] - qn, 2) / 2.0 / pow(sigma_n, 2)) / (sqrt(twopi) * sigma_n);

    // Put it all together and return
    return TMath::PoissonI(n, par[4]) * par[8] * gn;
}

```

Figure A.4: In this final screenshot, the signal contribution is computed for the n^{th} PE peak. The variable, n , is looped from min-PE to max-PE which are parameters 10 and 11 respectively. The modified version of the signal is also shown which does not include any exponential decay. This algorithm comes from [6].

```

////////// DONE FITTING ///////////
printf("\nDone fitting. \n");

// Grab some stats info from the fit
Double_t chi = fit_func->GetChiSquare();
Int_t ndf = fit_func->GetNDF();
Int_t nfitpoints = fit_func->GetNumberFitPoints();

// Get output values
Double_t wout = fit_func->GetParameter(0);
Double_t pedout = fit_func->GetParameter(1);
Double_t pedrmsout = fit_func->GetParameter(2);
Double_t alphaout = fit_func->GetParameter(3);
Double_t muout = fit_func->GetParameter(4);
Double_t sigout = fit_func->GetParameter(5);
Double_t sigrmsout = fit_func->GetParameter(6);
Double_t injout = fit_func->GetParameter(7);
Double_t realout = fit_func->GetParError(8);
Double_t wouterr = fit_func->GetParError(0);
Double_t pedouterr = fit_func->GetParError(1);
Double_t pedrmsouterr = fit_func->GetParError(2);
Double_t alphaouterr = fit_func->GetParError(3);
Double_t muouterr = fit_func->GetParError(4);
Double_t sigouterr = fit_func->GetParError(5);
Double_t sigrmsouterr = fit_func->GetParError(6);
Double_t injouterr = fit_func->GetParError(7);
Double_t realouterr = fit_func->GetParError(8);

// CALCULATE PMT GAIN USING AMPLIFICATION SETTING AND ADC CONVERSION FACTOR
Double_t gain = sigout * 25.0 / 160.217662;
Double_t gainError = sigouterr * 25.0 / 160.217662;
Double_t chiPerNDF = (double)(chi / ndf);
if (chiPerNDF > 1.0) {
    gainError = gainError * sqrt(chiPerNDF);
}
Double_t gainPercentError = gainError / gain * 100.0;

```

Figure A.5: The parameters are retrieved from the fit function and stored in a MySQL database along with the inputs required to produce the results. The gain is calculated from the number of ADC channels in Q_1 , and relative error is computed.

Appendix B

Gain Measurement Results

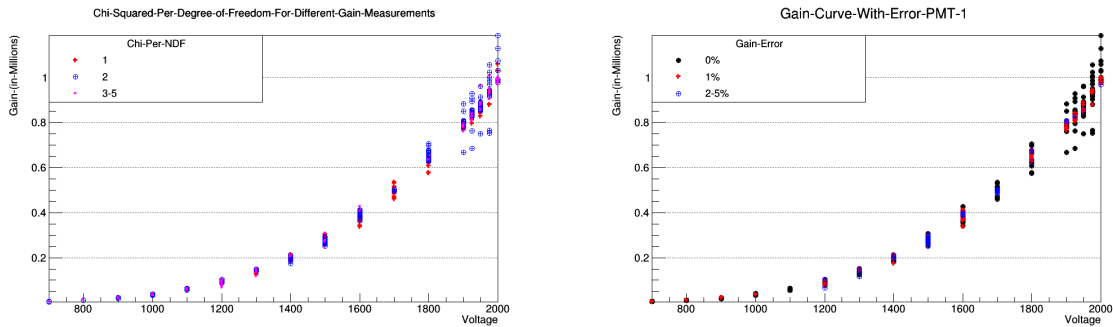


Figure B.1: PMT 1: The left plot shows the gain curves with fits of different χ^2 values. The plot on the right shows the error on the gain measurement (estimated by Root) from the same fits. These plots can be used to locate regions of predicted erroneous results.

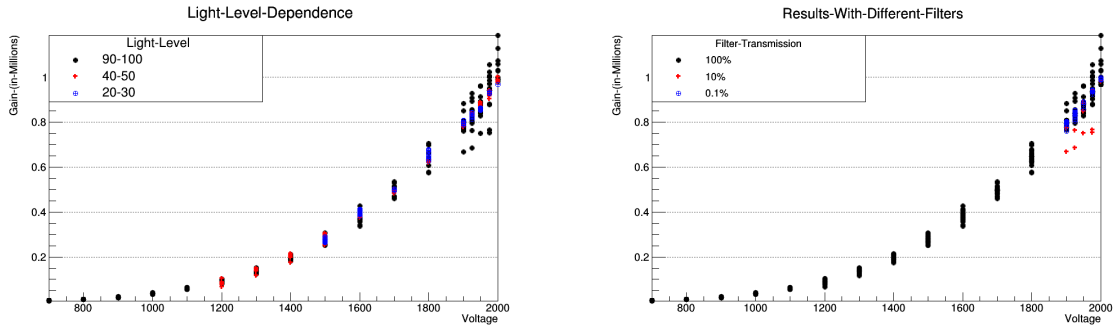


Figure B.2: PMT 1: These plots show how the light level or filter transparency affect the gain measurement. The left plot shows the intensity setting of the light pulses used for each run. The right plot shows which filter was being used to attenuate the pulses for the same runs. High-light data with no filtering produces a much larger spread of results than low-light data.

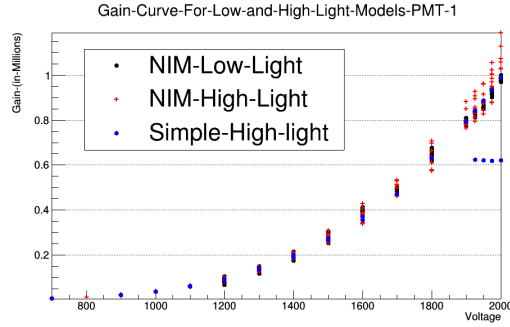


Figure B.3: PMT 1: This plot shows the gain curves predicted by 3 different models. The NIM low-light model is the main model of this thesis. The NIM high-light model is the same model, but constrained with light level information to produce reasonable results. The simple high-light model is a Gaussian pedestal and a Gaussian signal with an exponentially decaying tail. The simple high-light model is not able to predict anything below -1,900 V without filtering because the ADC saturates with charge at that light level.

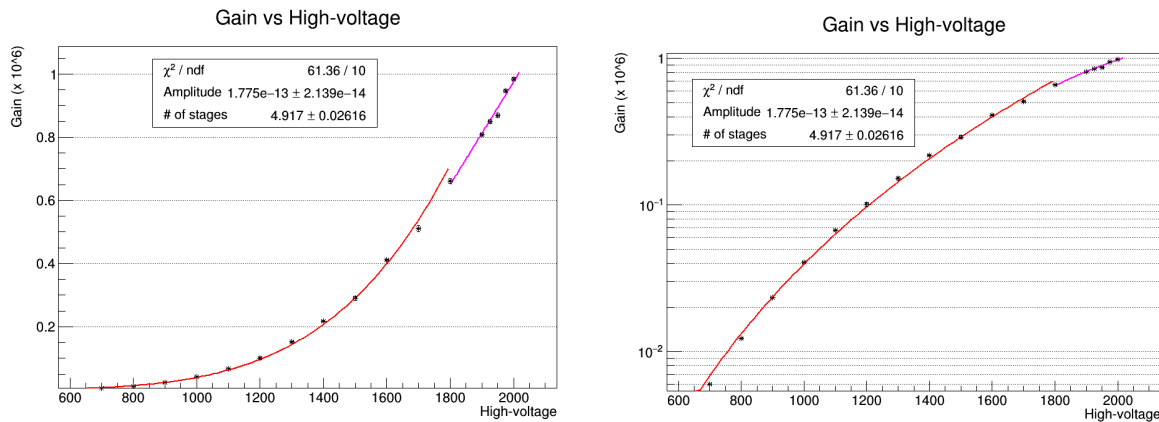


Figure B.4: PMT 1: These plots show a power curve fit ($G(V) = g(V/n)^n$) to the gain curve where V is voltage, g is amplitude, and n is the "number of stages". The error bar on the gain measurement is the estimated error on the gain measurement (from Root) scaled up by $\sqrt{\chi^2/NDF}$; the error estimate is never scaled down. The high voltage end is fit better to a line with slope 1.628×10^{-3} and y-intercept at -2.281. The right plot shows a log scale.

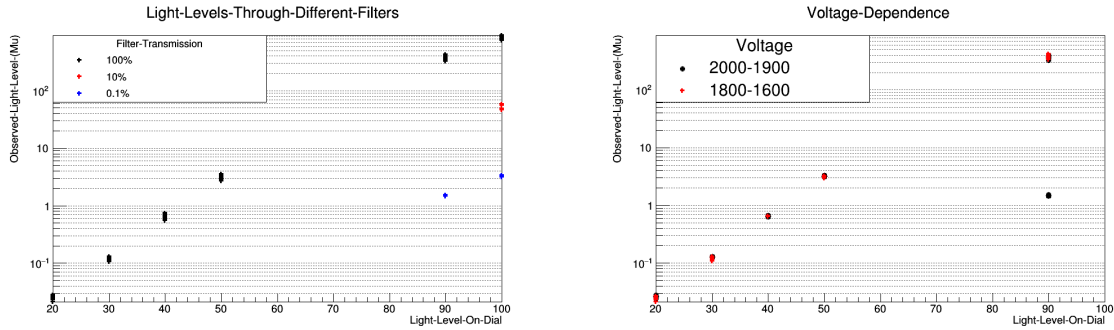


Figure B.5: PMT 1: These plots show the result of the light level calibration. The left plot shows the light level for different filter transparencies. The right plot shows which runs are high voltage and which are lower voltage.

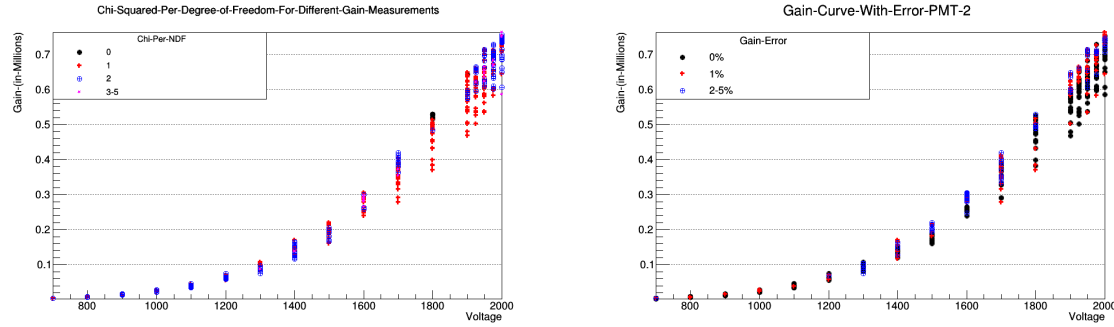


Figure B.6: PMT 2: The left plot shows the gain curves with fits of different χ^2 values. The plot on the right shows the error on the gain measurement (estimated by Root) from the same fits. These plots can be used to locate regions of predicted erroneous results.

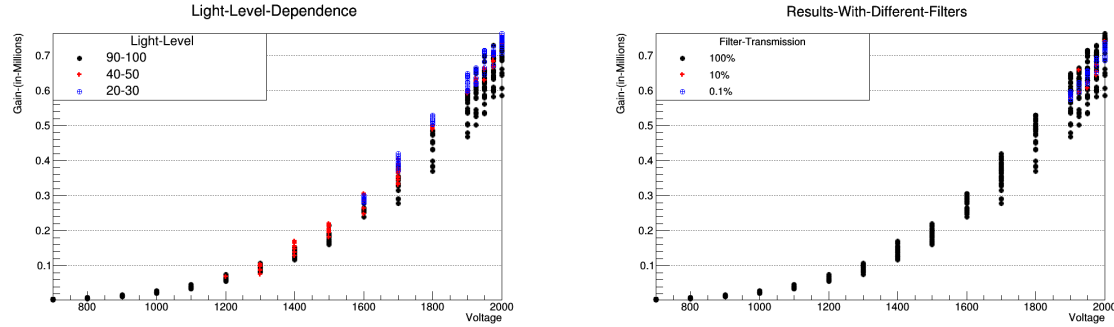


Figure B.7: PMT 2: These plots show how the light level or filter transparency affect the gain measurement. The left plot shows the intensity setting of the light pulses used for each run. The right plot shows which filter was being used to attenuate the pulses for the same runs. High-light data with no filtering produces a much larger spread of results than low-light data.

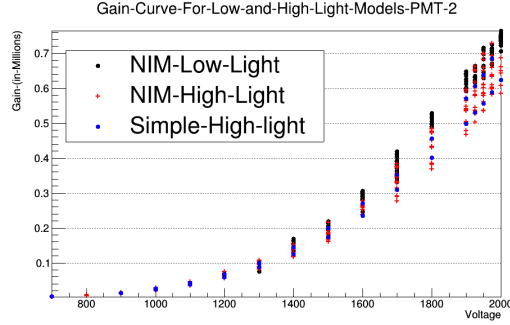


Figure B.8: PMT 2: This plot shows the gain curves predicted by 3 different models. The NIM low-light model is the main model of this thesis. The NIM high-light model is the same model, but constrained with light level information to produce reasonable results. The simple high-light model is a Gaussian pedestal and a Gaussian signal with an exponentially decaying tail.

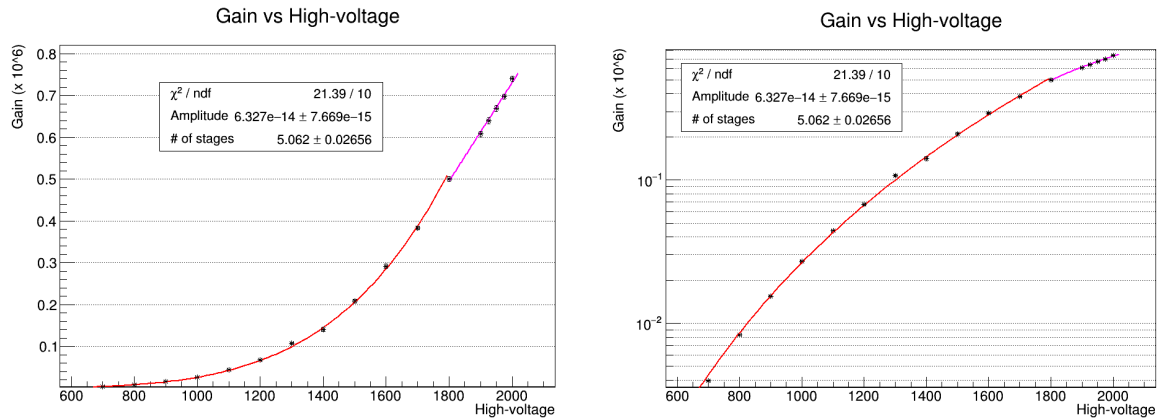


Figure B.9: PMT 2: These plots show a power curve fit ($G(V) = g(V/n)^n$) to the gain curve where V is voltage, g is amplitude, and n is the "number of stages". The error bar on the gain measurement is the estimated error on the gain measurement (from Root) scaled up by $\sqrt{\chi^2/NDF}$; the error estimate is never scaled down. The high voltage end is fit better to a line with slope 1.175×10^{-3} and y-intercept at -1.618. The right plot shows a log scale.

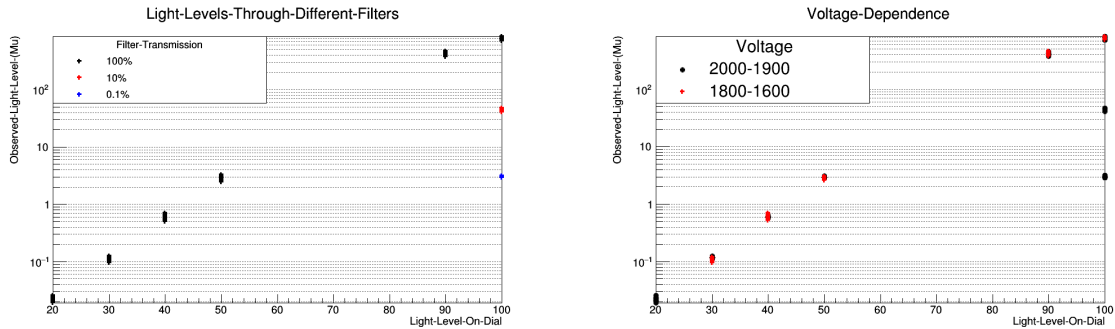


Figure B.10: PMT 2: These plots show the result of the light level calibration. The left plot shows the light level for different filter transparencies. The right plot shows which runs are high voltage and which are lower voltage.

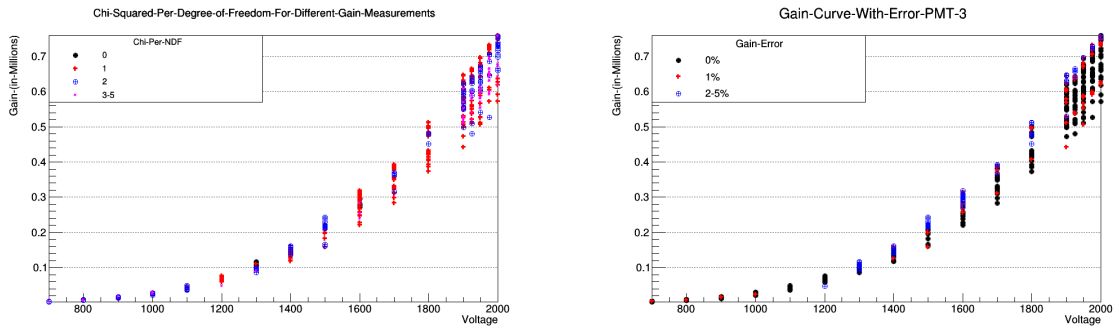


Figure B.11: PMT 3: The left plot shows the gain curves with fits of different χ^2 values. The plot on the right shows the error on the gain measurement (estimated by Root) from the same fits. These plots can be used to locate regions of predicted erroneous results.

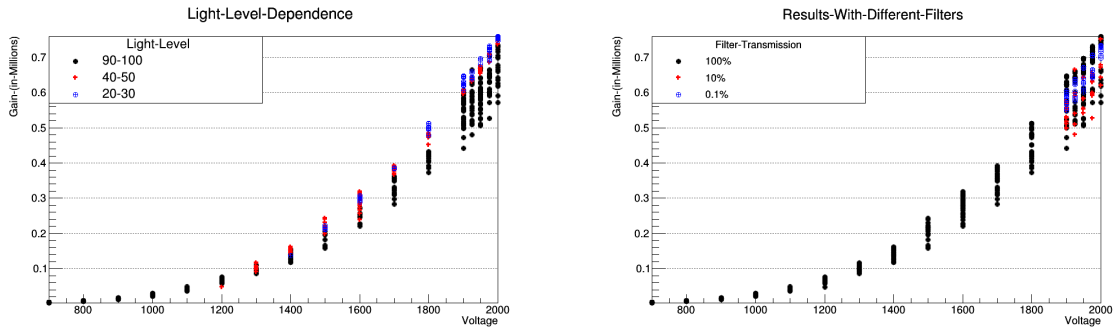


Figure B.12: PMT 3: These plots show how the light level or filter transparency affect the gain measurement. The left plot shows the intensity setting of the light pulses used for each run. The right plot shows which filter was being used to attenuate the pulses for the same runs. High-light data with no filtering produces a much larger spread of results than low-light data.

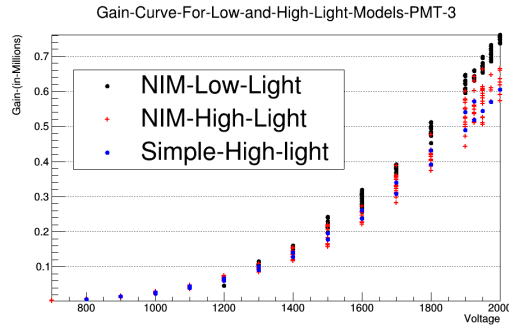


Figure B.13: PMT 3: This plot shows the gain curves predicted by 3 different models. The NIM low-light model is the main model of this thesis. The NIM high-light model is the same model, but constrained with light level information to produce reasonable results. The simple high-light model is a Gaussian pedestal and a Gaussian signal with an exponentially decaying tail.

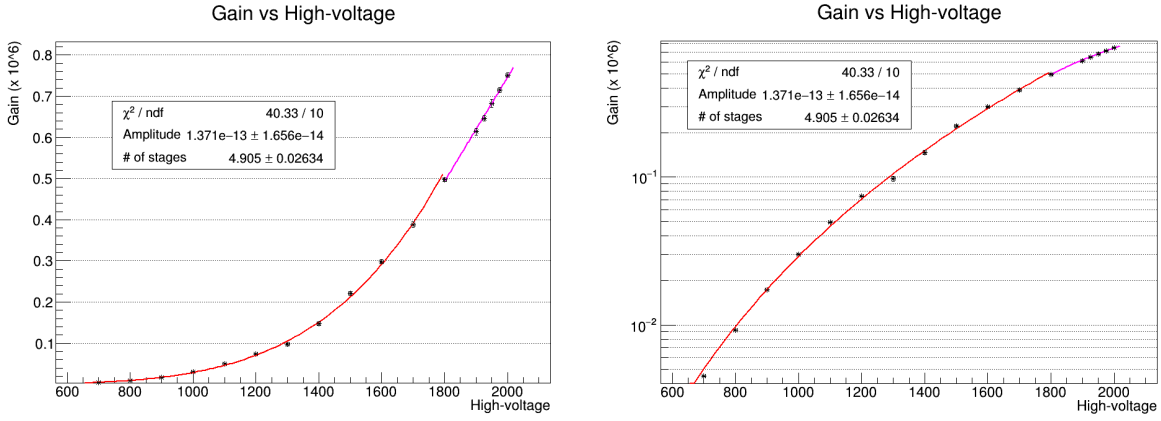


Figure B.14: PMT 3: These plots show a power curve fit ($G(V) = g(V/n)^n$) to the gain curve where V is voltage, g is amplitude, and n is the "number of stages". The error bar on the gain measurement is the estimated error on the gain measurement (from Root) scaled up by $\sqrt{\chi^2/NDF}$; the error estimate is never scaled down. The high voltage end is fit better to a line with slope 1.263×10^{-3} and y-intercept at -1.780. The right plot shows a log scale.

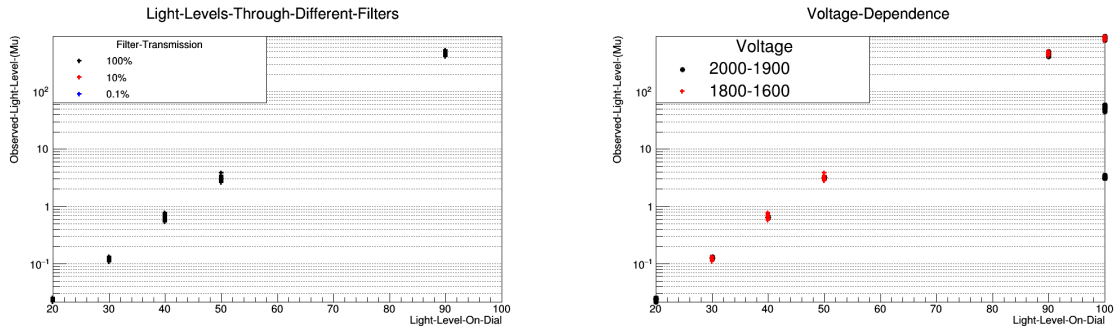


Figure B.15: PMT 3: These plots show the result of the light level calibration. The left plot shows the light level for different filter transparencies. The right plot shows which runs are high voltage and which are lower voltage.

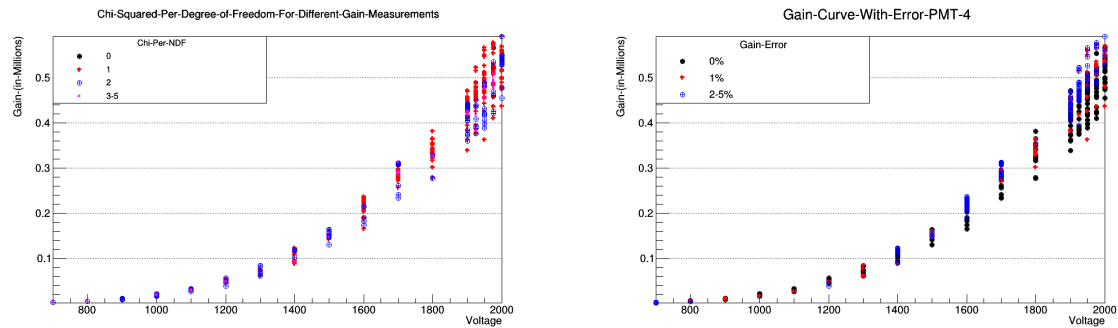


Figure B.16: PMT 4: The left plot shows the gain curves with fits of different χ^2 values. The plot on the right shows the error on the gain measurement (estimated by Root) from the same fits. These plots can be used to locate regions of predicted erroneous results.

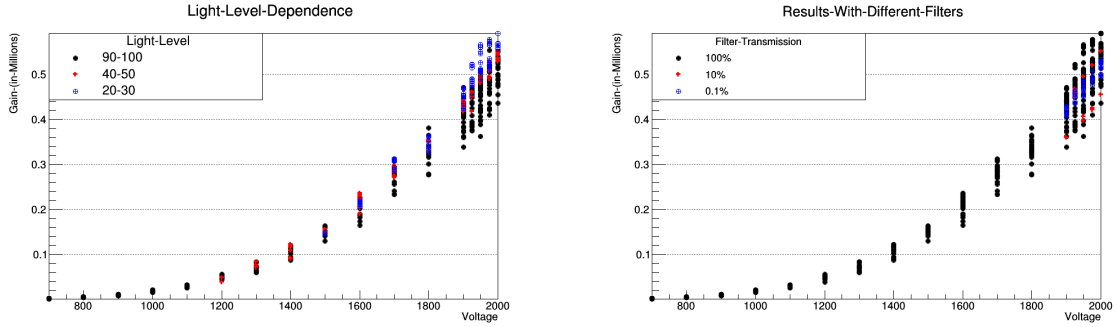


Figure B.17: PMT 4: These plots show how the light level or filter transparency affect the gain measurement. The left plot shows the intensity setting of the light pulses used for each run. The right plot shows which filter was being used to attenuate the pulses for the same runs. High-light data with no filtering produces a much larger spread of results than low-light data.

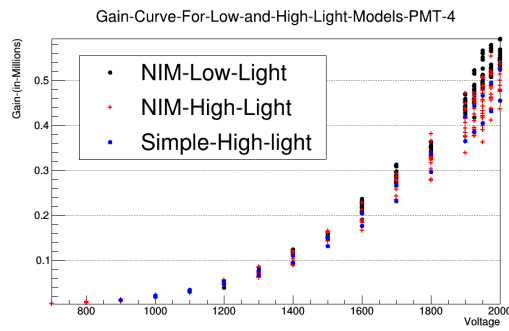


Figure B.18: PMT 4: This plot shows the gain curves predicted by 3 different models. The NIM low-light model is the main model of this thesis. The NIM high-light model is the same model, but constrained with light level information to produce reasonable results. The simple high-light model is a Gaussian pedestal and a Gaussian signal with an exponentially decaying tail.

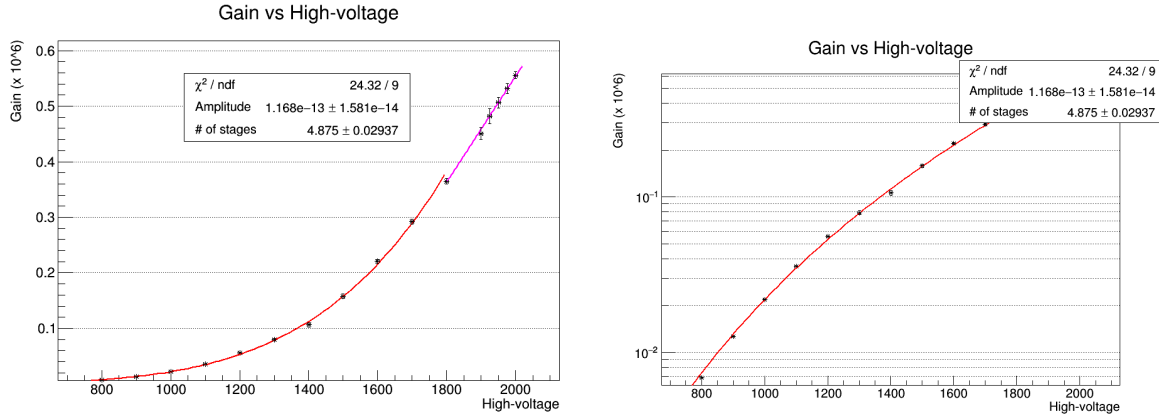


Figure B.19: PMT 4: These plots show a power curve fit ($G(V) = g(V/n)^n$) to the gain curve where V is voltage, g is amplitude, and n is the "number of stages". The error bar on the gain measurement is the estimated error on the gain measurement (from Root) scaled up by $\sqrt{\chi^2/NDF}$; the error estimate is never scaled down. The high voltage end is fit better to a line with slope 0.955×10^{-3} and y-intercept at -1.356. The right plot shows a log scale.

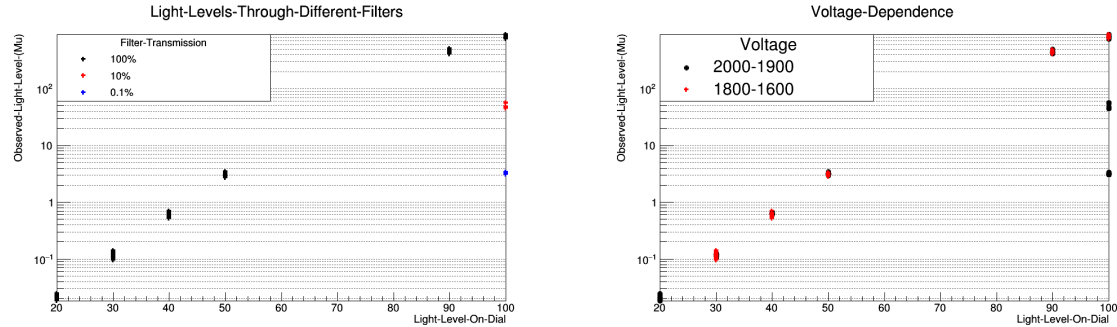


Figure B.20: PMT 4: These plots show the result of the light level calibration. The left plot shows the light level for different filter transparencies. The right plot shows which runs are high voltage and which are lower voltage.

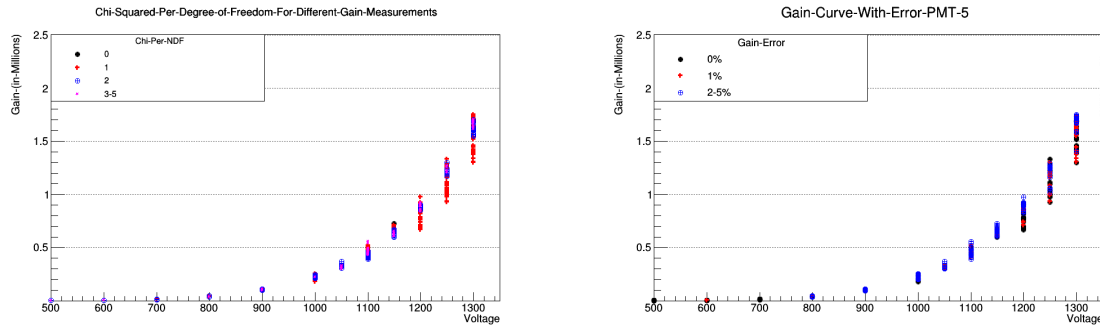


Figure B.21: PMT 5: The left plot shows the gain curves with fits of different χ^2 values. The plot on the right shows the error on the gain measurement (estimated by Root) from the same fits. These plots can be used to locate regions of predicted erroneous results.

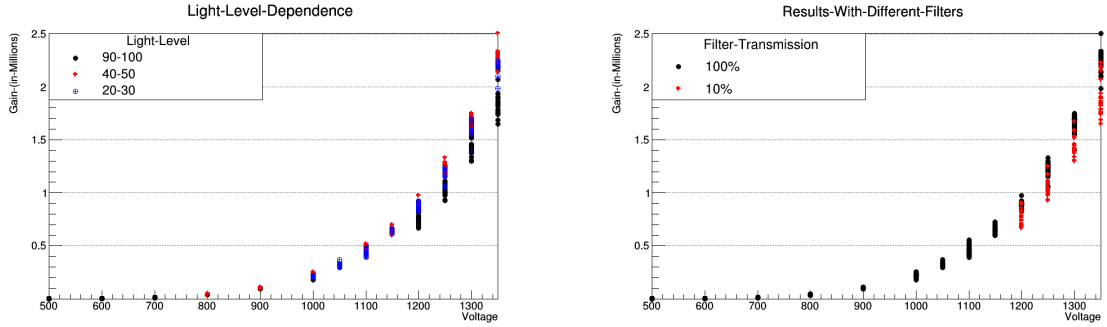


Figure B.22: PMT 5: These plots show how the light level or filter transparency affect the gain measurement. The left plot shows the intensity setting of the light pulses used for each run. The right plot shows which filter was being used to attenuate the pulses for the same runs. High-light data with no filtering produces a much larger spread of results than low-light data.

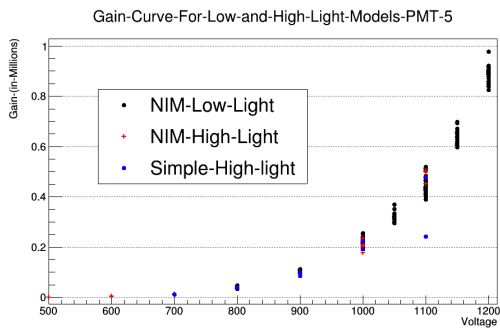


Figure B.23: PMT 5: This plot shows the gain curves predicted by 3 different models. The NIM low-light model is the main model of this thesis. The NIM high-light model is the same model, but constrained with light level information to produce reasonable results. The simple high-light model is a Gaussian pedestal and a Gaussian signal with an exponentially decaying tail.

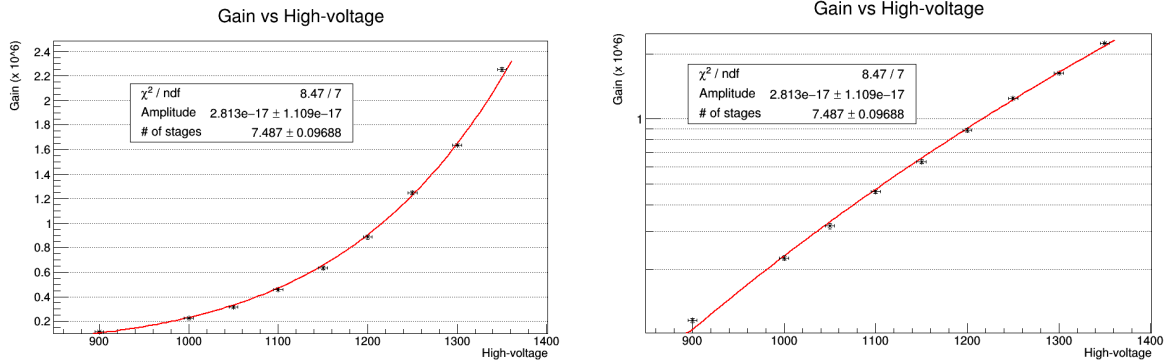


Figure B.24: PMT 5: These plots show a power curve fit ($G(V) = g(V/n)^n$) to the gain curve where V is voltage, g is amplitude, and n is the "number of stages". The error bar on the gain measurement is the estimated error on the gain measurement (from Root) scaled up by $\sqrt{\chi^2/NDF}$; the error estimate is never scaled down. The power curve fits this entire data range, perhaps because this is the only PMT without a modified base circuitry. The right plot shows a log scale.

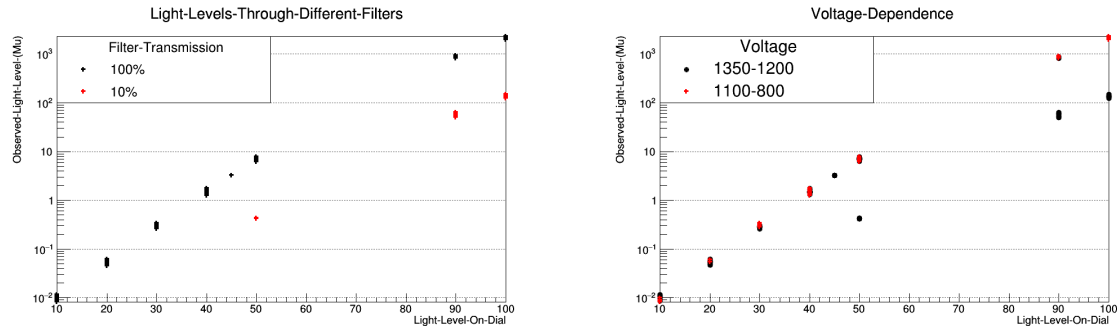


Figure B.25: PMT 5: These plots show the result of the light level calibration. The left plot shows the light level for different filter transparencies. The right plot shows which runs are high voltage and which are lower voltage.

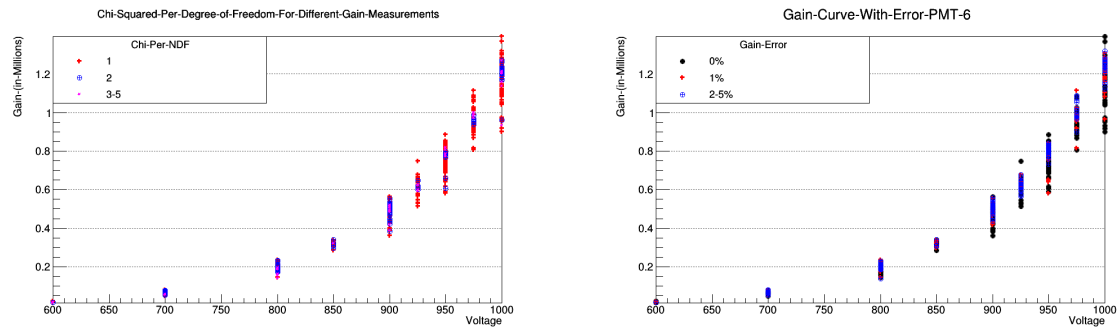


Figure B.26: PMT 6: The left plot shows the gain curves with fits of different χ^2 values. The plot on the right shows the error on the gain measurement (estimated by Root) from the same fits. These plots can be used to locate regions of predicted erroneous results.

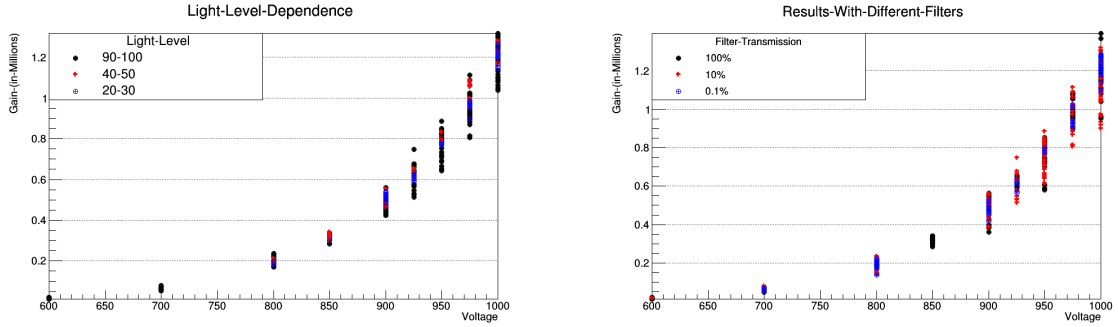


Figure B.27: PMT 6: These plots show how the light level or filter transparency affect the gain measurement. The left plot shows the intensity setting of the light pulses used for each run. The right plot shows which filter was being used to attenuate the pulses for the same runs. High-light data with no filtering produces a much larger spread of results than low-light data.

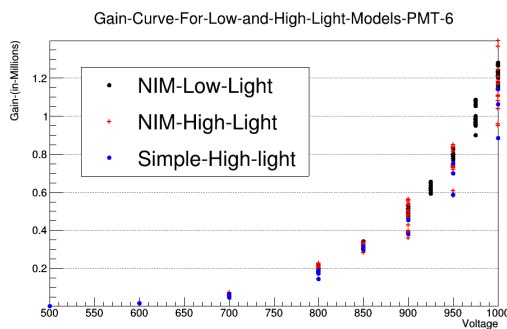


Figure B.28: PMT 6: This plot shows the gain curves predicted by 3 different models. The NIM low-light model is the main model of this thesis. The NIM high-light model is the same model, but constrained with light level information to produce reasonable results. The simple high-light model is a Gaussian pedestal and a Gaussian signal with an exponentially decaying tail.

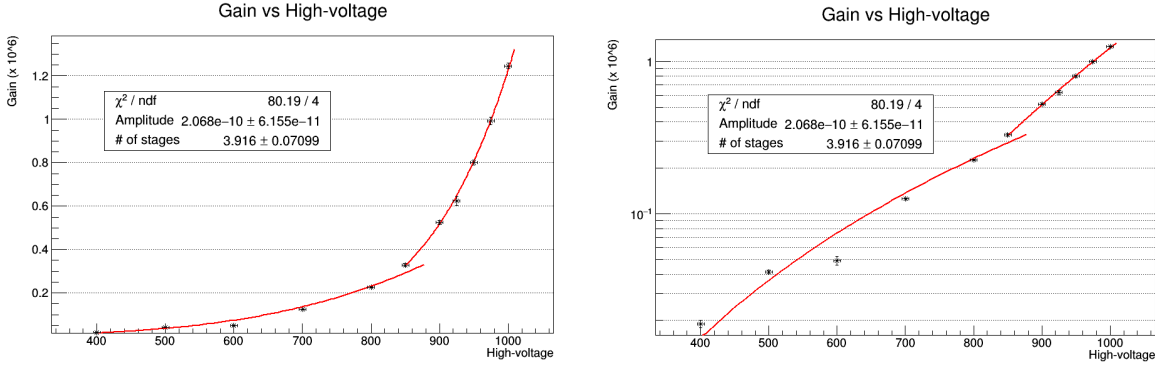


Figure B.29: PMT 6: These plots show a power curve fit ($G(V) = g(V/n)^n$) to the gain curve where V is voltage, g is amplitude, and n is the "number of stages". The error bar on the gain measurement is the estimated error on the gain measurement (from Root) scaled up by $\sqrt{\chi^2/NDF}$; the error estimate is never scaled down. The high voltage end is fit to a separate power curve with amplitude 1.089×10^{-17} and number of stages equal to 8.16675. The right plot shows a log scale.

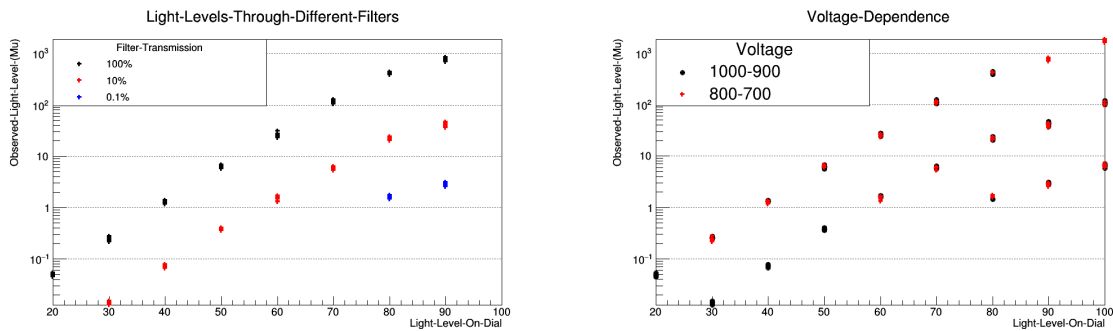


Figure B.30: PMT 6: These plots show the result of the light level calibration. The left plot shows the light level for different filter transparencies. The right plot shows which runs are high voltage and which are lower voltage.